UNIVERSITÉ LAVAL

Structures de glace des cours d'eau à forte pente : cristallographie et processus de croissance

Mémoire

Mathieu Dubé

Maîtrise en génie des eaux
Maître ès sciences (M. Sc.)

Québec, Canada

Résumé

Réunissant une série de trois articles scientifiques, ce mémoire offre une description et une quantification des processus dynamiques de glace dans les cours d'eau à forte pente. Menée sur trois cours d'eau du bassin versant de la rivière Montmorency (à proximité de Québec, QC, Canada), cette recherche démontre grâce à l'analyse par *CAT scan* que la glace de fond et les barrages de glace se développent principalement par croissance *in-situ* des cristaux de frasil-fixé. La porosité des structures de frasil-fixé varie entre 23% et 52% alors que celle de des structures de glace colonnaire, uniquement retrouvées dans les barrages de glace, varie entre 0% et 1,5%. De plus, les taux de croissance et de fonte des barrages de glace varient de façon importante autour d'une moyenne d'environ 1 cm/h. Le développement complet d'un barrage de glace a été simulé avec succès à l'aide d'un modèle physique comportant plusieurs degrés de liberté.

Abstract

Uniting three scientific papers, this thesis offers a description and a quantification of *dynamic* ice processes taking place in steep channels. This research was led on three channels located in the Montmorency River watershed near Quebec City, Canada. CAT scan analyses showed that the development of anchor ice and ice dams is mainly caused by in-situ growth of fixed-frazil ice crystals. Porosity of fixed-frazil ice structures ranges between 23% and 52% while porosity of columnar ice structures, only found in ice dams, ranges from 0% to 1.5%. Moreover, ice dam growth and decay rates greatly vary around the mean value of about 1 cm/h. The complete development of a single ice dam was successfully simulated using a physical model that demonstrated the large number of degrees of freedom inherent in the process.

Table des matières

Liste des tableaux

Liste des figures

Remerciements

La réalisation d'un projet de maîtrise nous amène à acquérir et perfectionner différentes compétences et qualités, non seulement des points de vue technique et scientifique mais également sur le plan personnel. Mener à bien cette étude de terrain hivernale m'a demandé patience, détermination et ténacité. Le support de mes proches a été une source de motivation tout au long du projet. Je tiens particulièrement à remercier ma copine Marie-Pier d'avoir été si compréhensive durant ces deux années. Merci à mes parents, Marc et Lise, de m'avoir encouragé à persévérer tout au long de ce cheminement.

Je remercie également les personnes et les instances suivantes pour leur contribution significative à ce projet de maîtrise :

- Brian Morse, mon directeur de recherche, pour son humilité, ses idées infinies, sa vision, son expérience, sa patience, son sens de l'humour, sa grande disponibilité et sa générosité. Il a été un véritable guide et m'a permis de constamment me dépasser.

- Benoit Turcotte, mon fidèle collaborateur, pour son aide précieuse, son temps, son écoute et pour avoir partagé de nombreuses données. Nos sorties de terrain et nos discussions étaient à chaque fois aussi intéressantes qu'instructives.

- Dany Crépault pour son aide à construire et réparer les équipements et les outils de terrain. Son savoir-faire et sa rapidité d'exécution ont grandement facilité mon travail.

- Marlyne Fergusson pour avoir préparé mes nombreux relevés de dépenses de terrain et pour sa bonne humeur contagieuse.

- Les propriétaires riverains qui m'ont si gentiment donné accès à leur terrain durant 8 mois. Merci à Lise, Claude et Denis.

- Le conseil de recherches en sciences naturelles et en génie du Canada (CRSNG) et la Fondation canadienne pour l'innovation (FCI) pour leur support financier à ce projet.

Avant-propos

L'introduction et la conclusion de ce mémoire, soit les chapitres 1 et 5, ont été entièrement rédigés par l'auteur du mémoire.

L'article présenté au chapitre 2 a été coécrit par Benoit Turcotte (candidat au doctorat), Brian Morse (directeur de recherche) et Edward Stander (professeur à SUNY Cobleskill). L'auteur de ce mémoire est l'auteur principal de l'article **tel que présenté** à la conférence du CRIPE (*Committee on River Ice Processes and the Environment*).

L'article présenté au chapitre 3 a été coécrit par Benoit Turcotte (candidat au doctorat) et Brian Morse (directeur de recherche). L'auteur de ce mémoire est l'auteur principal de l'article **tel que publié** dans la revue scientifique *Cold Regions Science and Technology* en 2014.

L'article présenté au chapitre 4 a été coécrit par Benoit Turcotte (scientifique de recherche) et Brian Morse (directeur de recherche). L'auteur de ce mémoire est l'auteur principal de l'article **tel que soumis** à la revue scientifique *Canadian Journal of Civil Engineering* en 2014.

1. Introduction

1.1 Mise en contexte

La formation de la glace dans les cours d'eau à forte pente en milieu nordique repose sur une série de processus dynamiques qui interagissent entre eux et qui sculptent le paysage fluvial en période hivernale. Principalement répertoriés dans les chenaux à lit graveleux ayant une pente de plus de 0.3%, ces processus de glace causent notamment l'augmentation des niveaux d'eau (e.g. Tesaker, 1996; Turcotte et al., 2013) et la modification des conditions d'écoulement (e.g. débit, vitesse), donnant ainsi lieu à la formation d'une couverture de glace suspendue (e.g. Tesaker, 1994; Turcotte et al., 2011) propre à ces cours d'eau.

Ces processus représentent le résultat d'une série de réactions en chaîne basée sur deux conditions devant obligatoirement être rencontrées : un niveau de **turbulence** de l'écoulement suffisamment élevé et des températures de l'air suffisamment sous le point de congélation occasionnant la **surfusion de l'eau** (*supercooling*). Ces deux conditions permettent la formation de cristaux de **frasil**, soit de fins disques de glace se déplaçant dans la colonne d'eau. Pouvant être formés (ou encore nucléés) selon différents processus (Michel, 1978), ces cristaux adoptent, au premier stade de leur développement, une morphologie discoïde (Tsang, 1982). Leur croissance est possible tant et aussi longtemps que la température de l'eau demeure sous le point de congélation (surfusion). À ce moment considérés dans une phase active (e.g. Tesaker, 1994), les disques de frasil on la propriété de s'agglomérer entre eux ou encore d'adhérer sur les surfaces submergées ayant une température de 0°C ou moins.

Toute accumulation de glace formée sur une surface submergée est appelée **glace de fond** (*anchor ice*). Dans les cours d'eau à forte pente, la glace de fond présente une structure poreuse plus ou moins dense prenant la plupart du temps une apparence nuageuse (Figure 1.1). Elle peut se former de façon sporadique ou encore recouvrir le lit du chenal d'une large et épaisse couverture de glace (e.g. Stickler and Alfredsen, 2009). Depuis les premières publications sur le sujet (e.g. Barnes, 1906; Altberg, 1936) elle a été étudiée sur le terrain (Hirayama et al., 1997; Kempema and Ettema, 2011; Terada et al., 1998) et en laboratoire (e.g. Clark and Doering, 2004; 2006; Qu and Doering, 2007). Plusieurs chercheurs ont tenté d'expliquer les caractéristiques de la glace de fond (masse volumique, forme, répartition spatiale) en utilisant les caractéristiques d'écoulement représentées par les nombres de Froude et de Reynolds (e.g. Kerr et al., 2002; Stickler and Alfredsen, 2009). Toutefois, alors que certaines études révèlent une relation claire (e.g. Doering et al., 2001), d'autres ne révèlent aucun lien ou encore une relation faible (e.g. Yamazaki et al., 1996).

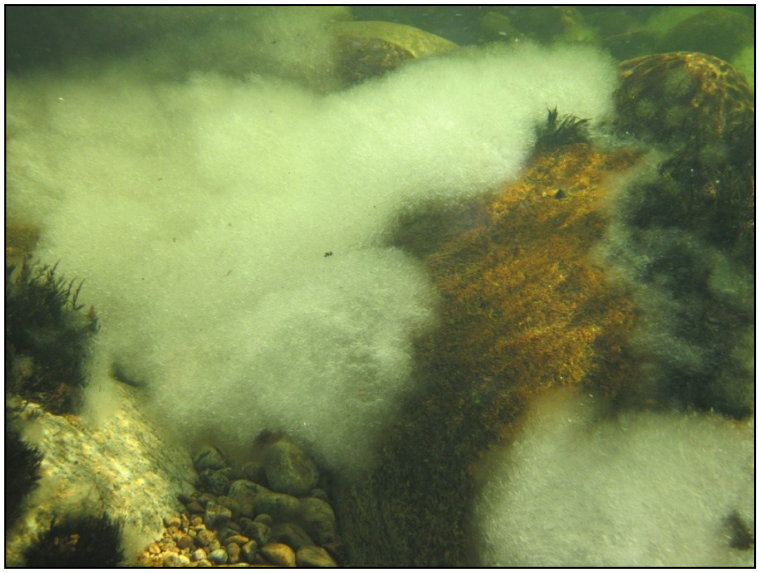

Figure 1.1. Accumulation de glace de fond sur un lit graveleux. L'écoulement est dans la direction de la caméra.

De plus, les processus d'initiation et de développement de la glace de fond sont encore débattus à ce jour. En effet, les chercheurs ne sont pas unanimes à savoir si la glace de fond est « uniquement » formée par l'attachement des cristaux de frasil (Kerr et al., 2002), « principalement » formée par l'attachement des cristaux de frasil (e.g. Qu and Doering, 2007; Yamazaki et al., 1996), formée par croissance en place (*in situ*) de cristaux de glace (e.g. Tesaker, 1994) ou encore formée par une combinaison de ces deux processus (e.g. Kempema and Ettema, 2009; Tsang, 1982).

De façon générale, les seuils et des rapides représentent deux unités géomorphologiques (Montgomery and Buffington, 1997) où la glace de fond se développe rapidement dans le temps et connait une croissance verticale importante, contrôlant ainsi les niveaux d'eau dans les sections mouille (*pool*) entre les seuils et les rapides. Lorsqu'une accumulation de glace de fond émerge, partiellement ou sur toute la largeur du seuil (ou du rapide), elle devient par définition (e.g. Turcotte et al., 2013) un **barrage de glace** (*ice dam*). Composés à la fois de glace de fond poreuse et de glace dense formée par cristallisation successive de fines couches d'eau appelée glaçage (*icing*), les barrages de glace (Figure 1.2) sont historiquement moins documentés que la glace de fond et ce, malgré leur impact important sur les conditions d'écoulement. Étant souvent considérés comme une condition particulière du développement de la glace de fond, rares sont les études qui mettent l'emphase sur les caractéristiques propres aux barrages de glace (e.g. Tesaker, 1994; 1996). De plus, aucune publication n'a, jusqu'à présent, permis de d'identifier des distinctions entre la structure interne et les propriétés cristallographiques de la glace de fond et celles des barrages de glace.

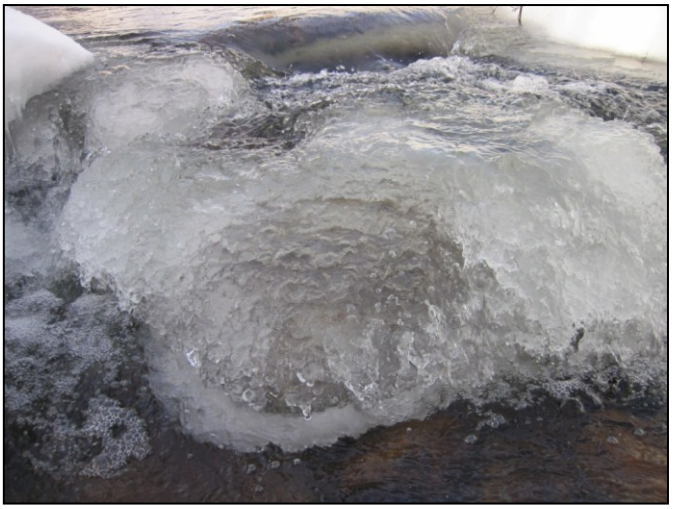

Figure 1.2. Barrage de glace composé de glace de fond et recouvert de glaçage. L'écoulement est dans la direction de la caméra.

Plus récemment, certaines publications ont mis en lumière l'influence des barrages de glace sur l'hydrologie et l'hydraulique des cours d'eau (e.g. Stickler et al., 2010). L'une de ces études (Turcotte et al., 2013) présente notamment les taux de croissance de barrages de glace situés dans différents chenaux à l'intérieur d'un bassin versant. Les résultats montrent une variabilité inter-chenal marquée et laissent entrevoir un niveau de variabilité à l'échelle d'un même chenal. De plus, cet article présente un modèle basé sur un bilan thermique adapté aux particularités des échanges thermiques dans les cours d'eau à forte pente. La simulation réalisée permet de prédire les événements de surfusion de l'eau ainsi que la durée des périodes de développement des barrages de glace. Le modèle n'est toutefois pas conçu pour simuler la hauteur d'eau stockée (*backwater*) à l'amont d'un barrage de glace en fonction des conditions environnementales locales.

1.2 Objectifs

Ce projet de recherche a pour but de non seulement combler certaines lacunes retrouvées dans la littérature sur la glace de fond et les barrages de glace, mais également d'approfondir la compréhension des processus de formation de ces deux types de glace par l'utilisation d'outils d'analyse et de modélisation innovateurs. De façon plus spécifique, ce projet de maîtrise en deux étapes vise dans un premier temps à 1) documenter et caractériser la structure interne et la cristallographie des barrages de glace et de la glace de fond, 2) quantifier les caractéristiques structurales propres à ces deux types de glace et 3) déterminer le(s) processus responsable(s) de leur développement. Cette première étape est donc consacrée à l'étude microscopique de la formation de la glace dans les cours d'eau à forte pente. Le champ de recherche est ensuite étendu au niveau macroscopique avec le second volet qui a pour objectifs de 4) quantifier la variabilité du taux de croissance des barrages de glace à l'échelle d'un chenal et 5) d'expliquer cette variabilité en quantifiant l'influence des paramètres environnementaux sur le développement des barrages de glace.

Cette recherche a été menée dans le bassin versant de la rivière Montmorency au nord de la région de Québec durant quelques semaines de l'hiver 2011-2012 et durant la totalité de l'hiver 2012-2013. Les sorties de terrain réalisées lors du premier hiver (2011-2012) ont permis de récolter des échantillons de barrage de glace qui ont ensuite été analysés à l'aide d'un tomodensitomètre (CAT scan). La méthodologie employée et les résultats obtenus sont présentés dans un premier article (Chapitre 2) tel que présenté à la conférence du CRIPE (*Committee on River Ice Processes and the Environment*) tenue à Edmonton en Alberta en juillet 2013. Lors du deuxième hiver (2012-2013), une nouvelle série d'échantillons de glace a été récoltée et encore une fois analysée à l'aide du CAT scan. Cette fois, la glace de fond a également été échantillonnée et des méthodes d'analyse plus sophistiquées ont été employées. Les résultats sont présentés dans un second article (Chapitre 3) tel que publié en 2014 dans la revue scientifique *Cold Regions Science and Technology*. En plus des nombreux échantillons recueillis, l'hiver 2012-2013 a permis de récolter une grande quantité de données hydrauliques, hydrologiques et météorologiques durant une période de 242 jours (23 octobre 2012 au 22 juin 2013). Parmi ces données, les taux de formation et de fonte des barrages de glace ont été comparés à six différents sites répartis sur près de 800 mètres à l'intérieur du même cours d'eau. De plus, l'environnement d'un barrage de glace spécifique a été intensément instrumenté, permettant ainsi d'en modéliser son développement. Ces différentes données et ce modèle sont présentés dans un troisième article (Chapitre 4) tel que soumis à la revue scientifique *Canadian Journal of Civil Engineering* en septembre 2014.

Chacun des chapitres (articles) de ce mémoire présente un ouvrage complet en soit qui comprend une revue de littérature, une description de la méthodologie employée, une présentation et une analyse des résultats, une discussion et une bibliographie. Ces chapitres représentent une suite logique de caractérisation, de quantification et de modélisation des processus développement de la glace de fond et des barrages de glace, s'étendant de l'échelle micro-locale jusqu'à l'échelle du cours d'eau.

Références

Altberg, WJ. 1936. Twenty years of work in the domain of underwater ice formation, 1915-35. International Union of Geodesy and Geophysics, International Association of Scientific Hydrology 23: 373-407.

Barnes, HT. 1906. Ice Formation with Special Reference to Anchor-Ice and Frazil. John Wiley & Sons: New York, 257 pp.

Clark, S., Doering, J.C., 2004. A laboratory study of frazil ice size distributions. Proceedings of the 17th International IAHR Ice Symposium, Saint Petersburg, Russia, 291-297.

Clark, S., Doering, J. C., 2006. Effect of turbulence intensity on frazil formation. Proceedings of the 18th International IAHR Ice Symposium, 267-275.

Doering, J.C., Bekeris, L.E., Morris, M.P., Dow, K.E., Girling, W.C. 2001. Laboratory Study of Anchor Ice Growth. Journal of Cold Regions Engineering, March 2011, p. 60-66.

Hirayama K, Terada K, Sato M, Hirayama K, Sasamoto M, Yamazaki M. 1997. Field measurements of anchor ice and frazil ice. In: Proceedings of the 9th CGU-HS CRIPE Workshop on the Hydraulics of Ice Covered Rivers, Fredericton, NB, Canada.

Kempema, E. W., Ettema, R. 2009. Variations in anchor-ice crystal morphology related to river flow characteristics. Proceedings of the 15th CGU-HS CRIPE Workshop on River Ice, St. John's, Newfoundland and Labrador, Canada.

Kempema, E. W., Ettema, R. 2011. Anchor ice rafting: observations from the Laramie River, River research and applications, Volume 27, Issue 9, p. 1126-1135

Kerr DJ, Shen HT, Daly SF. 2002. Evolution and hydraulics of anchor ice on gravel bed. Cold Reg. Sci. Technol. 35: 101–114.

Montgomery, D.R., Buffington, J.M., 1997. Channel-reach morphology in mountain drainage basins. GSA Bulletin 109 (5), 596-611.

Michel, B., 1978. Ice Mechanics, Les Presses de l'Université Laval, Québec.

Qu, Y.X., Doering, J., 2007. Laboratory study of anchor ice evolution around rocks and on gravel beds. Canadian Journal of Civil Engineering 34, 46–55.

Stickler M, Alfredsen KT. 2009. Anchor ice formation in streams: a field study. Hydrol. Process. 23: 2307–2315. DOI: 10.1002/hyp.7349.

Stickler M, Alfredsen KT, Linnansaari T, Fjeldstad H-P. 2010. The influence of dynamic ice formation on hydraulic heterogeneity in steep streams. River Res. Applic. 26: 1187–1197. DOI: 10.1002/rra.1331.

Tesaker E. 1994. Ice formation in steep rivers. In: Proceedings of the 12th International IAHR Ice Symposium.

Tesaker E. 1996. Interaction between ice and water flow in rapids. In: Proceedings of the 13th International IAHR Ice Symposium.

Terada K, Hirayama K, Sasamoto M. 1998. Field measurement of anchor and frazil ice. In: Proceedings of 14th International IAHR Ice Symposium.

Tsang, G. 1982. Frazil and Anchor ice: A Monograph. National Research Council of Canada, Associate Committee on Hydrology, Subcommittee on Hydraulics of Ice Covered Rivers.

Turcotte B, Morse B, Anctil F. 2011. Steep channels freezeup processes. Proceedings of the 16th CGU-HS CRIPE Workshop on the Hydraulics of Ice Covered Rivers, Winnipeg, MB, Canada.

Turcotte, B., Morse, B., Dubé, M., Anctil, F., 2013. Quantifying steep channel freezeup processes, Cold Regions Science and Technology 94, 21-36.

Yamazaki, M., Hirayama, K., Sakai, S., Sasmoto, M., Kiyohara, M., Takiguichi, H., 1996. Formation of frazil and anchor ice. Proceedings of the IAHR Ice Symposium, pp. 488–496.

2. Formation and inner structure of ice dams in steep channels

Mathieu Dubé[1], Benoit Turcotte[2], Brian Morse[3] and Edward Stander[4]

[1,2,3]Université Laval, 1065, av. de la Médecine, Québec City, QC/Can, G1V 0A6

[1]*mathieu.dube.4@ulaval.ca*; [2]*benoit.turcotte.1@ulaval.ca*; [3]*brian.morse@gci.ulaval.ca*

[4]SUNY Cobleskill, Department of Natural Sciences, Cobleskill, New York, 12043

standeej@cobleskill.edu

Résumé

Les barrages de glace sont des structures fascinantes qui se forment spontanément dans les cours d'eau à forte pente durant la période de prise de glace. Ils augmentent dramatiquement les niveaux d'eau à l'amont et peuvent causer des inondations. Lorsqu'ils se forment à l'aval de stations hydroélectriques, ils peuvent réduire significativement la hauteur de chute et donc l'énergie produite. Jusqu'à présent, leur structure interne et leur porosité moyenne n'ont pas été documentées. Cette étude vise à comprendre la formation des barrages de glace en répondant à quatre questions spécifiques : Quels processus cryologiques expliquent leur développement? De quels types de cristaux sont-ils faits? Quelle est leur porosité? Quel est leur profil typique?

Cet article présente des données originales recueillies sur deux chenaux du bassin versant de la rivière Montmorency où le développement des barrages de glace est connu pour son intensité. Les différentes mesures regroupent des photographies à intervalle, l'évolution du niveau d'eau ainsi que les températures de l'eau et de l'air. Le tout a été recueilli lors de deux événements de prise de glace durant l'hiver 2011-2012. Des échantillons de barrage de glace on été analysés à l'aide de la technologie *CAT scan* et de l'analyse par sections minces. Les résultats du *CAT scan* ont révélé la composition interne et la porosité des échantillons de barrages de glace et ont été interprétés pour comprendre leur développement. Les sections minces ont permis de confirmer ce que le *CAT scan* a mesuré. En plus de l'originalité des résultats présentés, ce projet est innovateur, car il utilise la technologie du *CAT scan* comme une méthode d'analyse non destructrice des structures complexes et multidimensionnelles des barrages de glace.

Abstract

Ice dams are fascinating structures that spontaneously form across steep channels during the freezeup period. They dramatically increase the water level upstream and can cause overbank flooding. When they form downstream of hydroelectric dams, they can significantly reduce the available head and hence energy production. So far, their internal structure and overall porosity have not been documented. This study aims at understanding the formation of ice dams by answering four specific questions: What cryologic processes explain their development? What type of ice crystals are they made of? What is their porosity? What is their typical profile?

This paper presents original data from two channels of the Montmorency River watershed known for their intense ice dam development activity. Measurements include time-lapse photographs, water level records, and water and air temperatures collected during two freezeup events of the 2011-2012 winter. Ice dam samples were analyzed using CAT scan technology and thin sections. CAT scans revealed the inner composition and the porosity of ice dam samples and were interpreted to understand their development. Thin sections aided to understand what the CAT data quantified. Beyond the originality of the results presented in this work, this project is innovative because it uses CAT scan technology as a non-destructive method to analyze complex, multi-dimensional ice structures.

2.1 Introduction

Ice dams are fascinating ice structures that form in steep creeks, streams and rivers affected by subfreezing air temperatures. Despite their dominant presence in most cold regions gravel bed channels, ice dams remain poorly documented in the river ice literature. Recent studies have shown that they generate important channel blockage, they drastically raise water levels (e.g., Tesaker, 1994; Turcotte et al., 2013a), they affect flow patterns and water velocities that affect the conditions for ice cover formation (e.g., Stickler et al., 2010; Turcotte and Morse, 2010), they store a significant amount of water, thereby affecting downstream hydrological conditions (Turcotte et al., 2013b), and they lead to the development a unique, suspended ice cover that is supported by emerging rocks and banks (e.g., Tesaker, 1994; Turcotte et al., 2011). Ice dams seem to initially develop primarily under supercooling conditions but also buildup when the water temperature is at zero degree. Under a protracted period of cold air temperature, ice dams continue to grow and can eventually occupy the entire channel section despite a very small flow rate (Turcotte et al., 2013a).

In January 2012, ice dams were sampled in order to explore their internal structure and better understand their buildup dynamics. This paper presents a first attempt to classify their internal geometries, crystallography, and quantify their porosities. It will also describe the development processes as a function of air temperatures and local water levels.

2.2 Background

Ice processes taking place along low-gradient rivers have received substantial research attention over the last few decades. This research effort ultimately led to mitigation techniques that can prevent or minimize damage to infrastructures and improve local residents' safety (e.g. Ashton, 1986 and Prowse, 1955). In contrast, relatively few research efforts have specifically addressed steep channels ice processes.

Anchor ice represents the most documented steep channel ice form. It has been studied in the field (Bisaillon and Bergeron, 2009; Hirayama et al., 1997; Kempema and Ettema, 2011; Parkinson, 1984; Terada et al., 1998; Yamakazi et al., 1996) and in the lab (Clark and Doering, 2004; 2006; Kerr et al., 2002; Qu and Doering, 2007). Most anchor ice studies reported anchor ice release at sunrise or assumed that anchor ice was ephemeral. Relatively recently, complex, stable, anchored ice features such as ice dams have been described in detail (Stickler et al. 2010; Stickler and Alfredsen, 2009; Tesaker, 1994; 1996, Turcotte and Morse, 2010; Turcotte et al., 2011) and their thermal and hydrological impacts have been documented (Turcotte et al., 2012, 2013a,b). However, so far, no study has focused on the physical structure and unique buildup process of ice dams.

The characterization of ice structures is usually performed by analysing thin sections of ice under crossed polarizers (Michel 1978). Through crystallographic analysis (thin sections), one can define the growth properties of ice samples, as well as their deformational history. A detailed description of the technique can be found in Michel (1978), who separated low gradient freshwater ice into seven classes based on microstructure.

More recently, ice structures have been characterized through the use of non invasive techniques such as Computed Axial Tomography (CAT). In a recent study, Gherboudj et al. (2007) used CAT scans to characterize air inclusions in river ice cores. This technology allows the visualization of the shape and size of air inclusions, and provides a method to quantify ice porosity.

2.3 Sampled sites

The Montmorency River drains 1100 km² of hilly forested terrain north of Quebec City, Canada (Fig. 2.1). Ice dam samples were collected from two different reaches: in the River itself and in the much smaller (watershed of 8 km^2) Lepine Creek. The sampled River reach is 50 m-wide, presents a slope of 1%, and consists of rapids with numerous emergent boulders at low flow. At freezeup, the reach develops successive ice dams (Figs. 2.2 & 2.3), some of which have been observed to buildup to the floodplain level (1.5 m or so). Two ice samples (submerged [S1] and emerged [E1]; Fig. 2.2) were collected from an active (building up, water flowing on the dam crest) ice dam on Jan. 16th 2012.

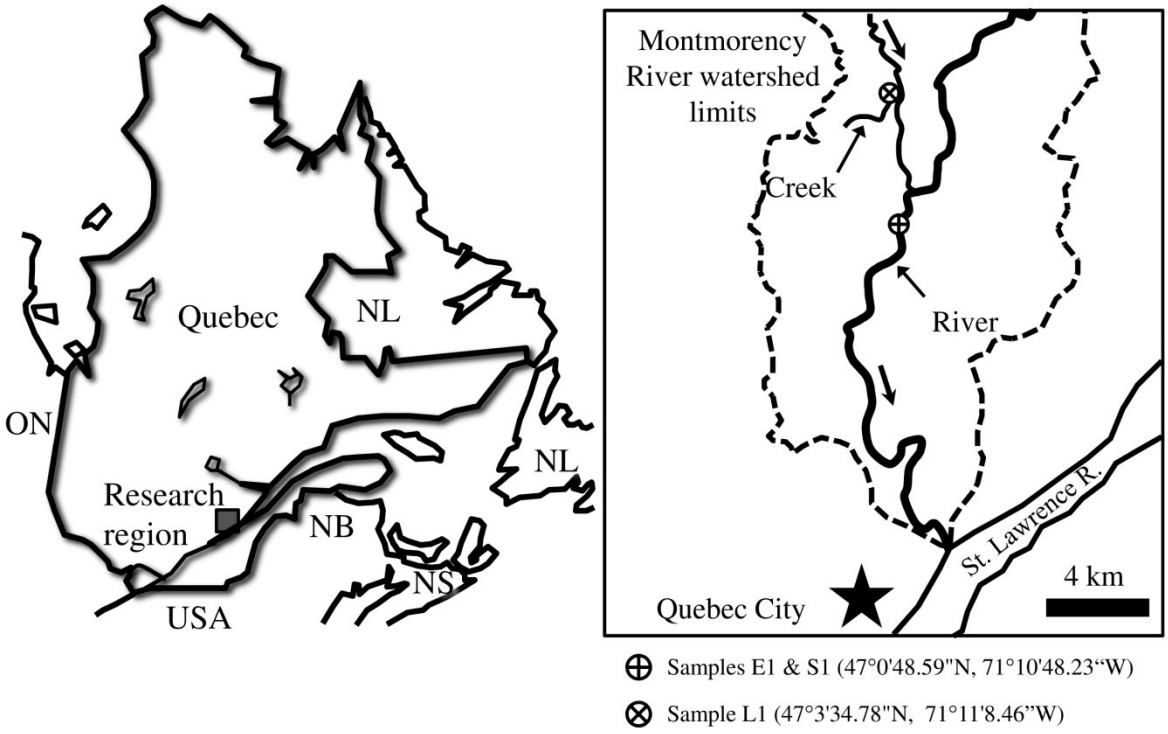

Figure 2.1. Research region and sampling sites, Montmorency River watershed, Quebec, Canada.

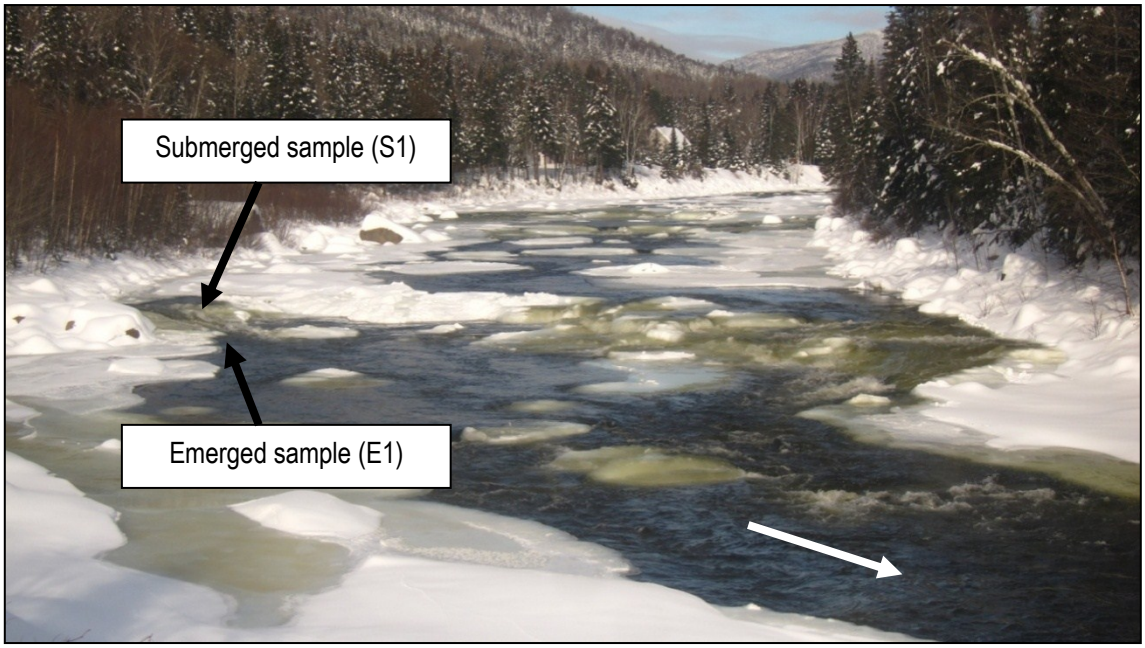

Figure 2.2. Study site, Montmorency River, Quebec, Canada. The channel is 50 m-wide. The white arrow indicates flow direction.

Figure 2.3. Looking across the channel where the emerged ice dam sample (E1) was collected. Note the ice dam extension in the background.

The sampled step-pool Creek reach is 4 m-wide and presents a slope of 2%. At freezeup, ice dams develop on each step. Some dams grow faster, drowning one or few upstream steps. One ice sample (L1; Fig. 2.4) was collected from a breached ice dam on Jan. 23rd 2012.

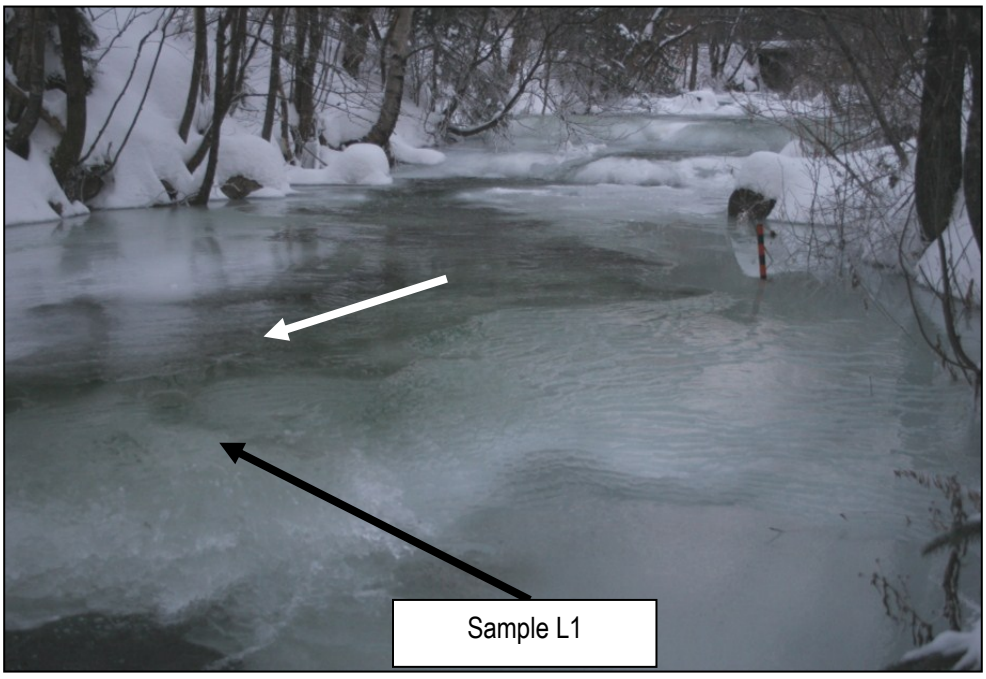

Figure 2.4. Sampled ice dam on Lepine Creek. Note the development of ice dams in the background. The white arrow indicates flow direction and the channel width is about 4 m.

2.4 Hydrological and weather conditions during ice formation

Figure 2.5 presents the measured air temperature, discharge (Obtained from the Quebec Government), water depth, and water temperature data for the Montmorency River during the weeks prior to sampling. The water depth and water temperature data were recorded on an hourly basis using a YSI 6600 probe located 1.3 km upstream of the sampling site. Despite the two short cold spells that occurred between Jan. 1st and Jan. 7th, the water temperature in the River only dropped to 0˚C after Jan. 8th. From that date, the water depth gradually increased while the discharge was decreasing (Fig. 2.5). Photographs taken by a fixed camera confirm that anchor ice and ice dam development began on Jan. 8th to 9th. On Jan. 16th (sampling date), ice dams were still building up, a process that ended few days later.

Figure 2.6 presents the weather (air temperature) and hydrological (discharge, water depth and temperature) conditions at the Creek site during the weeks prior to sampling. The discharge was obtained from an upstream hydrometric station that was not affected by ice (Turcotte et al., 2013b) whereas the water depth and temperature were recorded on an hourly basis using a YSI 6600 probe located about 50 m upstream of the sampled ice dam. The structure of the sampled dam was formed by four distinct buildup events, each one

characterized by a rise and a subsequent drop in the measured water depth and by a water temperature equal to 0°C (Fig. 2.6).

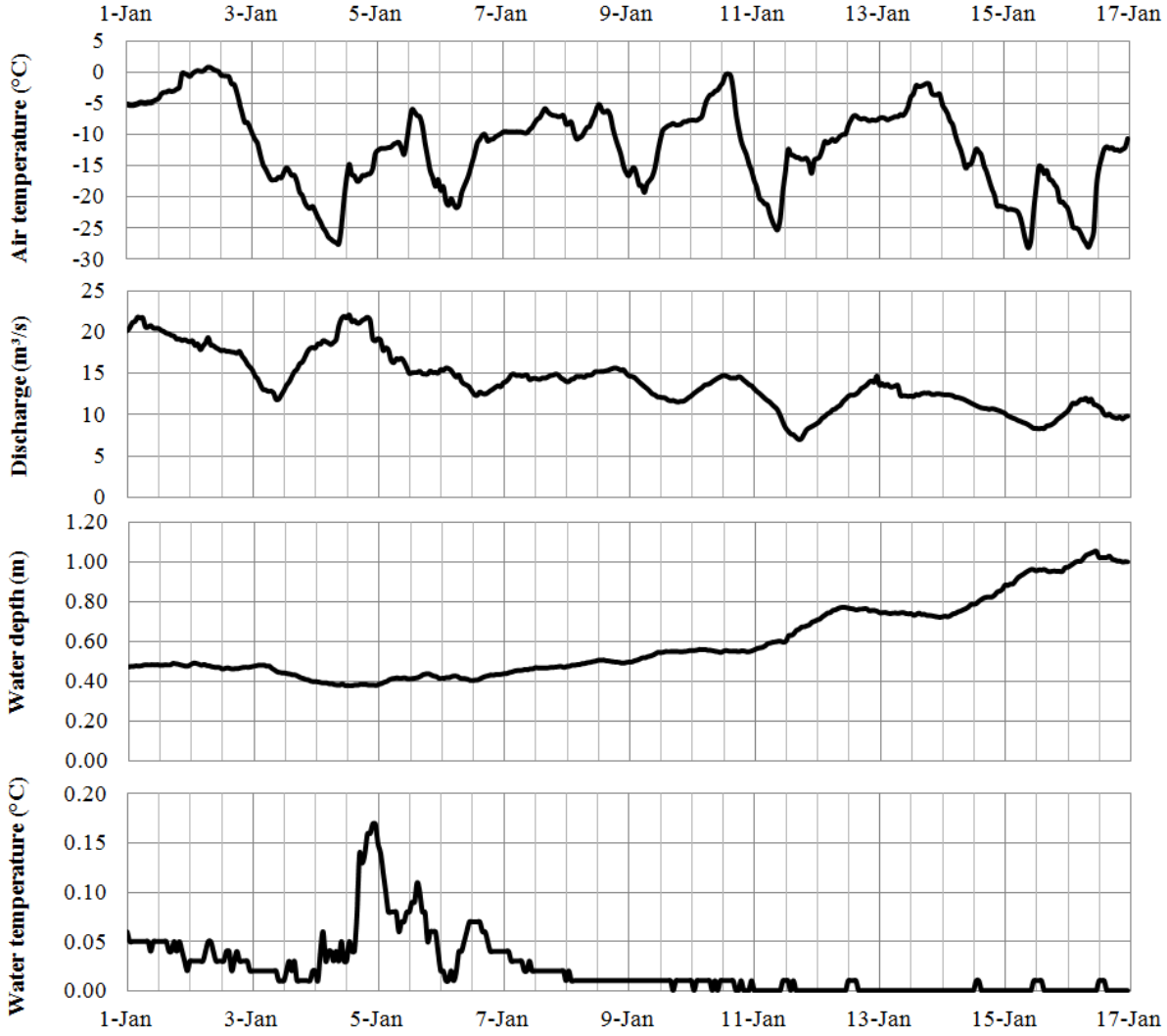

Figure 2.5. Montmorency River data (Jan. 2012): water depth, water temperature and air temperature were recorded 1,3 km upstream of sampled ice dams E1 and S1. The River discharge was obtained from the Provincial Government (CEHQ) hydrometric station located about 20 km downstream.

Figure 2.6. Lepine Creek data (Dec. 2011 - Jan. 2012): air temperature, discharge, water depth and water temperature were recorded 50 m upstream of the sampled ice dam L1.

2.5 Sampling methodology

The two ice samples (E1: 15 x 26 x 27 cm & S1: 22 x 27 x 16 cm) were collected from a well-developed ice dam of the Montmorency River using a pickaxe. The structure of the samples was not altered by the axe strike as its rupture was sudden and fragile. The submerged sample S1 appeared to consist exclusively of anchor ice (Fig. 2.7), while the second sample E1 appeared to be composed of both anchor ice and solid ice. This sample was collected in a low-turbulence zone beside the main flow (Fig. 2.3). Once retrieved (Fig. 2.8), both samples were gravity-drained in order to remove as much interstitial water as possible and stored in sealed plastic bags at -10°C to prevent internal structure alteration.

The ice dam sample from Lepine Creek (L1: 18 x 18 x 29 cm) was collected from the surface part of a breached ice dam. Figure 2.9 clearly shows the impressive height of this ice dam (roughly 1.5 m). This figure also shows that this ice structure was completely dry at the moment of sampling, unlike E1 and S1 samples. Sample L1 was also collected using a pickaxe and stored in a sealed plastic bag at -10°C.

Figure 2.7. The submerged ice dam sample (S1) being collected.

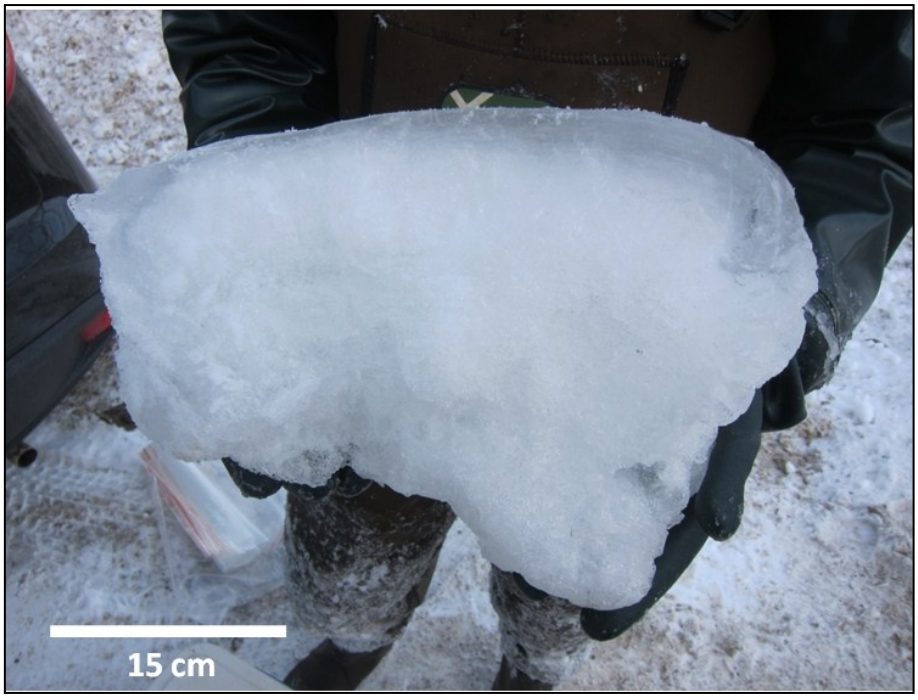

Figure 2.8. Ice dam sample E1 drained with layer of solid ice visible on the upper surface.

Figure 2.9. Sampled ice dam on Lepine Creek. The flow is toward the camera.

2.6 CAT scan analysis

The internal structure of all samples was analyzed using a medical CAT scan (*Siemens SOMATOM Sensation 64*). As the CAT scanning was necessarily conducted at room temperature, the operations were limited to less than 5 minutes for each sample to prevent significant melting. The resulting output for each sample was hundreds of DICOM images, each of which corresponded to one vertical slice (0.6 mm thick) through the sample formed of pixels of 0.55 x 0.55 mm in a 512 x 512 matrix. These images were analysed using *Fiji* free software.

DICOM files consist of 16-bit grayscale images. Brightness is defined by the pixel value, and ranges from -1024 to over 500. The higher the pixel value, the denser is the material. A value of 0 corresponds to pure water. By applying *Fiji*'s selection tools, it is possible to create a histogram and a statistical report (max, min, mean, standard deviation) of the brightness variation within a selected sub-area. Calibration of the pixel values to obtain ice porosity was done by comparing the solid ice value (zero porosity) to that of air (100% porosity). Sub-areas were then analysed and the resulting porosity value was calculated using the following equation:

$$Porosity\,(\%) = \frac{Mean\ pixel\ value - Solid\ ice\ pixel\ value}{Air\ pixel\ value - Solid\ ice\ pixel\ value} x100$$

2.7 Results interpretation

The CAT scan data were used to visualize the inner components of each sampled ice dam and to determine the porosity of specific ice structures within those dams. Since sample E1 and L1 display similar ice structures, they are interpreted first, followed by the sample S1.

2.7.1 Emerged sample (E1)

Figure 2.10 presents a vertical slice of sample E1 showing multiple ice structures of variable porosity values (sub-areas are numbered with increasing porosity values). The entire lower structure (sub-areas 3 & 6) is anchor ice as typically described in the literature. It is composed of acicular crystals up to 10 mm in length (Fig. 2.11), apparently oriented randomly. This supports the possibility that anchor ice can form by the adhesion of frazil ice particles drifting in the water column and intercepted by a porous ice matrix (e.g., Kerr et al., 2002; Qu and Doering, 2007). Figure 2.11 further suggests that some frazil particles (as pointed by arrows) continued to grow in place after being intercepted by the anchor ice mass. Those crystals probably achieved a longer size than others because local, micro hydraulic conditions were favorable to their growth orientation.

The CAT scan data also reveal that the anchor ice portion of sample E1 have an overall porosity of 28-36%. This value lies between the low turbulence (Type I) and high turbulence (Type II) anchor ice types identified by Stickler and Alfredsen (2009), but it represent a fairly low porosity range compared with what has been reported by Parkinson (1984; 71-84%). This range is also dramatically different from the porosity values typically measured from a floating, frazil ice cover, whose porosity value tends to range from 1 to 18% (Gherboudj et al., 2007). This suggests that the anchor ice mass was submerged during the first stage of the ice dam buildup process, which impeded heat loss to the atmosphere and thus the freezing of interstitial water. By comparison, interstitial spaces within floating frazil ice pans exposed to cold air temperatures can freeze as they readily lose heat to the atmosphere.

As expected, the solid ice cap covering the sample (Fig. 2.10, sub-area 1) presents a very low porosity value (0.6%) and essentially consists of pure ice. Sub-area 2 (one of many ball-shaped structures) presents another pure ice structure with a porosity value close to 0%. The ice cap developed by progressive flooding and freezing (icing) and presents the same crystal characteristics (Fig. 2.12) as thermal ice (S2 in Michel, 1978) commonly found within floating ice covers. The solid ice in sub-areas 1 and 2 consists of long, thick crystals oriented perpendicularly to the surface from which they developed. However, unlike typical thermal ice forming downward at the undersurface of an existing floating ice cover, this thermal ice grew upward from the submerged ice dam surface into the water flowing on top. This growth mechanism also applies to the ball-shaped structures as suggested by the horizontal thin section presented in Figure 2.13. The large crystals diameters suggest that thermal growth was indeed the dominant mechanism and their orientation suggests

that they also formed upward in a relatively thin water layer (possibly sprayed water droplets on emerged ice) that allowed full freezing.

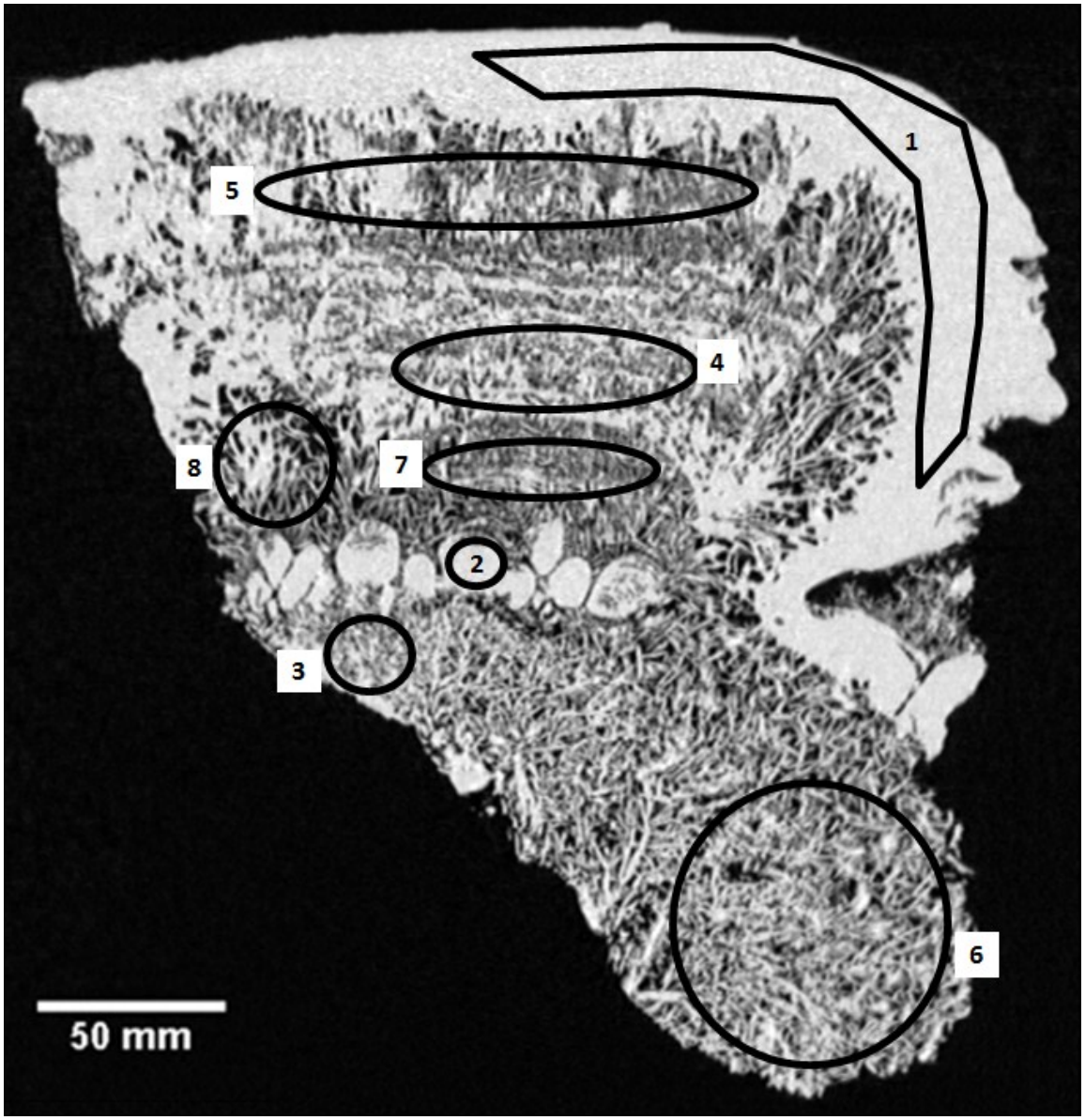

Sub-area	1	2	3	4	5	6	7	8
Porosity value	0.6%	1.5%	28%	28%	34%	36%	43%	48%

Figure 2.10. Inner structure and porosity values of sample E1 – The flow is from left to right the sample is oriented vertically as found in the field.

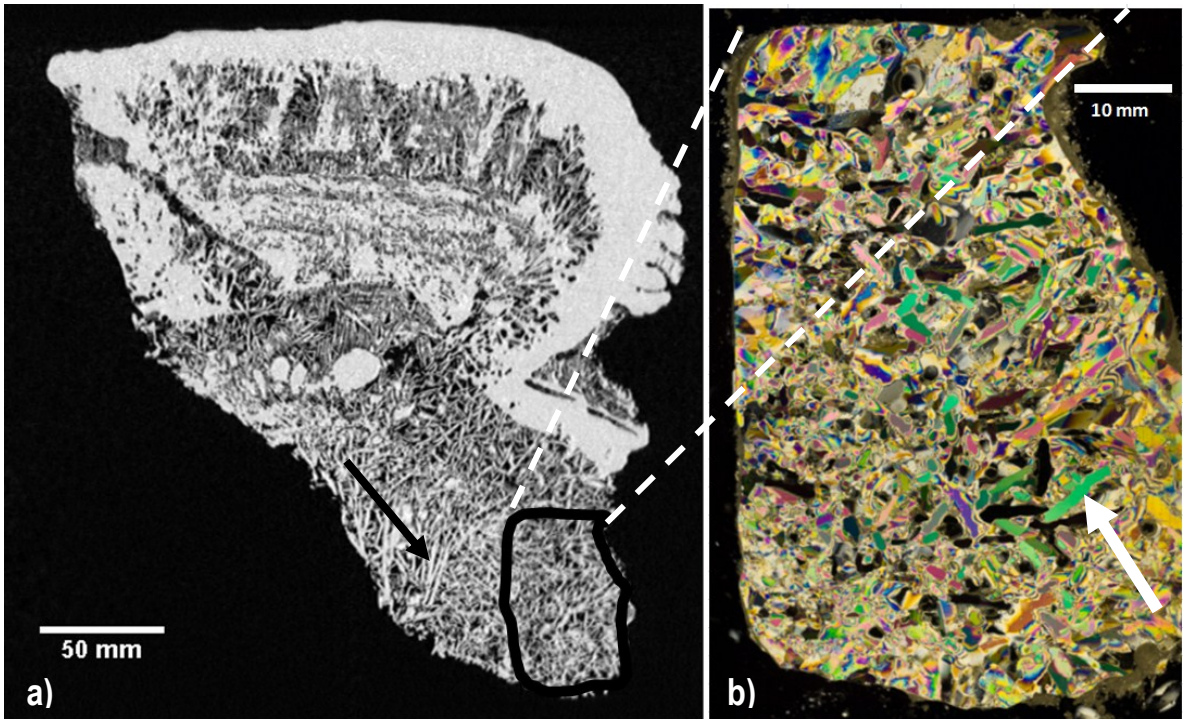

Figure 2.11. CAT scan (a) of sample E1 showing crystal orientations and porosity (grayscale) and (b) thin section using X polarizers (identified in 11a) showing the crystallography of an anchor ice sub-area.

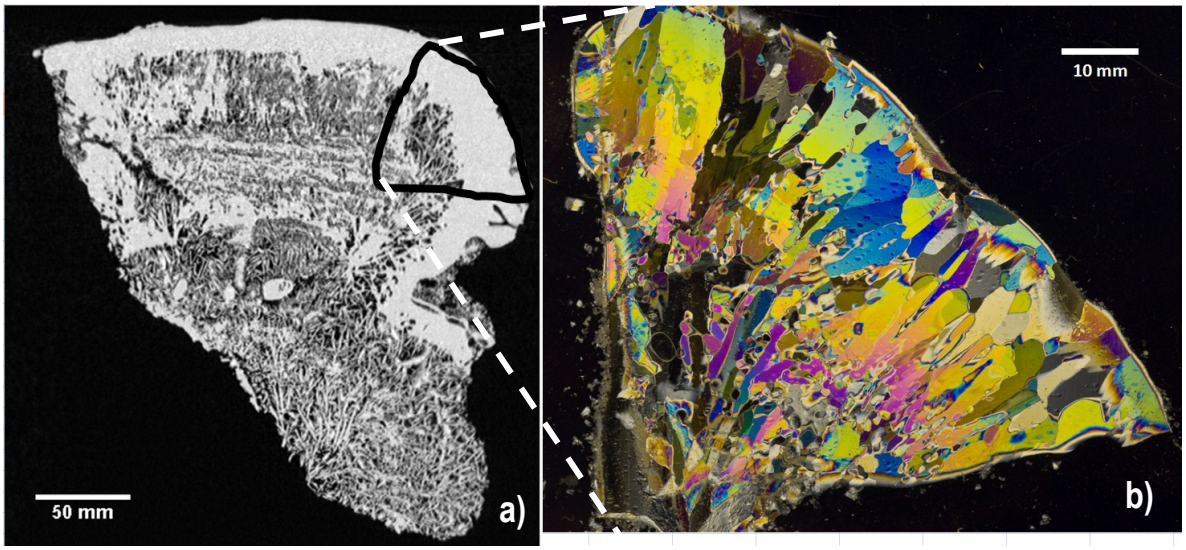

Figure 2.12. CAT scan (a) of sample E1 showing crystal orientations and density (gray scale) and (b) thin section using X polarizers (identified in 12a) showing the crystallography of the ice cap and of the anchor ice immediately below.

At a later development stage, the ball-shaped ice structures probably became flooded. This would explain why a majority of ice crystals growing in the water preferentially oriented themselves perpendicularly to the surface of each ball. Since the favorable growth orientation of ice crystals is parallel to the heat flow (Michel, 1978), in this case upward toward the water surface, crystals that were initially favorably oriented progressively

consumed the unfavorably oriented ones. Thus, the preferential orientation became perpendicular to the water surface as the ice dam developed over the ball-shaped solid ice (Fig. 2.10).

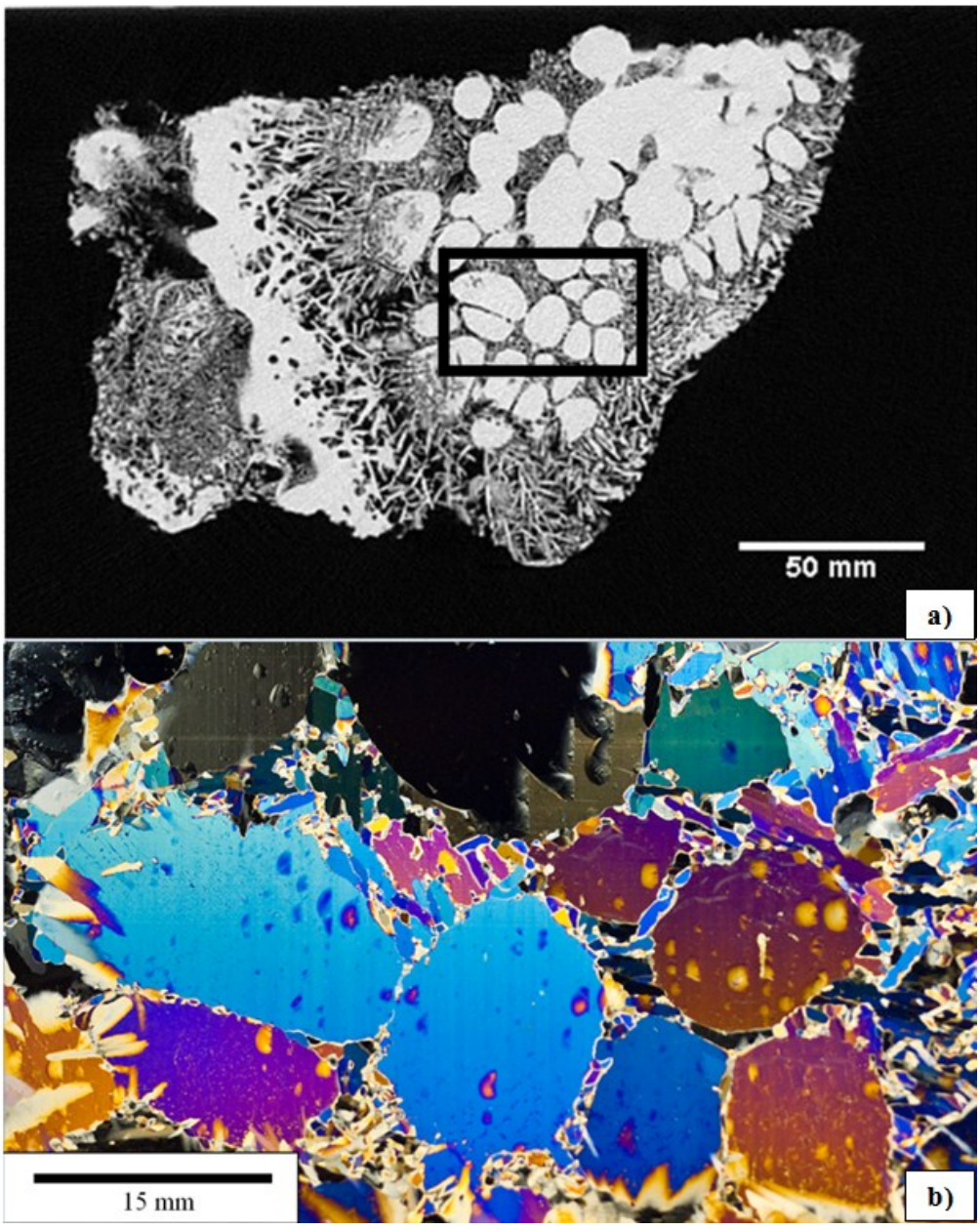

Figure 2.13. (a) Horizontal CAT scan slice of sample E1 showing the ball-shaped solid ice and general porosity (grayscale) and (b) thin section using X polarizers (identified in 13a) showing the crystallography of the ball-shaped solid ice separated by relatively porous anchor ice.

The entire sample portion located between the solid ice balls and the solid ice cap is composed of layers with different porosities (sub-areas 4, 5, 7 & 8). There are three possible conditions or combinations of conditions that could explain these ice structures: (1) this layering could develop as a result of variations in ice growth: rapid crystal growth resulted in a greater amount of air entrainment, while slower crystal growth allowed the air

to escape while the crystals were developing. (2) The observed layering can also be explained by the water depth flowing over the ice dam during its development. A shallow flow results in a denser ice structure (icing) while a deeper flow lead to the development of a more porous structure corresponding to typical anchor ice. (3) Since these crystals present preferred orientations and relatively high porosity values (28-48%), it is believed that they nucleated on and grew upward from deposited layers of fine frazil ice. Snow entrained in the water and snow falling directly on the ice dam crest (the site received about 15 cm of snow between Jan. 12th and Jan. 14th) might also have provided nuclei for the formation of these ice layers.

It is important to note that the ice dam sample E1 does not represent the entire vertical dam section. In fact, the lower part of the dam could not be collected due to the strong adhesion to the bed and to the hazardous conditions of the site. This also applies to sample S1 presented in section 2.7.3.

2.7.2 Lepine Creek breached ice dam (L1)

Sample L1 presents multiple inner structures (Fig. 2.14) that are similar to those found in sample E1. First of all, sub-areas 1, 2 & 3 show porosity values close to 0% and therefore represent pure ice formed by the same icing process as described above. Moreover, sub-areas 4 and 5 present ice structures with porosity values comparable to that of anchor ice as presented in Fig. 2.10. The random orientation of the ice particles in those sub areas supports the possibility of frazil ice interception. On the other hand, the largest crystals stress the possibility of subsequent *in situ* growth in a deep, cold water environment.

The lower part of the sample (sub-areas 7 & 8) is composed of small round-shaped particles that are not observed in sample E1. This structure presents a much higher porosity (59-70%) than the anchor ice of sub-areas 4, 5 & 6 (31-45%) and the anchor ice of sample E1 (28-36%; Fig. 2.10, sub-areas 3 & 6). The thin section of this part of the sample (Fig. 2.15) suggests that it is composed of frozen snowflakes. The bottommost part (sub-area 8) presents a higher porosity value than the part located immediately underneath (sub-area 7) a thin, solid ice layer. An analysis of the time-lapse photographs (Fig. 2.16) confirmed that the lower part of sample L1 was formed after a snowfall that took place between two ice dam buildup phases. Two freezeup processes might explain the variable porosity of this ice structure: (1) the flooding of the snow surface (as the water level began to increase) resulted in the fast development of a thin solid ice layer before the entire snow column (sub-areas 7 and 8) could get drowned. The porous ice in sub-area 8 would therefore be considered as dry-frozen snow whereas the development of normal snow ice implies slushing before complete freezing. (2) The entire snow column was indeed completely drowned as the water level increased but the air temperature was not cold enough to freeze the entire slush depth (sub-areas 7 and 8). As a result, some water remained unfrozen as the ice dam kept building up and this water was drained from the ice dam core when it got breached under milder air temperatures. Additional ice dam samples analysis combined with

complementary data should contribute in identifying the most probable freezeup process for this type of ice structure.

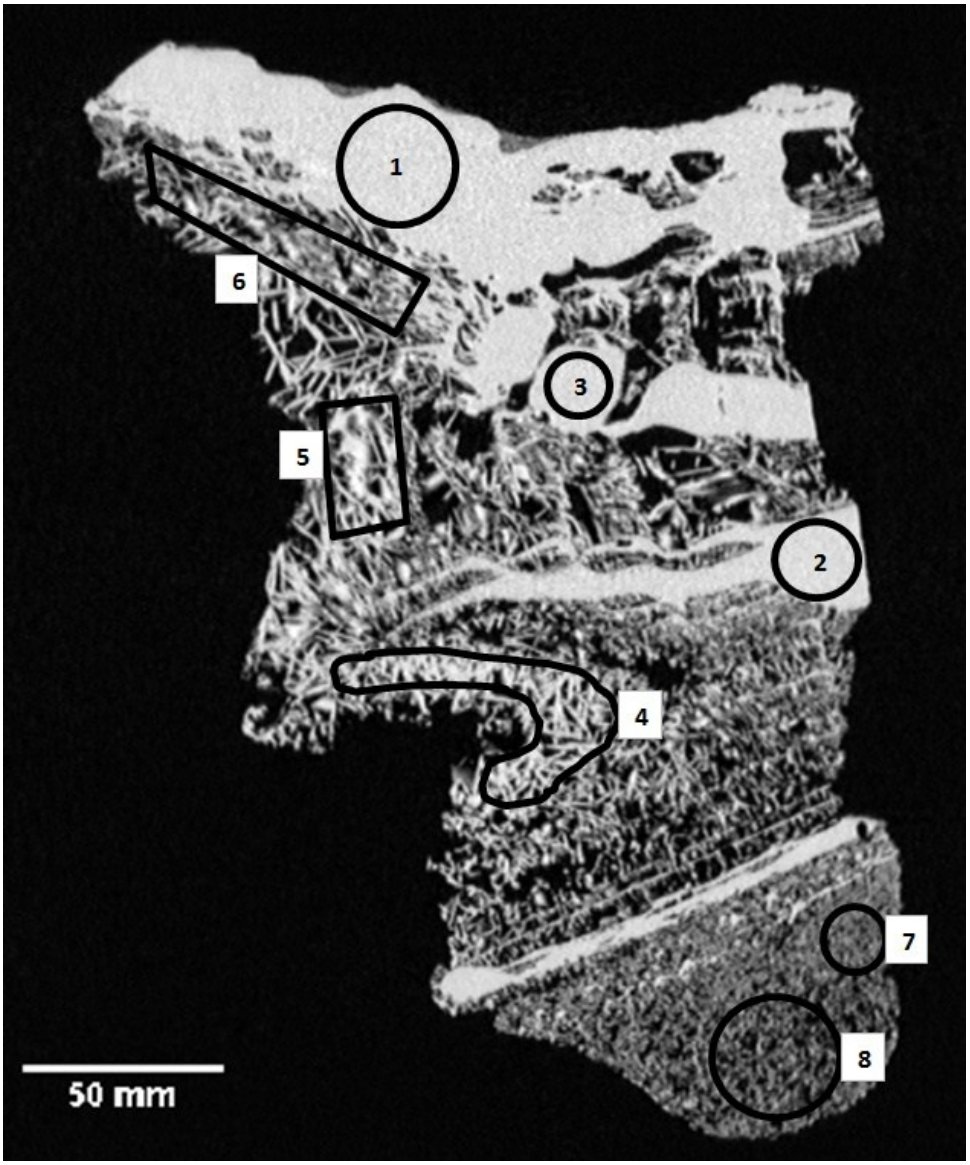

Sub-area	1	2	3	4	5	6	7	8
Porosity value	0%	1%	1%	31%	35%	45%	59%	70%

Figure 2.14. Inner structure and porosity values of sample L1 –flow is from left to right. The sample is tilted about 30° to the left from its vertical position.

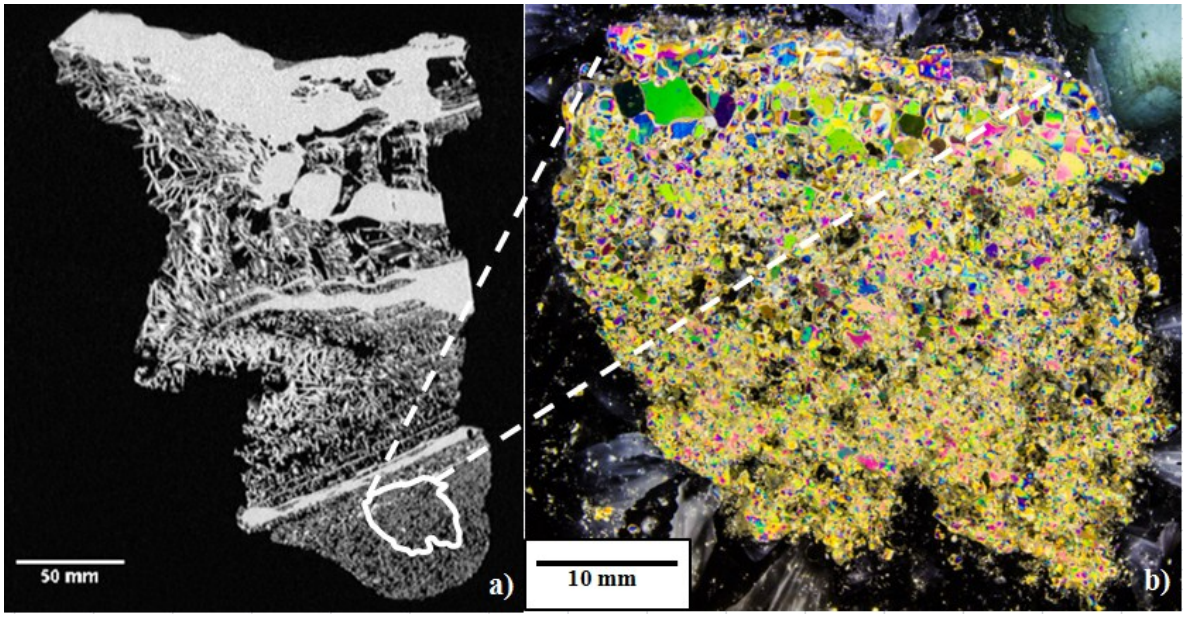

Figure 2.15. (a) Vertival CAT scan slice of sample L1 showing snow ice (bottom of the sample) and general porosity (grayscale) and (b) thin section using X polarizers (identified in 15a) showing the crystallography of the snow ice.

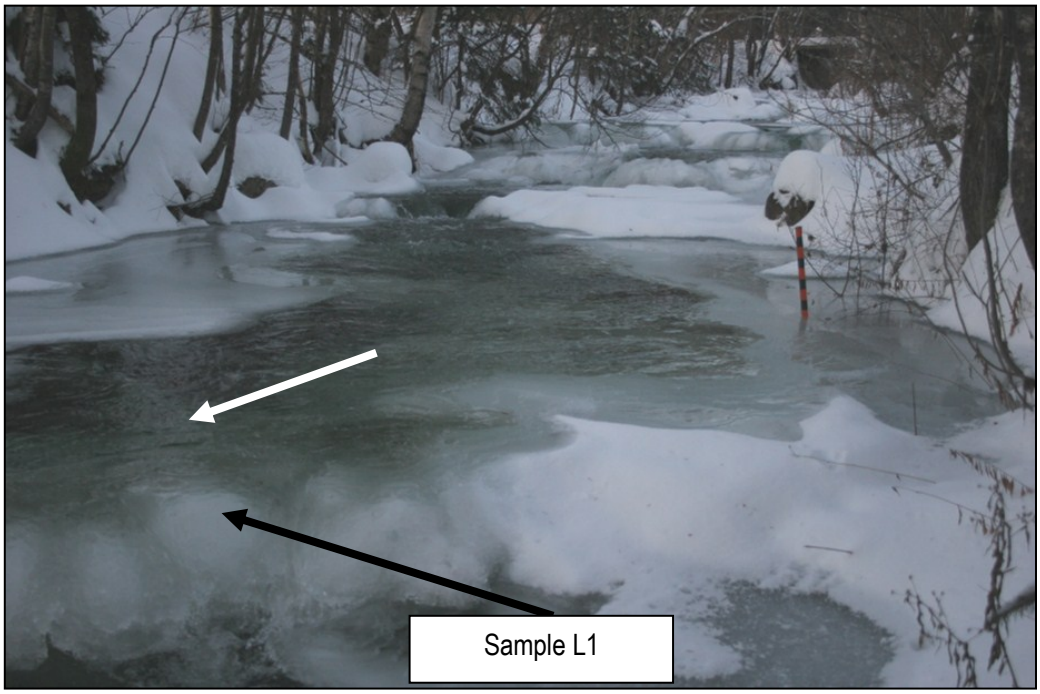

Figure 2.16. Flooded snow accumulation on the sampled ice dam's crest (L1) on Dec. 20th 2012. The arrow is indicates the flow direction.

2.7.3 Submerged sample (S1)

Figure 2.17 presents the internal structure and porosity values of different selected sub-areas found in sample S1. Similarly to samples E1 and L1, sample S1 is composed of ice structures with porosity values close to that

of pure ice (sub-areas 1, 2 & 3). It is likely that these layers formed by progressive flooding and freezing of thin water layers (icing process) during a freezeup phase characterized by the partial emergence of this ice dam portion. Nearer the surface of the sample, the pure ice (sub-area 2; slow flooding rate allowing all the water to freeze) give way to repeated horizontal solid ice layers separated by thin, porous anchor ice layers (sub-area 6; moderate flooding rate). Figure 2.18 shows a thin section of this type of alternating layers. The layers then evolve upward into long (25 mm in length), thick crystals with no horizontal stratification (Fig. 2.17, sub-area 7; *in situ* crystal growth in a largely submerged, possibly supercooled environment). The ice crystal growth rate in sub-area 7 was therefore slower than the flooding rate (controlled by downstream ice development).

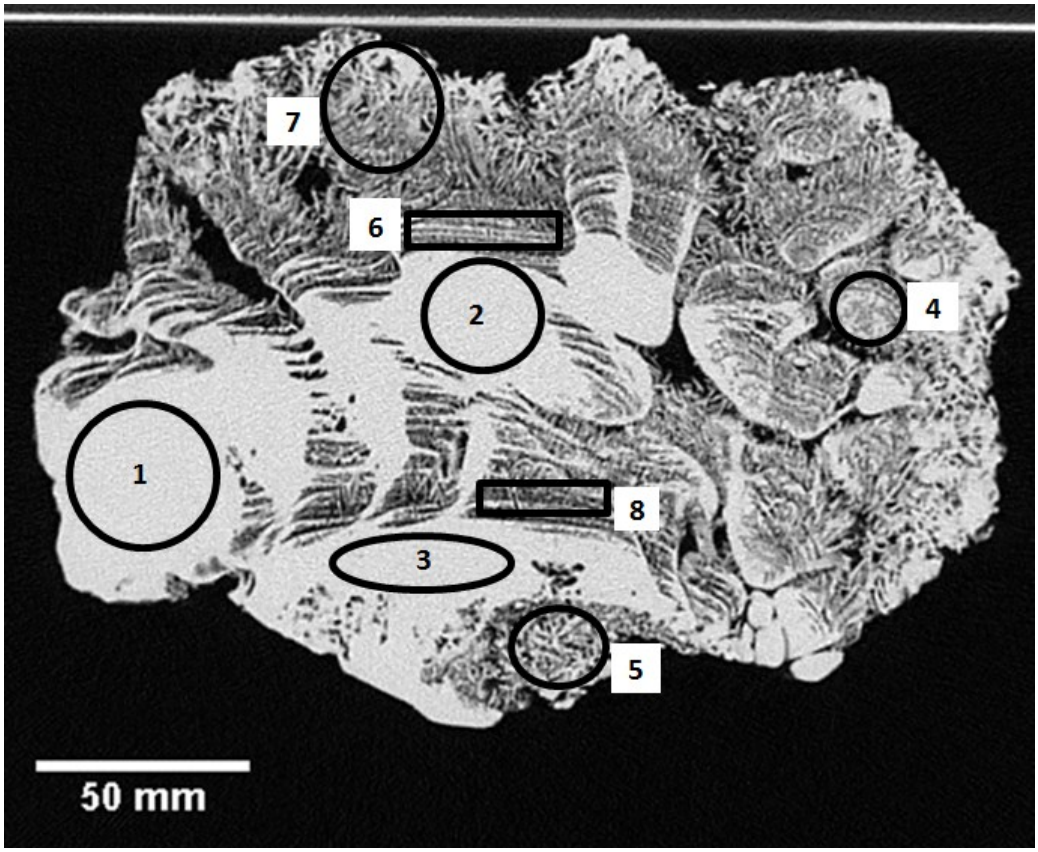

Sub-area	1	2	3	4	5	6	7	8
Porosity value	0.3%	0.6%	1.1%	23%	35%	37%	37%	47%

Figure 2.17. Inner structure and porosity values of submerged sample S1. Cut made through the sample perpendicularly to the flow direction. The sample is oriented vertically as found in the field.

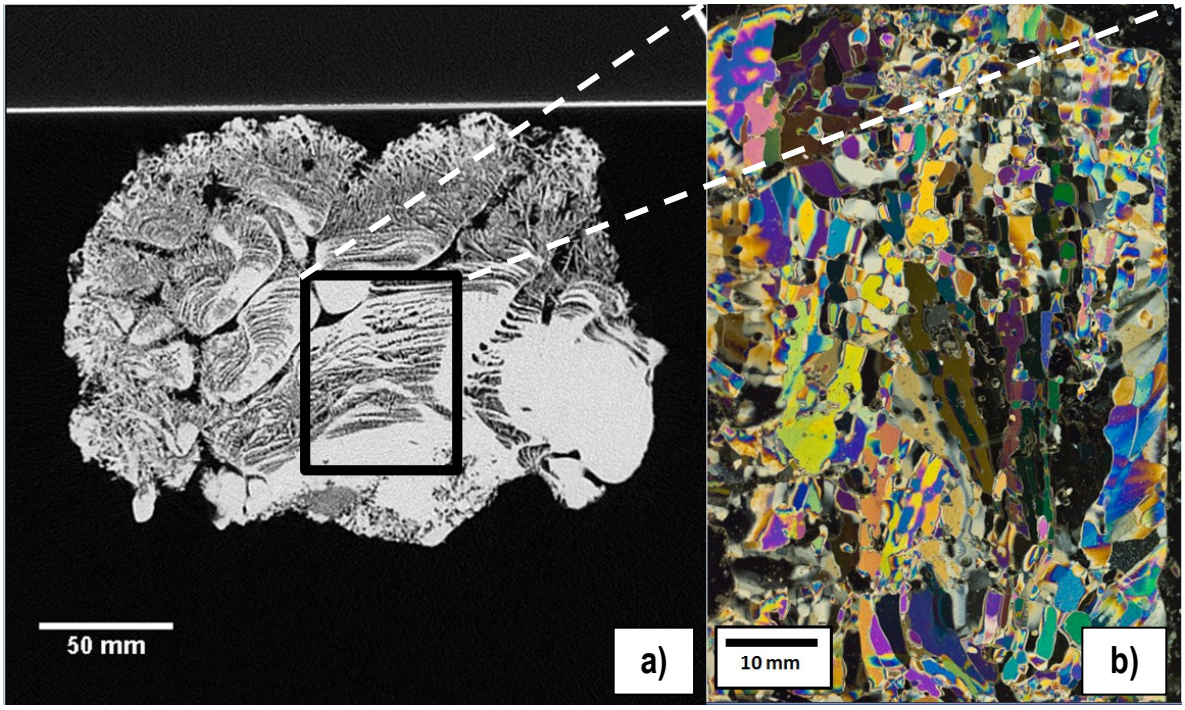

Figure 2.18. a) CAT scan of sample S1 showing crystal orientation and density (grayscale) and (b) thin section using X polarizers (identified in 18a) showing the crystallography of alternating solid-anchor ice layers.

2.8 Discussion

The combination of traditional thin section techniques and CAT scan analyses has proven to be a powerful tool to reveal the inner structure of ice dam samples. It allowed determining the porosity of ice dams, and provided detailed information on both crystal size distribution and orientation as well as on the different structures that can be found within ice dams. Interestingly, no typical ice dam profile was found throughout this analysis. This suggests that the inner composition of ice dams is most likely defined by local hydraulic and environmental conditions. As a consequence, two ice dams that develop on consecutive steps can display very different inner structures. Sixteen additional samples were retrieved during winter 2012-2013. Some, collected only a few meters apart showed important ice structure variations.

The Montmorency River and Lepine Creek ice dam samples consisted of both anchor ice and solid ice (icing). The porosity of the anchor ice structures varied between 28% and 45%. As a result, it is believed that, in the absence of preferential water conduits within the ice dam core and if buildup has not been interrupted by melting periods, only a small ratio of the channel discharge could flow through ice dams' core. This would further explain the constant flooding and freezing as well as the upward development of ice dams under cold air temperatures.

Results presented here suggest that classic anchor ice structures found within ice dams initially form by the deposition and interception of frazil ice particles. This is based on the fact that anchor ice sub-areas displayed nearly identical crystal sizes and shapes everywhere in the samples, with no initial preferential orientation. Afterward, favorably oriented crystals can grow to achieve impressive sizes. In turn, the solid ice structures were produced (1) when thin water layers were overtopping the dam surface and freezing afterward and (2) when water was sprayed on existing, emerged ice accumulations. The porosity of these structures was typically between 0% and 1.5% (effectively pure ice).

Ice dam development is a very dynamic freezeup process which takes place in steep channels. The buildup rates, known to range from 0.5 to 3.0 cm/hr (Turcotte et al., 2013 a), depends primarily on weather conditions and a feedback loop exists between growth rates and varying water levels (water storage reducing the discharge and water level). If the water level rises rapidly, some ice dam sections become submerged. In turn, slowly rising, stable, or ephemerally dropping water levels can lead to the emergence of anchor ice accumulations and to the development of denser ice structures. These ice structures will likely contribute to increase the strength of ice dams. This suggests that an ice dam that forms faster during one intense, cold spells could be more fragile than an ice dam that forms during multiple, successive cold spells alternating with partial melting periods. Further research on the topic is underway.

References

Bisaillon, J-F., Bergeron, N.E. 2009. Modeling anchor ice presence-absence in gravel bed rivers. Cold Regions Science and Technology, 55, p. 195-201.

Clark, S., Doering, J.C., 2004. A laboratory study of frazil ice size distributions. Proceedings of the 17th International IAHR Ice Symposium, Saint Petersburg, Russia, 291-297.

Clark, S., Doering, J.C., 2006. Effect of turbulence intensity on frazil formation. Proceedings of the 18th International IAHR Ice Symposium, 267-275.

Gherboudj, I., Bernier, M., Hicks, F., & Leconte, R. 2007. Physical characterization of air inclusions in river ice. Cold Regions Science and Technology, 49(3), p. 179–194.

Hirayama K, Terada K, Sato M, Hirayama K, Sasamoto M, Yamazaki M. 1997. Field measurements of anchor ice and frazil ice. In: Proceedings of the 9th CGU-HS CRIPE Workshop on the Hydraulics of Ice Covered Rivers, Fredericton, NB, Canada.

Kempema, E. W., & Ettema, R. (2011). Anchor ice rafting: observations from the Laramie River, River research and applications, Volume 27, Issue 9, p. 1126-1135

Kerr DJ, Shen HT, Daly SF. 2002. Evolution and hydraulics of anchor ice on gravel bed. Cold Reg. Sci. Technol. 35: 101–114.

Michel, B., 1978. Ice Mechanics, Les Presses de l'Université Laval, Québec.

Parkinson FE. 1984. Anchor ice effects on water levels in Lake St. Louis, St-Lawrence River at Montreal. In: Proceedings of the 3rd CGU-HS CRIPE Workshop on the Hydraulics of River ice, Fredericton, NB, Canada.

Qu, Y.X., Doering, J., 2007. Laboratory study of anchor ice evolution around rocks and on gravel beds. Canadian Journal of Civil Engineering 34, 46–55.

Stickler M, Alfredsen KT. 2009. Anchor ice formation in streams: a field study. Hydrol. Process. 23: 2307–2315. DOI: 10.1002/hyp.7349.

Stickler M, Alfredsen KT, Linnansaari T, Fjeldstad H-P. 2010. The influence of dynamic ice formation on hydraulic heterogeneity in steep streams. River Res. Applic. 26: 1187–1197. DOI: 10.1002/rra.1331.

Tesaker E. 1994. Ice formation in steep rivers. In: Proceedings of the 12th International IAHR Ice Symposium.

Tesaker E. 1996. Interaction between ice and water flow in rapids. In: Proceedings of the 13th International IAHR Ice Symposium.

Terada K, Hirayama K, Sasamoto M. 1998. Field measurement of anchor and frazil ice. In: Proceedings of 14th International IAHR Ice Symposium.

Turcotte B, Morse B. 2011. Ice processes in a steep river basin. Cold Reg. Sci. Technol. 67: 146-156. DOI:10.1016/j.coldregions.2011.04.002.

Turcotte B, Morse B, Anctil F. 2011. Steep channels freezeup processes. Proceedings of the 16th CGU-HS CRIPE Workshop on the Hydraulics of Ice Covered Rivers, Winnipeg, MB, Canada.

Turcotte, B., Morse, B., Anctil, F., 2012. Cryologic continuum of a steep watershed. Hydrol. Process. In press.

Turcotte, B., Morse, B., Dubé, M., Anctil, F., 2013a. Quantifying steep channel freezeup processes, Cold Regions Science and Technology, in press.

Turcotte, B., Morse, B., Anctil, F., 2013b. The hydro-cryologic continuum of a steep watershed at freezeup. Journal of hydrology, under review.

Yamazaki, M., Hirayama, K., Sakai, S., Sasmoto, M., Kiyohara, M., Takiguichi, H., 1996. Formation of frazil and anchor ice. Proceedings of the IAHRIce Symposium, pp. 488–496.

3. Inner structure of anchor ice and ice dams in steep channels

Mathieu Dubé[1*], Benoit Turcotte[2], Brian Morse[3]
[1,2,3]Université Laval, 1065, av. de la Médecine, Québec City, QC/Can, G1V 0A6

[1]mathieu.dube.4@ulaval.ca; [2]benoit.turcotte.1@ulaval.ca; [3]brian.morse@gci.ulaval.ca

Résumé

La formation dynamique de la glace, regroupant la glace de fond et des barrages de glace, est le processus dominant dans les cours d'eau à forte pente (> 0.3%) durant la période hivernale. Elle a pour effet de contrôler les niveaux d'eau, la résistance à l'écoulement, la bathymétrie, le débit, la qualité de l'eau et les habitats de poisson. Des modèles empiriques de ces processus sont disponibles mais dans l'optique de développer des modèles plus physiques, il est nécessaire d'approfondir les connaissances sur la nature de la glace retrouvée dans ces cours d'eau. Cet article présente des données originales recueillies sur deux chenaux du bassin versant de la rivière Montmorency où le développement des barrages de glace est connu pour son intensité. Les différentes mesures prises durant l'hiver 2012-2013 regroupent des photographies à intervalle, des photographies sous-marines, l'évolution du niveau d'eau ainsi que les températures de l'eau et de l'air. Des échantillons de glace de fond et de barrage de glace on été analysés à l'aide de la technologie *CAT scan* et de l'analyse par sections minces. Cette étude vise à comprendre les processus de développement de la glace de fond et des barrages de glace en s'attardant aux types et à la taille de cristaux qui les composent, à leurs mécanismes de croissance, à leur orientation et à leur porosité.

Deux principaux types de cristaux ont été observés : cristaux de glace colonnaire et cristaux de frasil-fixé. De larges cristaux de glace colonnaire ayant crû vers le haut, de façon perpendiculaire à la surface de l'écoulement ont seulement été observés dans les échantillons de barrages de glace. Les cristaux de frasil-fixé proviennent de la déposition ou l'interception de particules de frasil dérivant dans la colonne d'eau qui se sont fixé au lit et aux accumulations de glace existantes. Les résultats suggèrent que la croissance en place (*in-situ*) des cristaux de frasil-fixé est le processus de formation dominant pour la glace de fond et les barrages de glace. Les accumulations de frasil-fixé consistent en une masse de cristaux en forme de plaques interconnectés ayant une orientation préférentielle perpendiculaire au lit et à la surface de l'eau. Ces accumulations montrent une porosité variable ayant une valeur moyenne de 41%. Lorsqu'analysés en utilisant les images obtenues avec le *CAT scan*, les cristaux en plaques interconnectés apparaissent comme une structure dendritique en forme d'arbre. La taille moyenne des segments de cristaux et la taille maximale des cristaux de frasil-fixés sont significativement plus importantes pour les échantillons de barrages de glace que pour les échantillons de glace de fond.

Abstract

Dynamic ice growth (composed primarily of anchor ice and ice dams) is the dominant process in steep (slope > 0.3%) channels during winter. The ice growth (in all its manifestations) regulates water levels, flow resistance, bathymetry, flow rate, water quality and fish habitat. Empirical models of the processes are available but in order to develop more physically-based models, more knowledge about the nature of ice in these channels is required. This paper presents original data from two channels of the Montmorency River watershed known for their intense anchor ice and ice dam development activity. The data include time-lapse photographs, underwater photographs, water level records, and water and air temperatures collected during winter 2012-2013. Moreover, anchor ice and ice dam samples were analysed with thin sections and using computed axial tomography (CAT) scan technology. This study aims at understanding the development processes of both anchor ice accumulations and ice dams by investigating their crystal types and sizes, their growth mechanisms, patterns, and orientation, and their porosity.

Two main types of ice crystals were observed: columnar ice crystals and fixed-frazil ice crystals. Relatively large columnar ice crystals grew upwards (away from the bed) perpendicularly to the local flow surface and were only observed in ice dam samples. Fixed-frazil crystals originated from the deposition and/or interception of drifting frazil particles that became “fixed” to the bed and to existing ice accumulations. The data suggest that *in-situ* growth of fixed-frazil ice crystals was the dominant process (accounted for the most ice development) for both anchor ice and ice dams. Fixed-frazil ice consists of a bonded mass of interlocking plate shaped crystals demonstrating a preference for to be perpendicular to the bed and water surfaces. The mass displays some variability in porosity (mean value 41%). When analysed using CAT scan slices, the interlocking plates appear as a tree-like or dendritic structure. The average size of resulting crystal segments and the maximum size of individual whole crystals within fixed-frazil ice structures were significantly more important for ice dam samples than for anchor ice samples.

3.1 Introduction

Anchor ice accumulations and ice dams are fascinating structures that form across steep channels during the freezeup period (Fig. 3.1). Anchor ice forms below the water surface on the channel bed material and it represents the most documented steep (slope > 0.3%) channel ice type because of its important impact on flow conditions. It is indeed an ice process that is less dominant from a hydraulic point of view in low-gradient channels compared to the most documented floating ice cover. Anchor ice has been studied in the field (Hirayama et al., 1997; Kempema and Ettema, 2011; Parkinson, 1984; Terada et al., 1998; Yamakazi et al., 1996) and in the lab (Clark and Doering 2004; 2006; Kerr et al., 2002; Qu and Doering, 2007). Northern Europe scientists such as Stickler and Alfredsen (2009) and Tesaker (1994) have presented anchor ice as a submerged ice type forming on the channel bed that generates backwater effects. Many published studies either reported anchor ice release at sunrise or that anchor ice accumulations were ephemeral (e.g. Parkinson, 1984). More recently, complex, stable, anchored ice features such as ice weirs and ice dams have been described in detail (Stickler et al., 2010; Tesaker, 1996; Turcotte et al., 2011) and their thermal and hydrological impacts were documented (Turcotte et al., 2012, 2013, 2014). Submerged anchor ice weirs form at natural steps made of stone clusters or between dominant boulders where anchor ice accumulations can link across the channel which can in turn substantially increase the water level upstream. As weirs continue to develop at variable spatial rates (Dubé et al. to be submitted, Turcotte et al. 2013), parts of them can eventually emerge, thereby forming 'ice dams'. They cause significant backwater effects that can even extend to the floodplain.

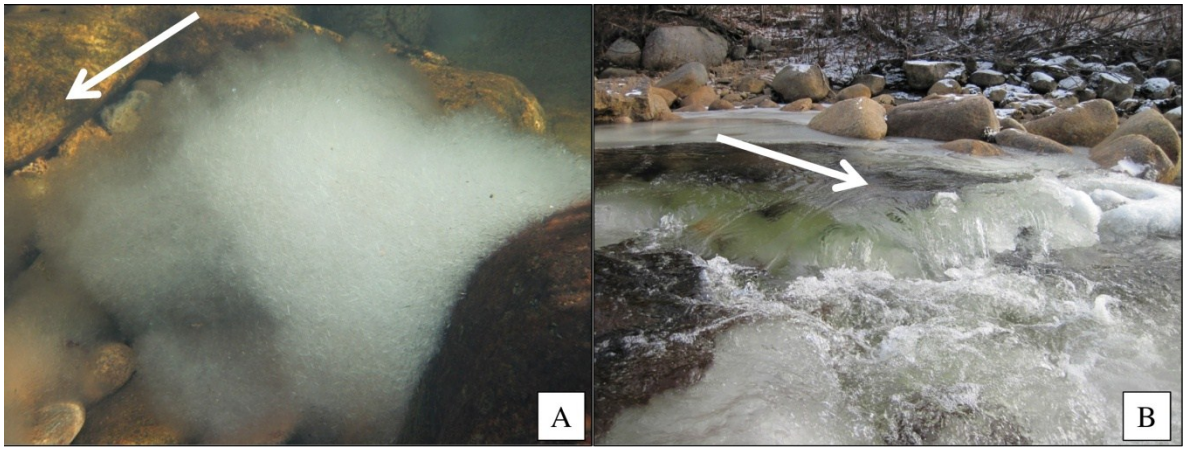

Figure 3.1. (A) Underwater photograph of an anchor ice accumulation in a pool section of the Stream and (B) photograph of a partially emergent ice dam in the Stream. White arrows indicate the flow direction.

Any hydraulic structure (dam, bridge, culvert, water intake, bank protection, habitat creation, etc.) built in a winter-affected steep stream must account for dynamic ice growth. Previous studies have shown that anchor ice and ice dams (especially during the freezeup period) may produce the highest water levels, the lowest flow

rates (because of increased hydraulic storage caused by ice), a completely changed river morphology (as rapid sections can become step-pool sections), a change in water current patterns (slower water at some places, concentrated jets at others), a completely different global resistance to flow and a regulated change in water temperature and water conductivity. The impact on local fish (e.g. Bradford and Heinonen, 2008) and flora habitat is self evident as the ice can cover the bed, flood the banks, and insulate water from the cold. As such, the study and modelling of those ice processes are of interest as steep stream are very abundant in nature. Generally, models, based on heat budgets and field observations have been empirical in nature. However, the recent observations and work are beginning to document the very structure of those ice features. This will open the doors to a more physically-based understanding and modelling of the processes and it is the intention of this paper to contribute to this initiative by presenting some new field data and ice structure analyses.

The first objective of this study is to describe the inner structure and crystal arrangements in anchor ice and ice dams as well as to identify their respective dominant growth mechanism. To do so, ice samples were collected during winter 2012-2013 from two channels known for their anchor ice and ice dam development (e.g., Turcotte et al., 2013). Computed axial tomography (CAT) scan analyses were performed on all samples while traditional thin section analyses were performed on selected ice structures of interest. The second objective of the study is to identify structural characteristics specific to anchor ice and ice dams. The results presented throughout this paper improve our understanding of 1) crystal types and sizes found it anchor ice and ice dams, 2) their growth mechanisms, patterns, and orientation, and 3) their porosity. One should note that the term “size” is used here to describe the crystal dimension in the a-axis (Michel, 1978).

The link between hydraulic conditions (e.g., Froude and Reynolds numbers) and anchor ice and ice dams development has received some attention in the literature. This paper adopts a different approach to explain the development of steep channel ice features by presenting and analysing their complex crystallographic arrangements. Building on the work presented by Kempema and Ettema (2009) and Dubé et al. (2013), this paper attempts to establish a linkage between crystal characteristics and their development mechanisms.

Kempema and Ettema (2009) investigated the composition of anchor ice accumulations and suggested that variations in anchor ice crystals morphology are primarily caused by their *in situ* growth. This process would directly account for the internal strength of the anchor ice mass and the bonding between anchor ice and the substrate. Most of their 72 anchor ice samples did not reveal the presence of disc-shaped frazil crystals as it is often reported to be found in the water column (e.g. Tsang, 1982). Moreover Kempema and Ettema did not find any link between hydraulic conditions and ice crystals morphology. In fact, crystals shape and size could vary significantly within the same sample.

The characterization of ice structures is usually performed by analyzing thin sections of ice under crossed polarizers. Through these crystallographic analyses, one can determine the growth properties of ice samples as well as their deformational history. A detailed description of the thin-section technique can be found in Michel (1978), who separated low gradient freshwater ice into seven classes based on microstructure interpretation. More recently, ice structures have been characterized through the use of non invasive techniques such as Computed Axial Tomography (CAT). In a recent study, Gherboudj et al. (2007) used CAT scans to characterize air inclusions in floating river ice covers. The technology allows for the visualization of the shape and size of air inclusions, and provides a method to quantify ice porosity. Dubé et al. (2013) applied CAT and thin section techniques to non-floating steep channel ice samples collected in 2011-2012. The porosities of different ice structures were quantified and ice crystal structures were presented.

3.2 Sampled sites, sample categories and methods

3.2.1 Sampled sites

Anchor ice and ice dam samples were collected during winter 2012-2013 in the 1,100 km^2 Montmorency River watershed located in a hilly-forested area north of Quebec City, Canada (Fig. 3.2). Samples were collected (location shown in Fig. 3.3) from two different instrumented channels: the *De l'Île* Stream (watershed of 80 km²) and the smaller *Lépine* Creek (watershed of 8 km²). Figure 3.3 shows the location of all the instruments used in the study including water pressure and temperature probes, air pressure and temperature probes, and fixed automated cameras oriented in the upstream direction. Throughout this paper, these two channels will be referred to as the *Stream* and the *Creek*.

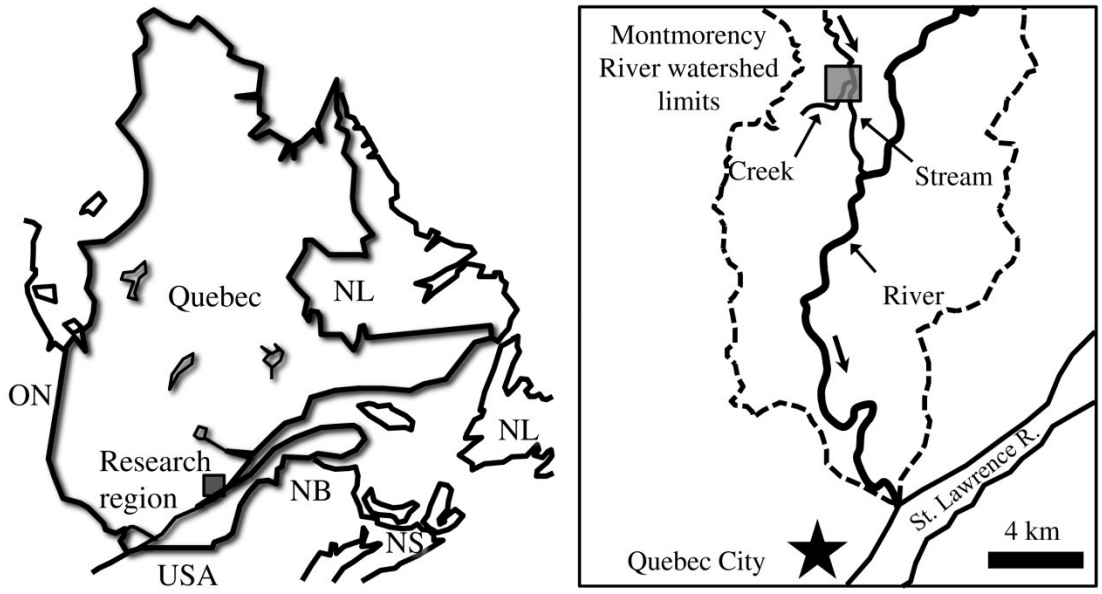

Figure 3.2. (A) Research region and (B) sampled channels (grey area) in the Montmorency River watershed, Quebec, Canada.

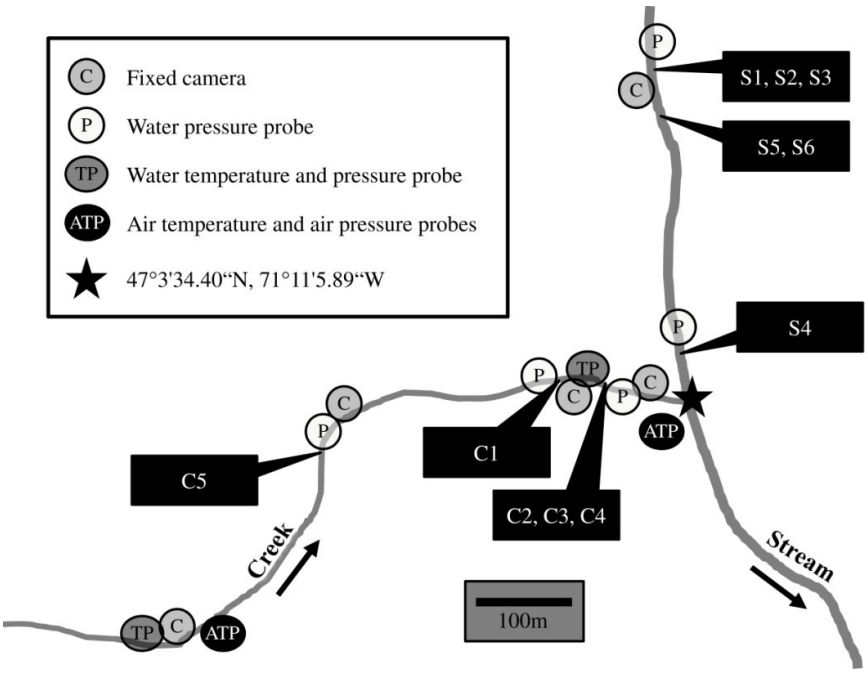

Figure 3.3. Instrumentation layout in the Stream and the Creek and sampling sites identification (black boxes).

The Stream's width is relatively constant at 18 m and its slope in the 500 m-long reach of interest is 1.5%. Based on the Montgomery and Buffington (1997) channel morphology classification, this reach consists of rapids with numerous emergent boulders locally forming incomplete steps. At freezeup, ice dams develop in the alignment of dominant emerging boulders. Some dams develop at faster rates resulting in the upstream drowning of slower developing dams. Six samples were collected along this reach. Four of them (S1, S2, S3 and S4) were retrieved before (Nov. 27th, Nov. 30th, and Dec. 12th, 2012) a mid-winter breakup that took place on Jan. 31st 2013. This event cleared the Stream from all its ice and was immediately followed by a new freezeup period. The two other samples (S5 and S6) were collected from a new ice dam on Feb. 7th 2013.

The Creek width is about 4 m and its average slope along a 700 m reach is 2%. It presents a well-defined step-pool morphology and, at freezeup, ice dams form on every step. Five anchor ice and ice dam samples were collected in the Creek reach: one of them (C1) was retrieved on Nov. 27th, 2012, three (C2, C3 and C4) were collected on Jan. 16th, 2013, and the last one (C5) was retrieved on Jan. 18th, 2013. Figure 3.4 presents CAT scans (vertical slices perpendicular to the channel bed and parallel to the banks) of the 11 ice samples. Arrows indicate the flow direction over the ice, white saw tooth lines show where samples were broken away from the rest of the ice accumulation, and double smooth white lines indicate where the ice was attached to the rock substrata. Two main ice types were found in the samples: columnar ice ('C' in sample S6; Fig. 3.4) and fixed-frazil ice ('FF' in sample S6; Fig. 3.4). The principal characteristics and growth processes of each ice type are presented below in section 3.4.

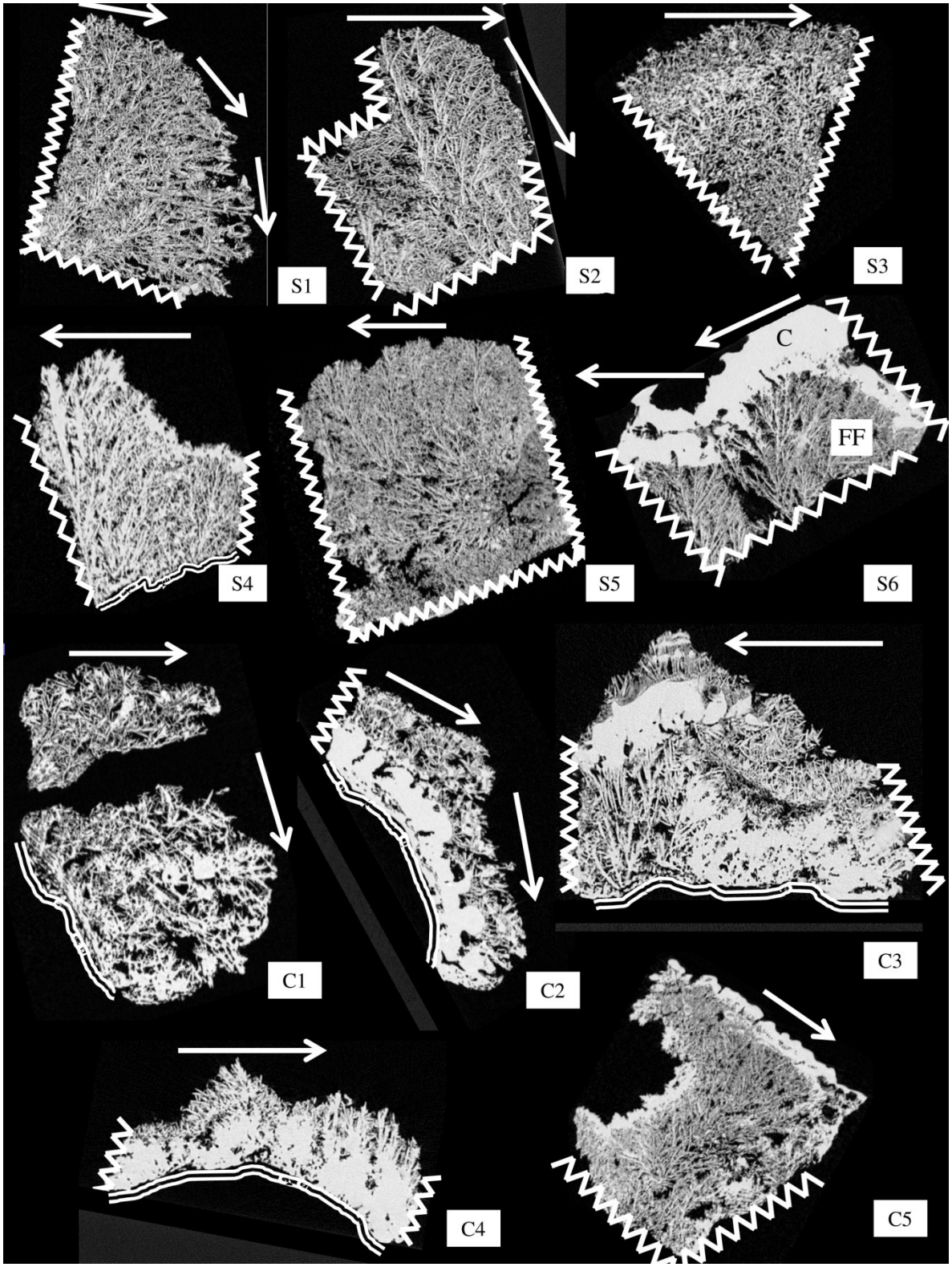

Figure 3.4. CAT scans of collected ice samples. Arrows indicate the scale with a distance of 10 cm along the flow direction. Saw tooth lines show where ice was broken away. Double white lines indicate the rock substrata surface. (Note that sample C1 was broken in two).

Table 3.1 presents detailed information about the origin of each sample, the ice crystal types found in their core and the water depth on top of them when they were retrieved. Ice dam samples S1, S5, C1, C2 and C3 were retrieved from the submerged sections of partly emergent ice dams.

Table 3.1. Ice sample identifications and characteristics.

Sample	Category	Overlying water depth (m)	Ice types
S1	Ice dam	0.10 – 0.20	Fixed-frazil
S2	Anchor ice	0.15 – 0.20	Fixed-frazil
S3	Anchor ice	0.50 – 0.60	Fixed-frazil
S4	Anchor ice	0.15 – 0.20	Dense fixed-frazil
S5	Ice dam	0.10 – 0.15	Fixed-frazil
S6	Ice dam	0 (emerged)	Fixed-frazil, columnar
C1	Ice dam	0.10 – 0.15	Fixed-frazil, dense fixed-frazil
C2	Ice dam	0.03 – 0.05	Fixed-frazil, columnar
C3	Ice dam	0.03 – 0.05	Fixed-frazil, dense fixed-frazil, columnar
C4	Anchor ice	0.15 – 0.20	Fixed-frazil, dense fixed-frazil
C5	Ice dam	0 (emerged)	Fixed-frazil, columnar

3.2.2 Ice sample categories

Ice samples were collected from developing anchor ice accumulations or ice dams. It is important to note that all active dams (those that are building up) present emerging sections and submerged sections (where a significant portion of the channel discharge flows) while breached ice dams are essentially emerged ice features. The inner structure of breached ice dams is expected to be different from that of newly forming ice dams as the formers are subjected to multiple water level variations and as most of their structure is exposed to cold air which can potentially modify their crystallographic arrangements.

Samples were categorized based on their origin. In the “anchor ice” category, sample S2 was retrieved from an ice weir, sample S3 was collected from an anchor ice accumulation in a deep pool between two steps, and samples S4 and C4 were collected from anchor ice accumulations located just upstream of a step in a moderately shallow flow. “Ice dam” category samples were mostly retrieved on the downstream side of ice dams but two samples, S5 and C3, were collected on the upstream part of a dam (Fig. 3.5).

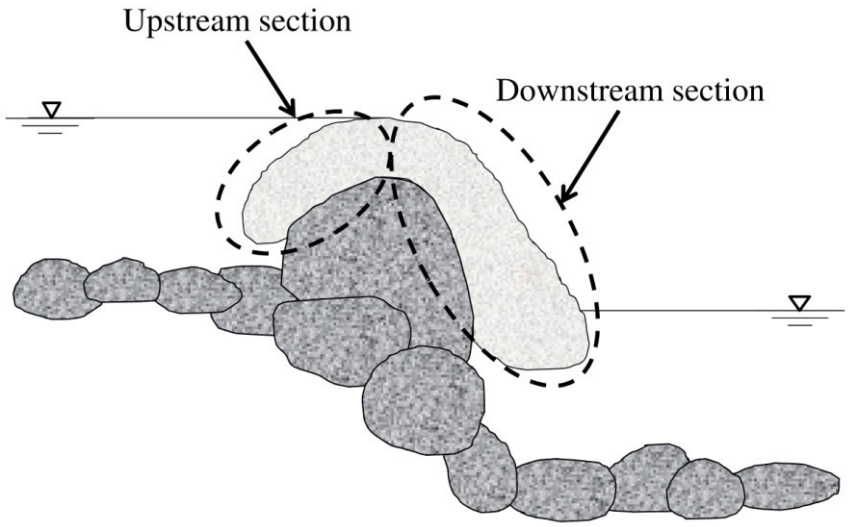

Figure 3.5. Typical ice dam profile showing upstream and downstream sampling locations.

3.2.3 Sampling methodology and CAT scan analysis

A pickaxe was used to retrieve samples as their structure was not altered by the pickaxe strike. This technique worked well with higher density samples. To retrieve more porous samples, the pickaxe was gently used to slice away the desired ice volume. Every sample collected was strong enough to be hand held outside the water without losing its structural integrity. Samples were then gravity-drained in order to remove as much interstitial water as possible. They were put in sealed plastic bags (to avoid ice sublimation) and were transported from the field in coolers filled with snow to protect the samples from breaking and to keep them cold during transport. They were then stored in a cold room at -10 °C.

The internal structure of the samples was characterised and analysed using a medical CAT scan (*Siemens SOMATON Sensation 64*). As the CAT scanning was necessarily conducted at room temperature, the operation was limited to less than 5 minutes for each sample in order to prevent melting. The resulting CAT output for each sample was hundreds of DICOM images, each of which corresponded to one vertical slice (0.6 mm thick) through the sample formed of pixels of 0.55 x 0.55 mm in a 512 x 512 matrix. These images (i.e. matrices) were analysed using *Fiji* software (ImageJ version 1.48d).

DICOM files consist of 16-bit grayscale images. Brightness is defined by the pixel value, and ranges from -1024 to over 500. The higher the pixel value, the denser is the material. By applying *Fiji*'s selection tools, it is possible to create a histogram and statistical reports (max, min, mean, standard deviation) of the brightness variation within a selected sub-area. Conversion of pixel values to ice porosity is done by comparing pure solid ice value (0% porosity) to the surrounding air value (100% porosity). Sub-areas can then be analysed and the resulting porosity value is calculated using the following equation:

$$Porosity(\%) = \frac{Mean\ pixel\ value - Solid\ ice\ pixel\ value}{Air\ pixel\ value - Solid\ ice\ pixel\ value} x100$$

After calibration tests, it was determined that the mean pixel value of pure solid ice was -85 ± 2 while the mean pixel value of air was -996 ± 1. While the latter was obtained with air surrounding the samples, pure solid ice pixel value was obtained with what appeared to be air-free crystal clear ice structures within the collected samples. This value was then compared with pixel value of floating border ice collected during the same winter. Resulting values were the same, which confirmed that the calibration procedure was correct.

3.3 Hydrological and weather conditions during ice formation

Figure 3.6 presents measured air temperatures (T_A) and water depths (Y) for the Stream and the Creek during the entire sampling period (Nov. 25th, 2012 to Feb. 8th, 2013).

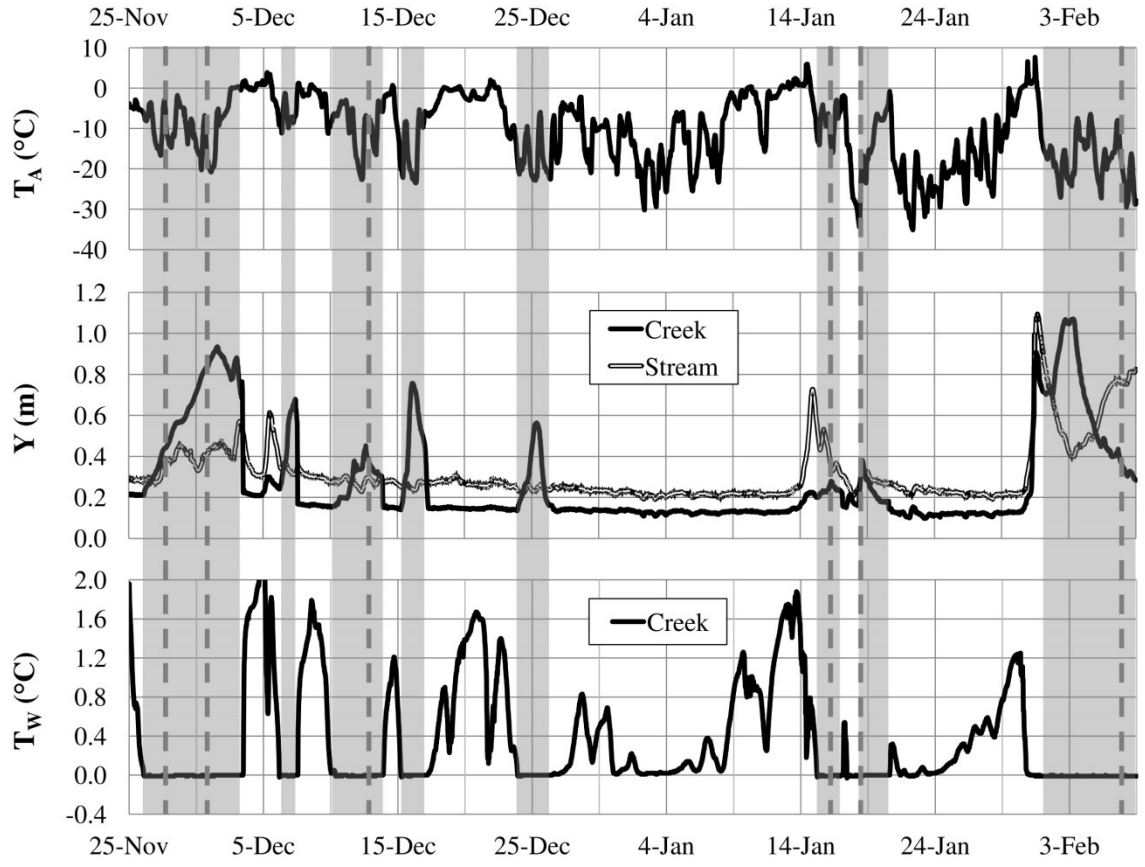

Figure 3.6.Stream and Creek environmental data (T_A, Y and T_W) for the entire sampling period (Nov. 25th, 2012 to Feb. 13th, 2013).

The air temperature was recorded on a 30 minute-basis using a HOBO U22 logger with ± 0.2 °C accuracy. Atmospheric and water level pressures were measured at the same rate using HOBO U20 loggers with

absolute ± 0.003 m accuracy. Water level loggers were anchored on the channel bed in order to detect variations induced by ice dams. Barometric pressure was subtracted from water pressure signals to obtain the actual water level with ± 0.002 m accuracy on relative variations. Fixed Canon 20D cameras located near sampling sites provided complementary data including ice dam growth rates. Finally, the water temperature (T_W) in the Creek was recorded using a YSI 6600 with a ± 0.02 °C accuracy. The periods during which ice dams were generating a backwater effect and the sampling dates are respectively indicated by grey areas and vertical dashed lines in Fig. 3.6. Ice dam buildup periods (Y increases) corresponded to water temperatures of 0.00°C or less. Maximum measured supercooling was -0.03°C and only lasted for few hours before T_W reached a plateau at 0.00°C. As supercooling is mandatory for anchor ice and ice dam development, it is likely that the instrument was not precise enough to measure slightly supercooled temperatures. To address this issue, the same YSI 6600 was compared with a RBR*solo* (± 0.002 °C accuracy) temperature logger during winter 2013-2014 in the same Creek. Results indicated that measured 0.00°C plateau (Fig. 3.6) actually corresponded to continuous water supercooling varying between -0.002°C and -0.012°C.

3.4 Ice crystal types

CAT scan images were initially used to identify different ice crystals and structures found within collected samples (Fig. 3.4). Traditional thin sections were then performed in order to relate various ice structures of interest to known ice types. While the CAT scan technology provided a complete 3D image of each samples, thin sections revealed the many individual ice crystals within complex sample sub-areas.

3.4.1 Columnar ice crystals

Figure 3.7A presents a vertical CAT scan slice of sample S6 while Figure 3.7B shows a subset thin section near the top of the sample. It is important to note that this sample only represents the upper part of an ice dam section. The lower part of the dam could not be collected due to the strong adhesion to the bed and to the difficult working conditions at the site.

The upper part of the sample presents itself as a distinct solid ‘ice cap’ that covers an underlying porous tree-like structure. The very low porosity of the cap (bright structure in Fig. 3.7A) suggests that it developed by progressive flooding and freezing of thin layers of water. This freezeup process, easily observed on timelapse photographs, is known as icing (e.g. Turcotte et al., 2011) and the resulting ice presents the same crystal characteristics as the ice structure known as S2-columnar ice commonly found within floating ice covers (Michel, 1978). The ice cap is therefore made of dense ice which structure consists of long, thick crystals oriented perpendicularly to the surface on which they grow (Fig. 3.7B). However, unlike typical columnar ice forming downward at the undersurface of an existing floating ice cover, this columnar ice grew upwards from the submerged ice dam surface into the water flowing on top. This upward growth is corroborated by the

crystal orientation that is generally perpendicular to the water surface as crystals grew in length and size. Crystal thickness increases toward the water surface and because preferred crystal orientations outgrow those that are not properly oriented. One should note that the black holes in top half of the thin section (Fig. 3.7B) do not represent an actual absence of ice but rather columnar ice crystals that were perfectly oriented parallel to the crossed polarizers and thus not diffracting the incoming light. The bright white color on the CAT scan image in the same region corroborates this fact (Fig. 3.7A).

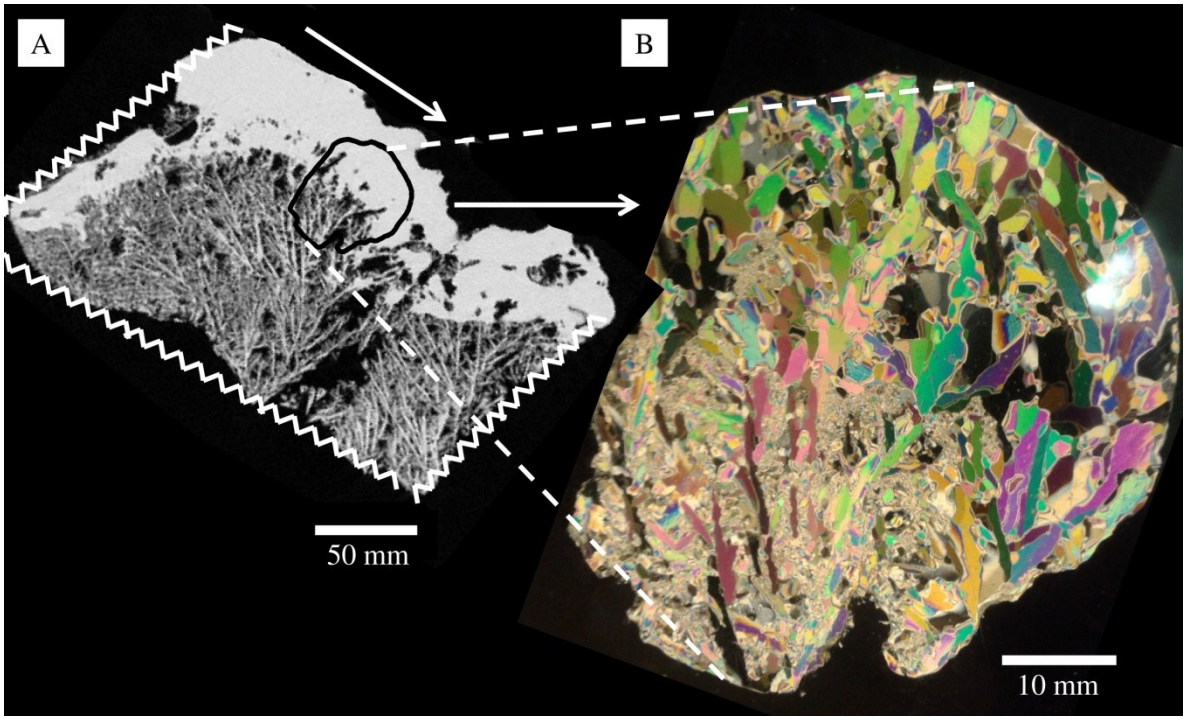

Figure 3.7. (A) Vertical CAT scan slice of sample S6 showing crystal orientations and porosity (grayscale) and (B) thin section (identified in 7A) showing the crystallography of the ice cap. The flow is from left to right and the sample is oriented vertically as found in the Stream.

Columnar ice crystals formed by spray ice process were also observed in ball-shaped ice structures (Fig. 3.8) in an ice dam sampled in the Montmorency River during winter 2011-2012 (Dubé et al., 2013). The thin section (Fig. 3.8B) indicates that these balls were also composed of large columnar ice crystals.

3.4.2 Fixed-frazil ice crystals

Figure 3.9 shows that the entire lower portion of sample S6 is made of porous ice composed of two dominant crystal shapes: 1) thick plate-like crystals as long as 30 mm with a dominant orientation and 2) fine to medium-grained crystals (less than 5 mm) randomly oriented. This crystal arrangement supports the previous assertions that anchor ice is initiated by the adhesion of suspended frazil ice particles (Kempema and Ettema 2009, Kerr et al. 2002, Qu and Doering 2007, Stickler and Alfredsen 2009, Terada et al. 1998, Tsang 1982).

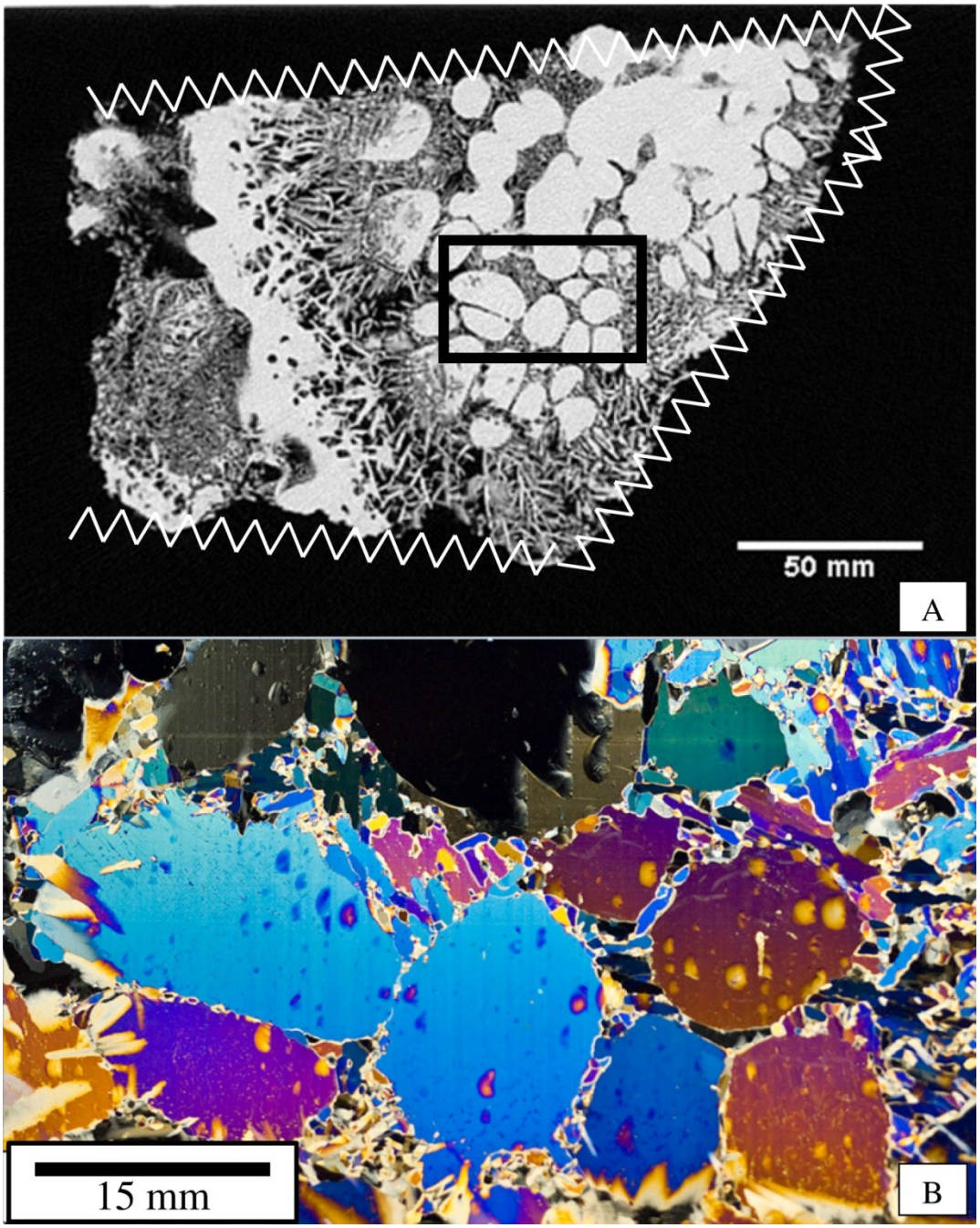

Figure 3.8. (A) Horizontal CAT scan slice showing crystal orientations and porosity (grayscale) and (B) thin section of the zone identified in 8A showing the crystallography of the ball-shaped ice. The flow is from right to left. (Adapted from Dubé et al., 2013).

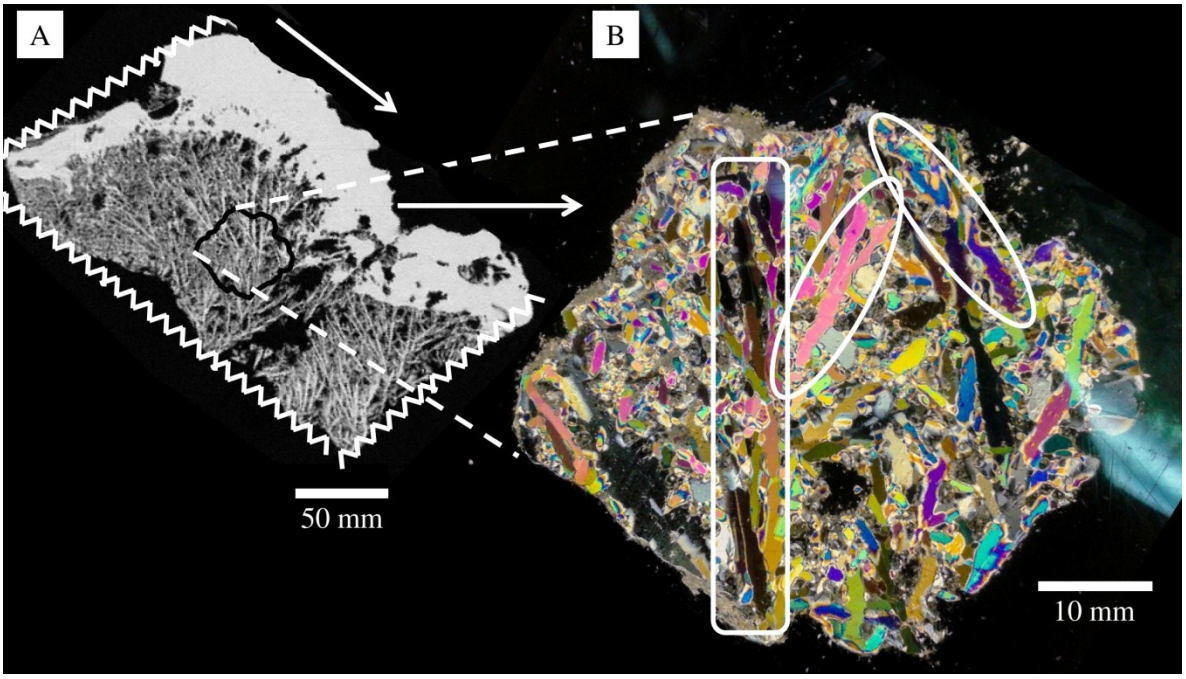

Figure 3.9. (A) Vertical CAT scan slice of sample S6 showing crystal orientations and porosity (grayscale) and (B) thin section showing the crystallography of fixed-frazil ice of the zone identified in 9A. The flow is from left to right and the sample is oriented vertically as found in the field.

Figure 3.10 presents an underwater photograph of a waterproof glove taken in the Creek on Dec. 12th 2012 at 07:00 (before sunrise) while the air temperature was -23 °C. Figure 3.10B is a close up of the spacing between two fingers with what appear to be hundreds of disc shaped frazil ice particles (maximum size of about 1 mm) that are drifting in the water column. This agrees with typical observation of flat disk being the dominant shape of ice crystals that grow at the supercooling levels found in turbulent water bodies (Daly, 1994). While half of the crystals are disc-shaped (Fig. 3.10B), the other half presents a perceptible elliptical shape. It is possible that the observed particles were all disc-shaped frazil ice crystals oriented in different directions relative to the camera. The brightness of the elliptical crystals is explained by the orientation of their 'a-axis' more or less parallel to the camera view, causing reflection of the camera flash.

Some newly deposited frazil discoid particles are visible in the underwater photograph presented in Figure 3.11 (pointed by arrows in Fig. 3.11B). These semi-transparent ice crystals are attached (i.e. 'fixed-frazil') to the outer margin of a developing anchor ice accumulation in the Creek. The form of their crenulated edges indicates (e.g. Kempema and Ettema, 2009; Tsang, 1982) that the discs were growing at that very moment as the air temperature was -10°C.

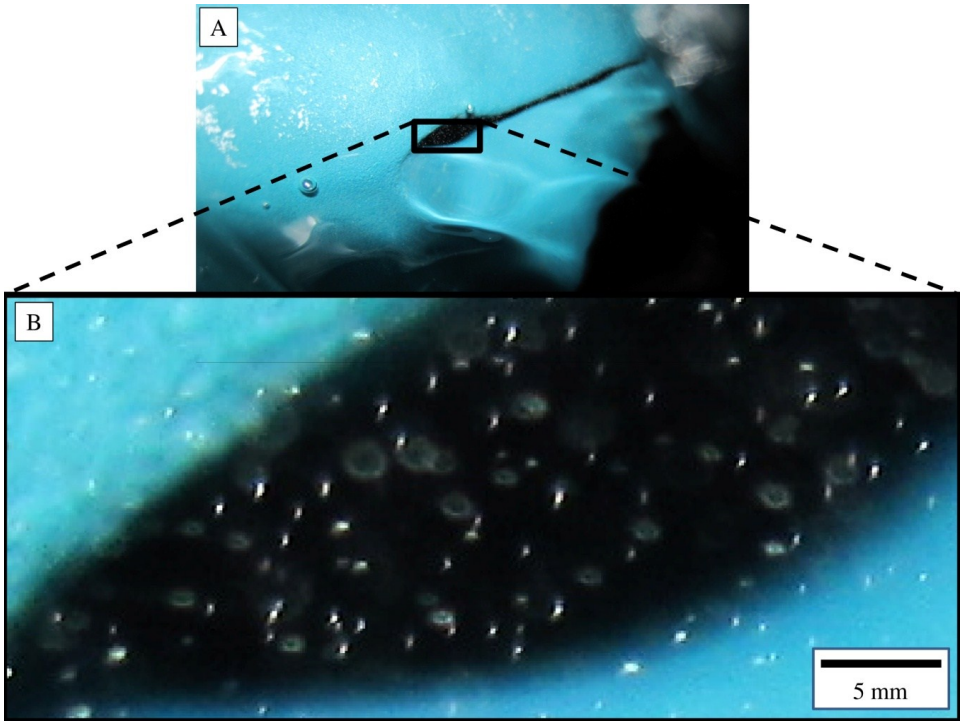

Figure 3.10. (A) Underwater photograph in the Creek of a waterproof glove showing (B) disc-shaped frazil ice in the spacing between two fingers.

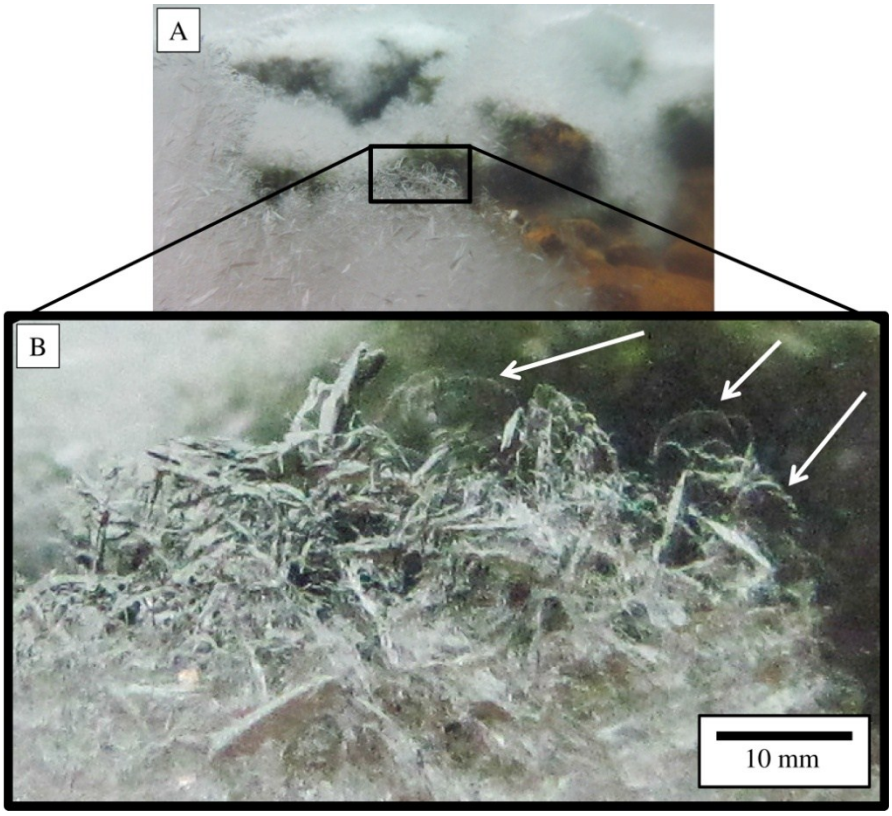

Figure 3.11. (A) Underwater photograph of anchor ice mass in the Creek and (B) close-up section showing transparent disc-shaped frazil ice particles actively growing (pointed by arrows).

However, small individual discoid particles, even the largest ones (~1 mm diameter), could not be identified within anchor ice accumulations. CAT scans and thin sections reveal that, in fact, most crystals were quite large suggesting that they grew *in-situ*. This supports a conclusion by Kempema and Ettema (2009) that discoid frazil particles grow extensively once they are intercepted. The presence of longer plate-like shaped crystals (examples highlighted by white shapes in Fig. 3.9B) indicates that some of them selectively kept on growing, sometimes achieving a substantial size (up to 30 mm). This dominant growth selection was probably based on the disk shape instability in that preferential orientation within local heat flow (Daly, 1994). The thin section in Figure 3.9B shows strikingly different ice crystal morphologies than those typically observed for primary ice nucleated from frazil (P3–ice) and for congealed frazil slush (S4-ice) in Michel (1978) where in both cases, crystals are defined to be less than 5 mm with random orientation.

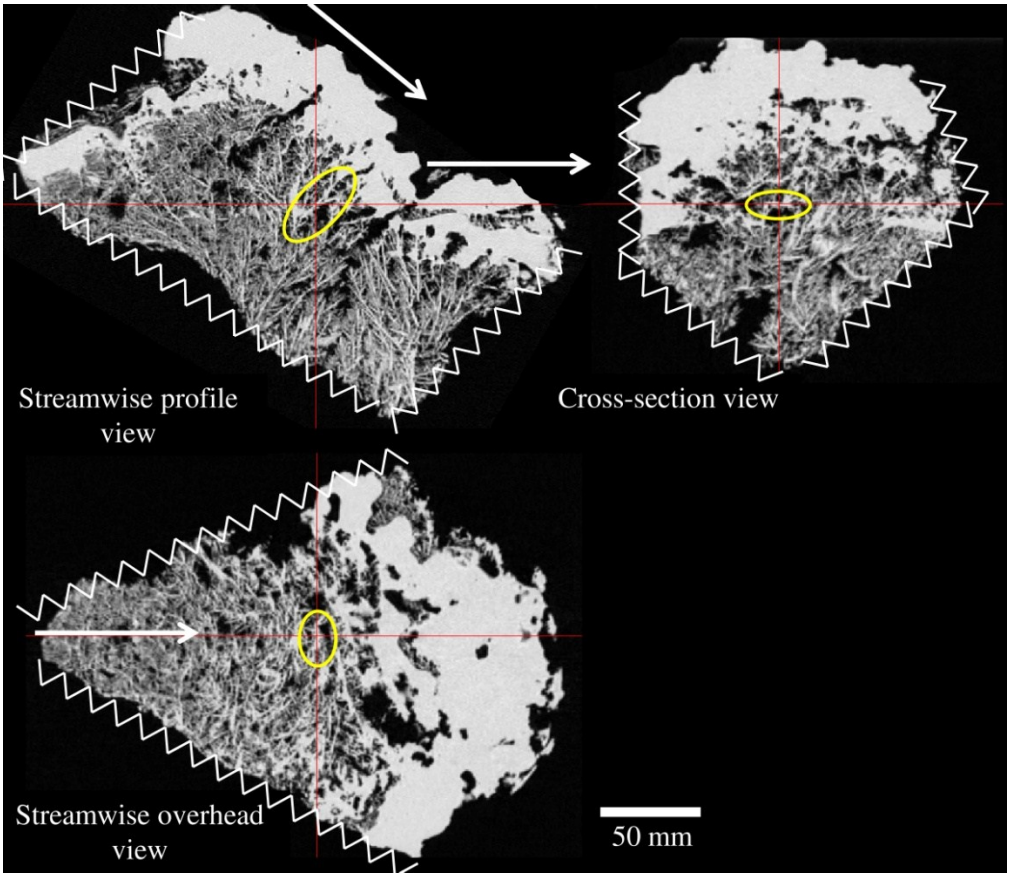

Figure 3.12. Spatial tracking of a single plate-like fixed-frazil ice crystal (enclosed in ellipse) using CAT scan analysis of sample S6. Straight lines indicate the location of the three perpendicular slices and their intersection point to the same fixed-frazil ice crystal.

Interestingly, acicular, needle-like or spicule shaped frazil crystals were seldom observed in sample S6. This also applies to every other collected sample. Tsang (1982) noted that in nature, at a supercooling of less than 0.1 °C, the frequency of occurrence of needle-shaped frazil ice is much lower than that of discoid frazil. The

measured water supercooling at both instrumented Creek sites was never more than 0.03 °C, which could explain the absence of spicule shaped crystals in the retrieved samples. One should note that the long crystals observed in the CAT scan image (Fig. 3.9A) are not needle-shaped because they display a significant length in the three perpendicular views (see Fig. 3.12). Otherwise, they would appear as a pin-point in at least one perpendicular view.

From this point on in the paper, ice structures found in anchor ice accumulations composed of long crystals that likely grew *in-situ* will be referred to as *fixed-frazil* ice (the word 'fixed' is used to indicate that the ice is not moving with the flow).

3.5 Ice structures' properties

3.5.1 Porosity

The porosity of different ice structures within each sample was determined using the CAT data. Figure 3.13 presents a vertical slice of sample S6 showing multiple sub structures of variable porosity.

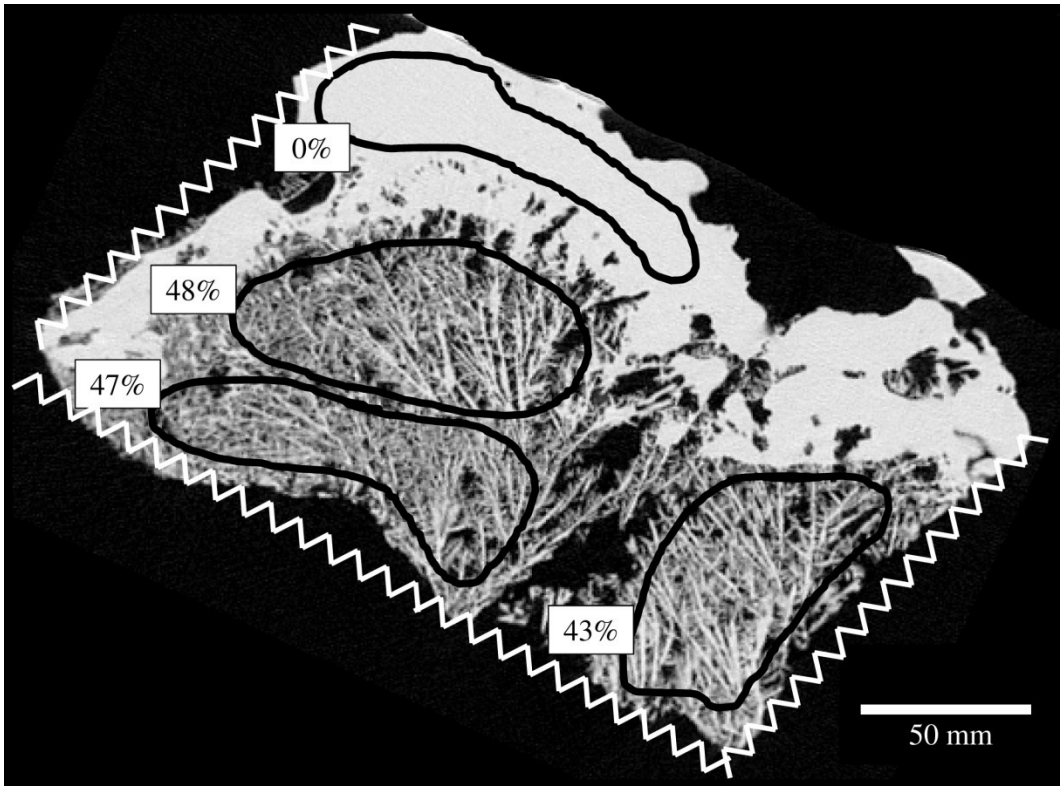

Figure 3.13. Vertical CAT scan slice of sample S6 showing inner structure and porosity values for sub-areas (including columnar ice and fixed-frazil ice). The flow is from left to right and the sample is oriented as found in the Stream.

The ice cap covering the sample presents a porosity of 0%, a value that is consistent with what was suggested in sub-section 3.4.1 (ice structure developed by an icing process and composed of columnar ice crystals).

Columnar ice structures found in other ice samples displayed porosity values varying between 0 and 1%. This narrow range suggests that columnar ice structures present a uniform, compact crystal arrangement and that the growth process is similar for all collected samples. Similarly, columnar ice found in a floating cover also displays porosity values close to 0% (Gherboudj et al. 2007).

The fixed-frazil ice portion of sample S6 presents an overall porosity of 43-48%. Fixed-frazil ice structures observed in the other samples display a porosity range of 24-52%, which compares with the anchor ice porosity range (23-48%) presented by Dubé et al. (2013) for samples collected a year earlier in the Creek and in the Montmorency River. These two ranges are comprised in both the low turbulence (Type I; 34-61%) and high turbulence (Type II; 2-31%) anchor ice identified by Stickler and Alfredsen (2009), but they are fairly low when compared with those reported by Parkinson (1984) for field data (71-84%) and by Qu and Doering (2007) for laboratory data (59-88%).

These ranges differ significantly from porosity values reported by Gherboudj et al. (2007) for congealed floating frazil ice covers (1-18%) wherein interstitial water freezes when floating frazil ice exposed to cold air. As a consequence, it can be stated that the anchor ice accumulations presented above were submerged during their entire development process, which prevented heat loss from the core of the samples and thus freezing of interstitial water.

Porosity values of fixed-frazil ice structures are presented in Table 3.2 where 'n' represents sample size. Results suggest that fixed-frazil ice porosity ranges are very similar for both ice type categories although the porous part of ice dams appear to be, on average, 6% more porous (not statistically significant with a 90% probability on a Student t-test) than anchor ice accumulations. This suggests the possibility of a relationship between porosity and flow velocity. Yamazaki et al. (1996) observed in their field study that anchor ice porosity decreased as a function of flow velocity (though their statistical relationship was also weak). This could explain the presence of dense fixed-frazil ice in some collected samples (see Table 3.1). This apparent relationship was also observed by Stickler and Alfredsen (2009) with reference to the Reynolds number.

Table 3.2. Fixed-frazil ice porosity of anchor ice and ice dams.

Category	Porosity			
	Max	Min	Mean	n
Anchor ice	52%	24%	38%	19
Ice dams	52%	27%	44%	35

3.5.2 Size of fixed-frazil ice crystals

CAT scan data were then used to calculate crystal size. Because *Fiji* uses an automated numerical algorithm to calculate crystals sizes, the number of calculations (n) far surpassed what could be done manually. However, with *Fiji*, it is not possible to calculate the entire length of each crystal because the software only calculates segment sizes between intersecting crystals. In order to help *Fiji* in its calculation task, basic CAT scan images need to be sharpened, transformed into black-white (binary image), and skeletonised. These operations transform, regardless of their thickness, all crystals into single lines. The length of each segment (line) for all samples was then calculated. Results are presented in the form of a cumulative frequency curve for both sample categories in Figure 3.14. The maximum and mean segment size and the number of segments are also presented in Fig. 3.14.

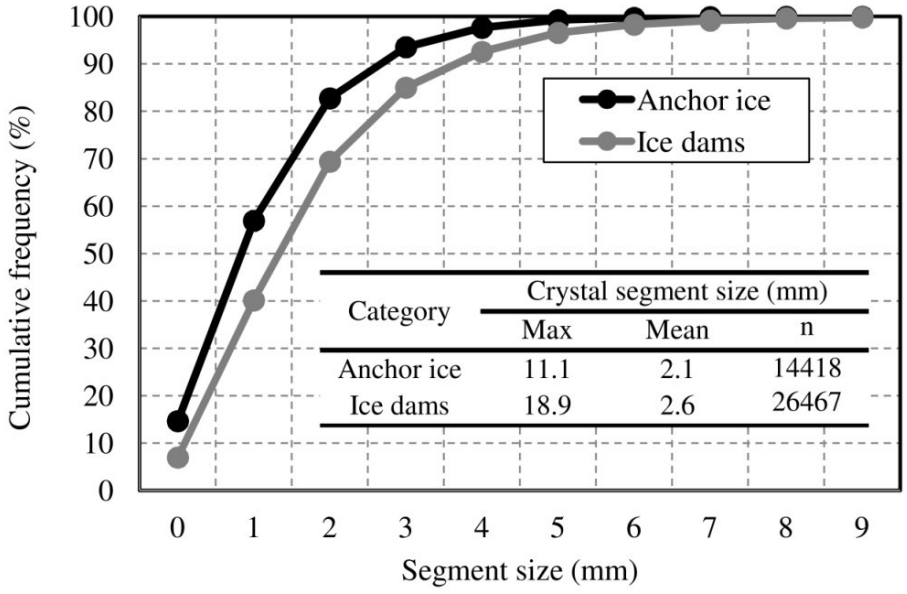

Figure 3.14. Cumulative frequency, maximum and mean values of crystal-segment size of fixed-frazil ice structures found in anchor ice and ice dams samples.

Both frequency curves present a similar trend but the segment size of fixed-frazil ice crystals in ice dams are generally greater than in the anchor ice samples (statistically confirmed with a Student t-test at the 95% confidence level) although this difference could simply be the result of less crystal intersections.

Individual whole ice crystal sizes were determined manually. For each sample, the (apparent) longest 10 crystals were manually measured and the longest crystal of each sample was sorted according to its category. Results presented in Figure 3.15 suggest that fixed-frazil ice structures found in anchor ice samples were shorter than those found within ice dams (statistically confirmed with a Student t-test at the 95% confidence level). These maximum measured crystal sizes are consistent with the findings of Kempema and Ettema

(2009) who reported that out of their 72 anchor ice samples collected, only 9 of them had maximum crystals sizes over 50 mm. Moreover, the vast majority of anchor ice crystals had a maximum size of less than 45 mm which compares with anchor ice category in Fig. 3.15 where all measured crystals were shorter than 42 mm.

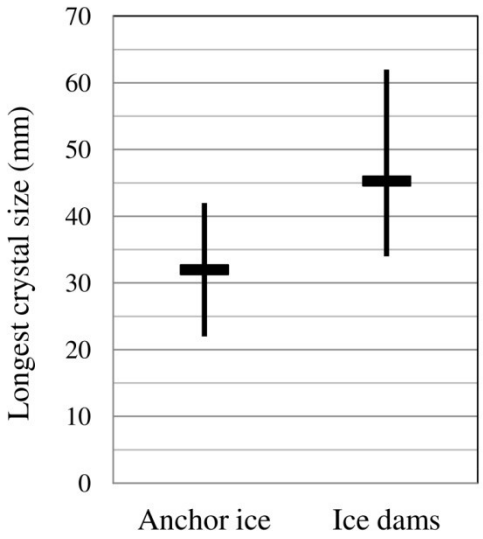

Figure 3.15. Distribution of the longest ice crystals measured in each anchor ice and ice dam sample. Vertical lines represent the measured size ranges and horizontal lines represent the mean values.

3.5.3 Orientation of fixed-frazil ice crystals

CAT scan images were also used to determine the orientation of ice crystals in fixed-frazil ice structures. The crystallographic orientation relative to the flow direction was determined numerically using *Fiji*. Since the sampling methodology and the site-to-site variability were not optimal for collecting samples of regular shapes, it was nearly impossible to CAT scan them with the same orientation relative to the flow direction. Nonetheless, based on supplemental photographs taken during sampling, the actual spatial orientation of each ice piece had been recorded and the numerical results from *Fiji* were rotated in order to set the water surface at a value close to 0° for each sample.

Regardless of their category (anchor ice or ice dam), at their first stage of development, fixed-frazil ice crystals were preferably oriented perpendicularly to the solid surface *upon which they developed* (sub-areas 1 and 2 in Fig. 3.16). This was observed for crystals growing on rock substrata and submerged columnar ice. As crystals grew, their orientation seemed to rapidly (at least in space) change to become perpendicular *to the water surface* (sub-areas 1 and 2 in Fig. 3.16). Sometimes the water surface was parallel to the substrata surface, in which case, the crystals orientation did not change (sub-area 2 in Fig. 3.16). Otherwise, crystals extended a relatively short length before evolving into longer crystals that became oriented towards the water surface. This whole process can be clearly observed in samples S1, S4, S6, C2, C3 and C4 (Fig. 3.4). In the case of

cascading flows on a developing ice dam, the crystals orientation was often curvilinear (see S2 and S5 in Fig. 3.4) due to the same growth process.

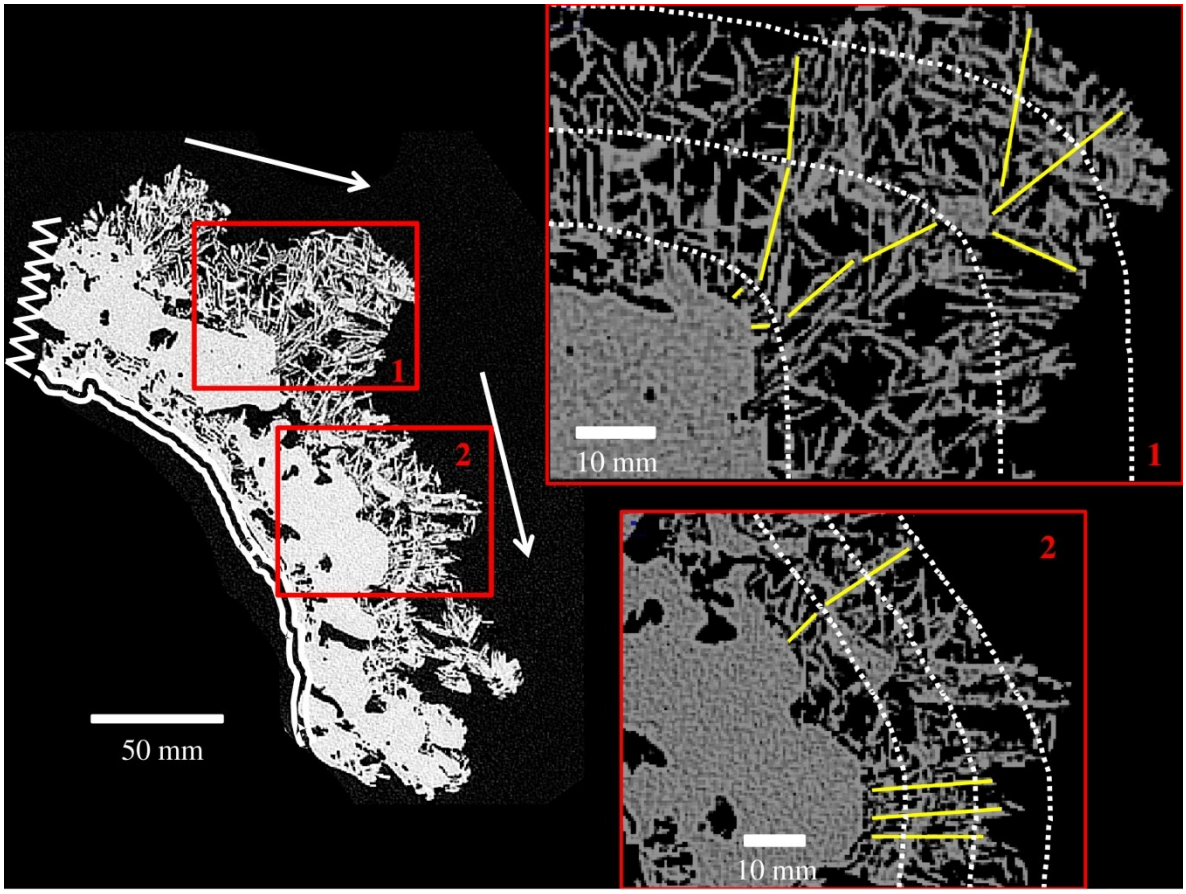

Figure 3.16. Vertical CAT scan slice of sample C2. Note ice crystal growth orientation (solid lines in sub-areas 1 and 2) and estimated evolution of the water depth over the sample (white dashed lines in sub-areas 1 and 2).

According to Michel (1978), these results indicate that *in situ* growth is the main fixed-frazil development mechanism since the most favorable ice crystals orientation for development is parallel to the heat flow, which, in this case, is eventually toward the water surface. Figure 3.16 presents estimated water surface location (white dashed lines) prevailing when crystals were growing. As a consequence, fixed-frazil ice crystals that were initially favorably oriented progressively dominated the unfavorably oriented ones, a process that compares with what was described earlier for columnar ice crystals. This also explains why the longest observed crystals in streamwise profile or cross-section (vertical planes) CAT scan slices were oriented perpendicularly to (and towards) the water surface (e.g. S1 in Fig. 3.4).

In turn, fixed-frazil ice crystals observed in streamwise overhead (horizontal plane) CAT scan slices displayed a rather short length and were mostly oriented perpendicularly to the flow direction (Fig. 3.12). A careful study of the crystal highlighted here shows that it resembles a plate having the approximate dimensions of 2 mm

thick, 20 mm wide and 40 mm long. It faces the flow but is leaning back on a 45° angle. Indeed, any multiple single-crystal spatial tracking reveal that *platelet* (or *plate-like*) is the dominant shape of fixed-frazil ice crystals found within samples. This agrees with previous field observations where platelets are noted as the dominant shape of anchor ice crystals (e.g. Kempema and Ettema, 2009; Yamazaki et al., 1996).

3.5.4 Dendrite structures development

Complementary observations of CAT scan data reveal that some shorter fixed-frazil crystals are attached to longer crystals and therefore are oriented in different directions. Figure 3.17 presents an example of such tree-like, dendritic structure presented in a vertical CAT scan slice of sample S6.

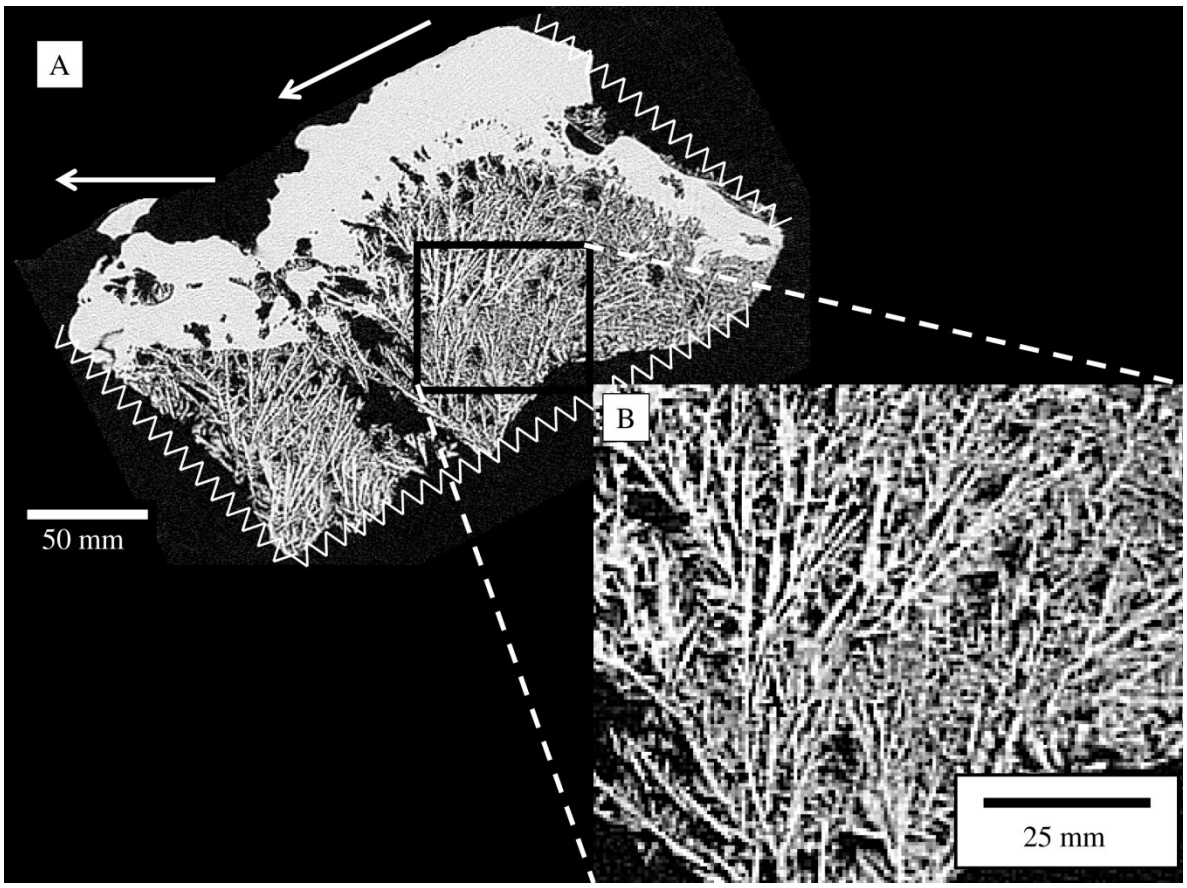

Figure 3.17. (A) Vertical CAT scan slice of sample S6 showing the dendritic growth of fixed-frazil ice crystals and (B) a close-up view.

The observed arrangement of fixed-frazil ice crystals into dendrites as observed in every sample is likely caused by intense heat loss to the surrounding water. The discoid frazil crystal morphology, once caught by the anchor ice matrix, gradually evolved into a plate-like morphology in order to enhance the crystal surface area and to release heat more efficiently. Daly (1994) assumed that the growth rate of the a-axis is controlled by the rate at which heat is transported away from the crystal/water interface. Thus, supercooled, turbulent fast

flowing waters of the Creek and the Stream are expected to provide important crystal growth rates. As the water was losing heat to the atmosphere, the favorably oriented (parallel to the heat flow) platelet crystals kept growing toward the water surface. This could have contributed to the development of the dendrite structure both mechanically and thermally. The mechanical development process is associated with the fast growing dominant crystals continually intercepting drifting frazil ice particles. The thermal growth process is associated with the "need" for the main crystals to release an increasing amount of latent heat by developing new growth paths in a tree branch-manner. From all the observed samples, it is believed that (active) frazil attachment or (passive) frazil interception only marginally contributed to the development of the tree-like fixed-frazil ice structures observed in CAT scan slices. Taking into account the extra complexity related to the interlocking nature of the platelets in fixed-frazil ice and the intergrowth at the bonds between crystals, it is probable that modified heat equations (possibly in matrix form) could describe the reason behind the 3D interconnecting structure geometry of the individual plates found in the fixed-frazil ice mass.

3.6 Discussion

Fixed-frazil ice structures found in anchor ice and ice dam samples were statistically significantly different from each other in terms of crystal segment size and maximum crystal size. However, the most striking difference between anchor ice and ice dam samples is that columnar ice structures were only present in ice dams. This implies that columnar ice crystals only grow from emergent surfaces exposed to cold air. Observations suggest that columnar ice in steep channels mostly form by (1) progressive flooding and freezing of thin water layers leading to a two-dimensional columnar ice cap or sheet, or (2) by constant splashing and freezing of sprayed water droplets leading to the development of largely three-dimensional structures such as "balls". A hybrid columnar ice formation process in steep channels is caused by wavelets at the turbulent water surface sporadically flooding cold surfaces. Considering this, an investigator unfamiliar with those ice processes would be surprised to find columnar ice structures well below the prevailing water surface or within fixed-frazil ice structures (C2 and C3 in Fig. 3.4; E1, L1 and S1 in Dubé et al., 2013). However, this simply indicates that the underlying material was emerging at an early ice dam development stage. Therefore, columnar ice development on fixed-frazil ice structures or at the bed level necessarily occurred when those structures were emerging. The clearly defined line between fixed-frazil ice and columnar ice in sample S6 (Fig. 3.17A) likely indicates the temporarily, slowly rising water surface level when fixed-frazil ice was emerging. The water level had to rise at a comparable or slower rate than columnar ice crystals could grow, a process that depends on the water layer thickness and on the local heat budget. In order to form anchor ice on top of a columnar ice structure, the later structure had to be flooded by a layer of water (hydraulic and hydrologic instabilities are frequent at that freezeup stage; Turcotte et al., 2014) that was too deep for columnar ice crystals to grow

upward. Instead, as the water became supercooled (once again), the fixed-frazil ice development process resumed and columnar ice crystals were "buried" in anchor ice.

The presence of columnar ice structures within ice dams could contribute in making them more resistant to collapse when the water level (or the channel discharge) varies. Ice dams are known to form mostly on existing steps (in step-pool channels or in cascades) or in the alignment of dominant boulders (in rapids or along riffles). As a result, the most structurally resistant ice features form where the water velocity is high, either at lateral flow constrictions or at vertical drops. In turn, anchor ice accumulations, only composed of fixed-frazil ice crystals, probably form anywhere in the channel where the water depth is significant and where flow velocity is high enough to bring supercooled water to the bed by turbulence. Such locations include largely variable flow conditions such as those prevailing at existing steps, along rapids and riffles, in natural pools (in steep-pool channels or between cascades), or in ice dam-induced pools.

In interpreting the data presented in this paper, one must consider that CAT scans and thin sections presented might have been affected by the sampling methodology. When samples were collected and gravity drained, their inner porous structures probably retained a certain amount of water (between crystal interstices and on crystal surfaces). Once exposed to cold air, this water could have contributed to the growth of fixed-frazil ice crystals, slightly altering their shape and size compared with their submerged state. This alteration was probably relatively more important for the smallest crystals and it is reasonable to assume that the reported porosity of fixed-frazil ice structures was somewhat influenced by the sampling methodology. In turn, the dominant fixed-frazil ice crystal analyses (segment size, maximum size, and orientation) presented here are probably not as significantly affected. Also, it is quite unlikely that the reported dendrite (tree-shape) arrangement of fixed-frazil ice structures observed in CAT scan slices was affected by the sampling methodology.

Because of their smaller crystal interstices and their slower drainage rate where ice structures were denser, more water per volume was probably retained than in other more porous samples. Therefore, reported porosities probably include a relative bias.

3.7 Conclusion

This field study was conducted in the Montmorency River watershed during winter 2012-2013. It had two objectives. The first objective was to investigate the inner structure of anchor ice accumulations and ice dams forming in steep channels. Two main types of ice crystals were identified: columnar ice crystals and fixed-frazil ice crystals. Evidence of disc-shaped frazil ice attachment were found although results suggested that *in-situ* growth of fixed-frazil ice crystals was the dominant growth process in both anchor ice and ice dams. The main

difference between anchor ice and ice dam structures was found to be the presence of dense columnar ice structures that contribute to the dams' resistance. These structures often presented themselves as caps but could be layered or even spherically-shaped. Ice emergence is a necessary condition for this columnar ice to form.

The second objective of the study was to identify characteristics that are specific to fixed-frazil ice structures found in anchor ice accumulations and ice dams. CAT scan data showed that the porosity was not significantly different for both ice samples categories. However, crystal segment sizes and maximum crystal sizes in fixed-frazil ice structures were significantly longer in ice dams. It was also proposed that the crystal orientation is initially perpendicular to the substrate but progressively evolves into an orientation perpendicular to the water surface (in the vertical plane) and to the water flow direction (in the horizontal plane). Finally, dendritic (or tree-like) growth was observed (using CAT scan slices) in every fixed-frazil ice structures.

Further anchor ice and ice dam sampling campaigns are needed to identify additional characteristics of steep channel ice features. These campaigns should include other sites. CAT scan analyses coupled with traditional thin sections proved to be a powerful tool combination for the analysis of complex, three dimensional ice structures. A hydraulic and meteorological study of the same winter and research sites is in progress. This study will further explain the conditions associated with the development of anchor ice and ice dams in steep channels. Quantifying the internal resistance of ice dams could be of interest to understand their storage capacity during a winter runoff event and prior to breakup. Finally, micro-scale models of ice growth need further development. As for individual frazil ice crystal particles, thermodynamic equations are required for the physical-based modelling of the platelet 3D complex structure of fixed-frazil ice. The equations applied to 'icing' may require some modification to account for the specifics of the growth of emergent columnar ice found in the ice dams. Both these models could form the basis of a better understanding about the fascinating dynamic ice processes found in steep channels.

Acknowledgments

This research was partially funded by the Canada Foundation for Innovation (CFI) and by the Natural Sciences and Engineering Research Council of Canada (NSERC). The CAT scan used in this paper is the property of the Institut national de la recherche scientifique (INRS) in Quebec City. The authors would also like to recognize the contribution of a number of river ice scientists and engineers who provided useful comments for the paper, particularly the two reviewers. Finally, field work was greatly facilitated at all levels by Dany Crepault from Laval University.

References

Bradford, M.J., Heinonen, J.S., 2008. Low flows, instream flow needs and fish ecology in small streams. (Technical report). Canadian Water Resources Journal, 33.2 (Summer 2008): 165(16).

Clark, S., Doering, J.C., 2004. A laboratory study of frazil ice size distributions. Proceedings of the 17th International IAHR Ice Symposium, Saint Petersburg, Russia, 291-297.

Clark, S., Doering, J.C., 2006. Effect of turbulence intensity on frazil formation. Proceedings of the 18th International IAHR Ice Symposium, 267-275.

Daly, S.F., Editor, 1994. International Association for Hydraulic Research, Working Group on Thermal Regimes: Report on Frazil Ice. International Association for Hydraulic Research, Working Group on Frazil Ice, Special Report 94-23.

Dubé, M., Turcotte, B., Morse, B., Stander, E. 2013. Formation and inner structure of ice dams in steep channels. Proceedings of the 17th CGU-HS CRIPE Workshop on River Ice, Edmonton, Alberta, Canada.

Dubé, M., Turcotte, B., Morse, B., to be submitted. Understanding complex behavior of ice dam development in steep channels.

Gherboudj, I., Bernier, M., Hicks, F., & Leconte, R. 2007. Physical characterization of air inclusions in river ice. Cold Regions Science and Technology, 49(3), p. 179–194.

Hirayama K, Terada K, Sato M, Hirayama K, Sasamoto M, Yamazaki M. 1997. Field measurements of anchor ice and frazil ice. In: Proceedings of the 9th CGU-HS CRIPE Workshop on the Hydraulics of Ice Covered Rivers, Fredericton, NB, Canada.

Kempema, E. W., Ettema, R. 2009. Variations in anchor-ice crystal morphology related to river flow characteristics. Proceedings of the 15th CGU-HS CRIPE Workshop on River Ice, St. John's, Newfoundland and Labrador, Canada.

Kempema, E. W., Ettema, R. 2011. Anchor ice rafting: observations from the Laramie River, River research and applications, Volume 27, Issue 9, p. 1126-1135

Kerr DJ, Shen HT, Daly SF. 2002. Evolution and hydraulics of anchor ice on gravel bed. Cold Reg. Sci. Technol. 35: 101–114.

Michel, B., 1978. Ice Mechanics, Les Presses de l'Université Laval, Québec.

Montgomery, D.R., Buffington, J.M., 1997. Channel-reach morphology in mountain drainage basins. GSA Bulletin 109 (5), 596-611.

Parkinson FE. 1984. Anchor ice effects on water levels in Lake St. Louis, St-Lawrence River at Montreal. In: Proceedings of the 3rd CGU-HS CRIPE Workshop on the Hydraulics of River ice, Fredericton, NB, Canada.

Qu, Y.X., Doering, J., 2007. Laboratory study of anchor ice evolution around rocks and on gravel beds. Canadian Journal of Civil Engineering 34, 46–55.

Stickler M, Alfredsen KT. 2009. Anchor ice formation in streams: a field study. Hydrol. Process. 23: 2307–2315. DOI: 10.1002/hyp.7349.

Stickler M, Alfredsen KT, Linnansaari T, Fjeldstad H-P. 2010. The influence of dynamic ice formation on hydraulic heterogeneity in steep streams. River Res. Applic. 26: 1187–1197. DOI: 10.1002/rra.1331.

Tesaker E. 1994. Ice formation in steep rivers. In: Proceedings of the 12th International IAHR Ice Symposium.

Tesaker E. 1996. Interaction between ice and water flow in rapids. In: Proceedings of the 13th International IAHR Ice Symposium.

Terada K, Hirayama K, Sasamoto M. 1998. Field measurement of anchor and frazil ice. In: Proceedings of 14th International IAHR Ice Symposium.

Tsang, G., 1982. Frazil and Anchor ice: A Monograph. National Research Council of Canada, Associate Committee on Hydrology, Subcommittee on Hydraulics of Ice Covered Rivers.

Turcotte B, Morse B. 2011. Ice processes in a steep river basin. Cold Reg. Sci. Technol. 67: 146-156. DOI:10.1016/j.coldregions.2011.04.002.

Turcotte B, Morse B, Anctil F. 2011. Steep channels freezeup processes. Proceedings of the 16th CGU-HS CRIPE Workshop on the Hydraulics of Ice Covered Rivers, Winnipeg, MB, Canada.

Turcotte, B., Morse, B., Anctil, F., 2012. Cryologic continuum of a steep watershed. Hydrol. Process. DOI: 10.1002/hyp.9629

Turcotte, B., Morse, B., Dubé, M., Anctil, F., 2013. Quantifying steep channel freezeup processes, Cold Regions Science and Technology 94, 21-36.

Turcotte, B., Morse, B., Anctil, F., 2014. The hydro-cryologic continuum of a steep watershed at freezeup. Journal of hydrology 508, 397-409

Yamazaki, M., Hirayama, K., Sakai, S., Sasmoto, M., Kiyohara, M., Takiguichi, H., 1996. Formation of frazil and anchor ice. Proceedings of the IAHR Ice Symposium, pp. 488–496.

4. Steep channel freezeup processes: understanding complexity with statistical and physical models

Mathieu Dubé[1*], Benoit Turcotte[2], Brian Morse[3]

[1,2,3]Université Laval, 1065, av. de la Médecine, Québec City, QC/Can, G1V 0A6

[1]*mathieu.dube.4@ulaval.ca*; [2]*benoit.turcotte.1@ulaval.ca*; [3]*brian.morse@gci.ulaval.ca*

Résumé

Le développement de barrages de glace dans les cours d'eau à lit graveleux affecte les niveaux d'eau, le débit et l'habitat aquatique au début de la période hivernale. Malgré leur présence marquée dans un type de cours d'eau commun, l'ingénieur en milieu fluvial dispose de peu d'information quantitative décrivant les processus de formation de ces structures de glace complexes. Cet article comble ces lacunes en présentant une imposante série de données décrivant le phénomène. La variation substantielle des taux de formation et de fonte des barrages de glace entre différents sites d'un même cours d'eau et d'une année à l'autre pour un même site sont expliquées par un modèle numérique qui inclut un bilan thermique appliqué à la séquence marche-mouille d'un ruisseau. Ce modèle physique simule avec succès le développement complet d'un barrage de glace et montre que ce processus dépend de nombreux paramètres, ou degrés de liberté. Il démontre également que les caractéristiques morphologiques d'un cours d'eau influencent grandement la dynamique des barrages de glace.

Abstract

The development of ice dams in steep channels dictates water levels variations and influences flow rates and habitat conditions. Despite the dominance of ice dam development in cold region gravel bed channels, practicing engineers and scientists have access to very little quantitative information describing this complex freezeup process. This paper aims to fill this gap by presenting a large data set on the process. The substantial variations observed in formation and melting rates from one site to the next and from one year to the next at the same site are explained with a physically-based numerical model that includes a complete heat budget applied to single step-pool sequence. The model successfully simulates the entire development of an ice dam and shows that the process depends on multiple parameters, or degrees of freedom. It also reveals that morphologic characteristics greatly influence ice dam dynamics.

4.1 Introduction

Cold regions steep streams are affected by singular ice processes at freezeup referred to as '*dynamic ice*' processes that mainly refer to anchor ice and ice dam development (e.g. Kerr et al., 2002; Stickler and Alfredsen, 2005; Stickler et al., 2010; Tesaker, 1994). Ice dams in steep channels are known to dramatically increase water levels, change hydraulic conditions and contribute to the development of a suspended ice cover (e.g., Turcotte et al., 2011) under which the water flows unaffected by ice. Winter surveys of the ice cover surface are compared to open water surveys for a comparable discharge in two reaches of a step-pool channel in Fig. 1. Photographs presented in Fig. 1B and 1D represent an intermediate ice cover state at the surveyed locations (Fig. 1A and 1C) during freezeup. At the end of freezeup, the suspended ice cover was locally more than one 1 m higher than the prevailing water surface and a dominant portion of the space between the ice surface and water was occupied by air, not by ice.

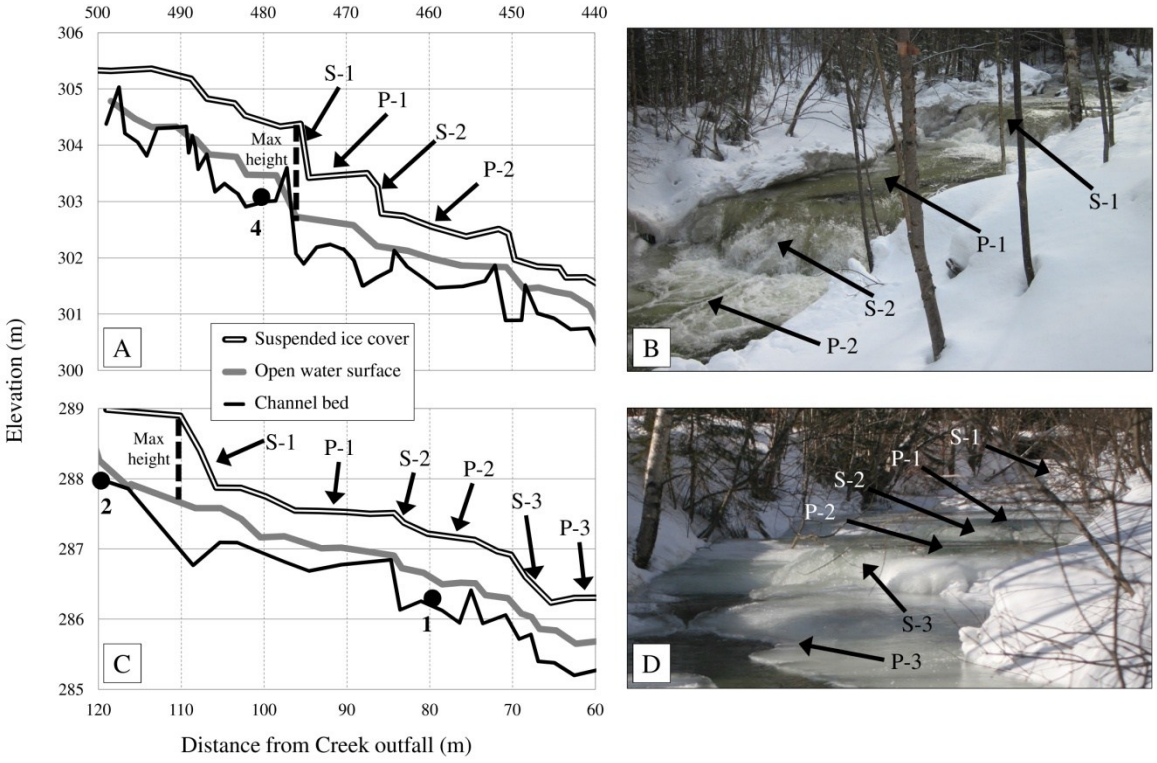

Figure 4.1. Land surveys of channel bed, open water surface (May 8th, 2013), and suspended ice cover surface (Feb. 18th, 2013) in two step-pool reaches. Arrows indicate location of steps (S) and pools (P). Flow is toward the camera in B and D. Site 4 (A & B) and sites 1 and 2 (C & D) are study sites presented in this work.

Despite the dominance of dynamic freezeup processes in cold region steep channels, few studies have presented quantitative field data or models that can readily be used by engineers and scientists. Turcotte et al. (2013) presented ice dam development and decay rates for channels of different Strahler orders of the same watershed. Tesaker (1996) presented a simple heat budget model for steep channels ice processes that was

improved by Turcotte et al. (2013). Turcotte et al. (2014) and Yamazaki et al. (1998) presented the effect of ice dam development on the channel discharge. Malenchak et al. (2006) and Malenchak et al. (2011) simulated the development of a single anchor ice weir in a large river. Ice processes along a relatively steep channel in Norway were adequately modelled (Timalsina et al., 2013) but ice dam development was neither reported nor simulated.

Most existing river ice models do not adequately simulate ice processes specifically taking place along chutes, rapids, and riffles and most existing heat budget models (e.g. Ashton, 1986) have been developed for large low gradient rivers and do not include thermal fluxes that are specific to small, steep channels. A physically-based model that can predict ice dam development and breaching would represent an important tool for cold region engineers and scientist working in gravel bed channels and it would inform them which field parameters should be assessed most carefully.

4.2 Objective

The overall objective of this paper is to provide a better comprehension of the spatial and temporal variability of ice dam growth/decay dynamics. The first section uses a statistical approach to demonstrate that a great variability exists in ice dam growth/decay rates from one channel type to the next, from a site to another in the same reach, and for a specific site from one year to the next. The second section presents a physically-based deterministic numerical model capable of simulating the growth and decay of a single ice dam. This model depends on multiple environmental parameters that must be measured or calculated in order to adequately simulate ice dam development and breaching. Both approaches (statistical or deterministic model) suggest that the design of hydraulic structures or the planning of restoration projects in steep channels must assess ice processes at the local scale.

4.3 Methodology

This paper presents field data from 18 sites of the Montmorency watershed located east of Quebec City, Canada during three consecutive winters (2011 to 2014). The most important data set was measured during winter 2012-2013 in the Lépine Creek watershed (47°3'34.40"N, 71°11'5.89"W), a hilly-forested area of 8 km^2. The Creek width varies from 2 and 4 m while its slope varies between 2% and 5% along the 800 m-long studied reach, a well-defined step-pool channel (Montgomery and Buffington, 1997). The inner structure, crystallographic arrangements, and growth processes of ice dam samples collected along the same reach were reported in Dubé et al. (2014).

Figure 2 presents the location (in meters from the outfall) of all instruments deployed at 6 research Creek sites. Four automated cameras (C in Fig. 2) were set to take a photograph every 30 minutes in order to visualize

freezeup processes and the overall ice cover spatial evolution. Water pressure was measured at the same rate using four HOBO U20 loggers (P in Fig. 2) and two YSI 6600V2 loggers (TP in Fig. 2) with a ± 2 mm accuracy. Atmospheric pressure was measured at sites 1 and 6 using two additional HOBO U20 loggers (ATP in Fig. 2). Water temperature and air temperature were respectively measured using two YSI 6600V2 loggers (TP in Fig. 2) with a corrected ± 0.01°C accuracy and two HOBO U22 loggers with a ± 0.2 °C accuracy. An additional HOBO U20 logger was anchored in the Creek 1.8 km upstream of Site 6. This upstream site is characterized by the absence of ice throughout winter and is used to quantify discharge variations in the reach.

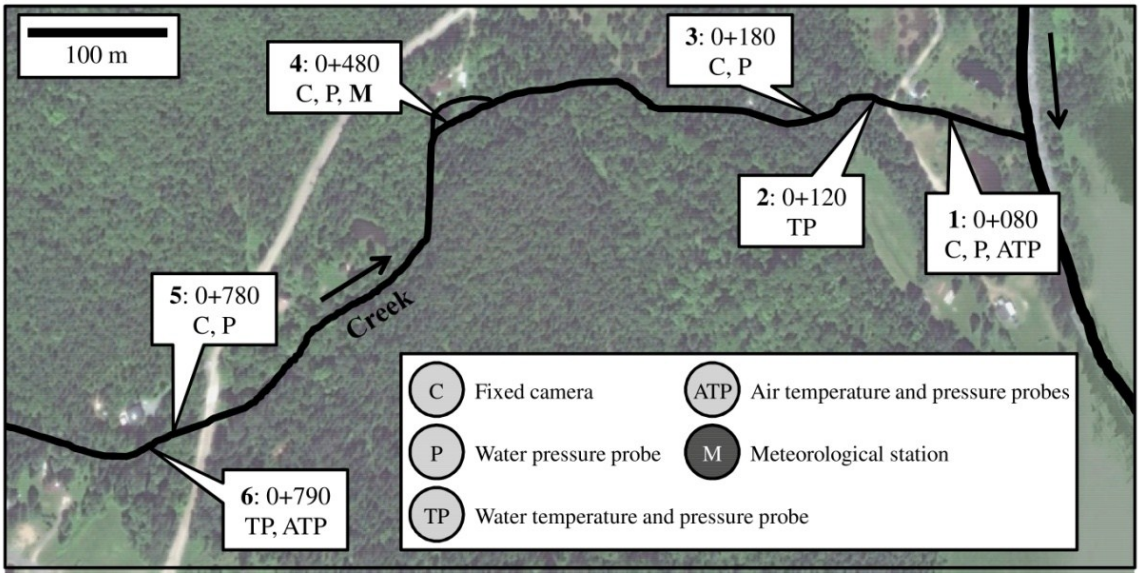

Figure 4.2. Deployed instrumentation in the Lépine Creek, Quebec (Canada).

A meteorological station (Fig. 3A) was installed at Site 4 (M in Fig. 2) at about 3 m from the channel banks. This site was located at a wide (about 15 m), lightly forested island. Measured parameters included air temperature, atmospheric pressure, wind speed and direction, and relative humidity on a one-minute basis using a CR5000 datalogger (the data was then average over 30 minutes). Short and long wave radiations were also measured downward and upward using a CNR4 (unventilated and unheated) net radiometer (Fig. 3B) placed 2 m above the water surface of the secondary channel.

4.4 Ice dam development rates

4.4.1 Data overview

Figure 4 presents the data from a first freezeup cycle (Nov. 26th to Dec. 3rd 2012). As proposed by Turcotte et al. (2013), a freezeup cycle starts and ends when the water depth is not measurably affected by ice (no backwater). The water depth (Y) in Fig. 4 was measured at Site 3 while the air temperature (T_{air}) and the water temperature (T_w) were respectively measured at Sites 1 and 2.

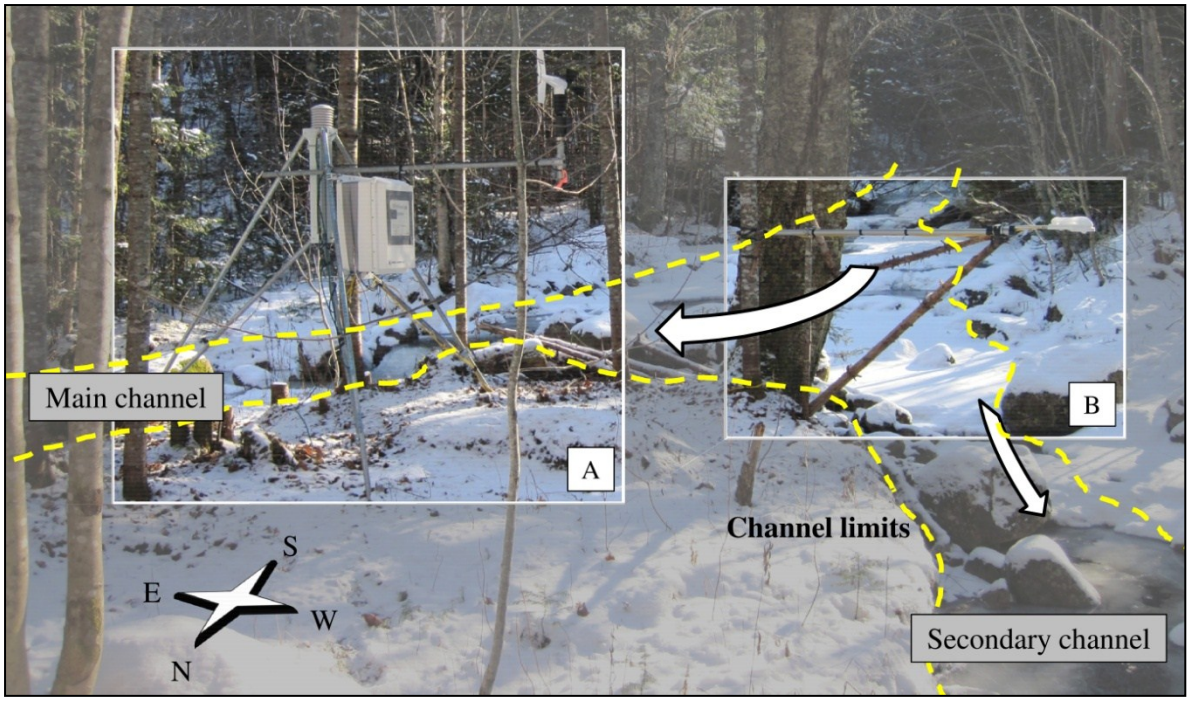

Figure 4.3. (A) Meteorological station and (B) net radiometer at Site 4.

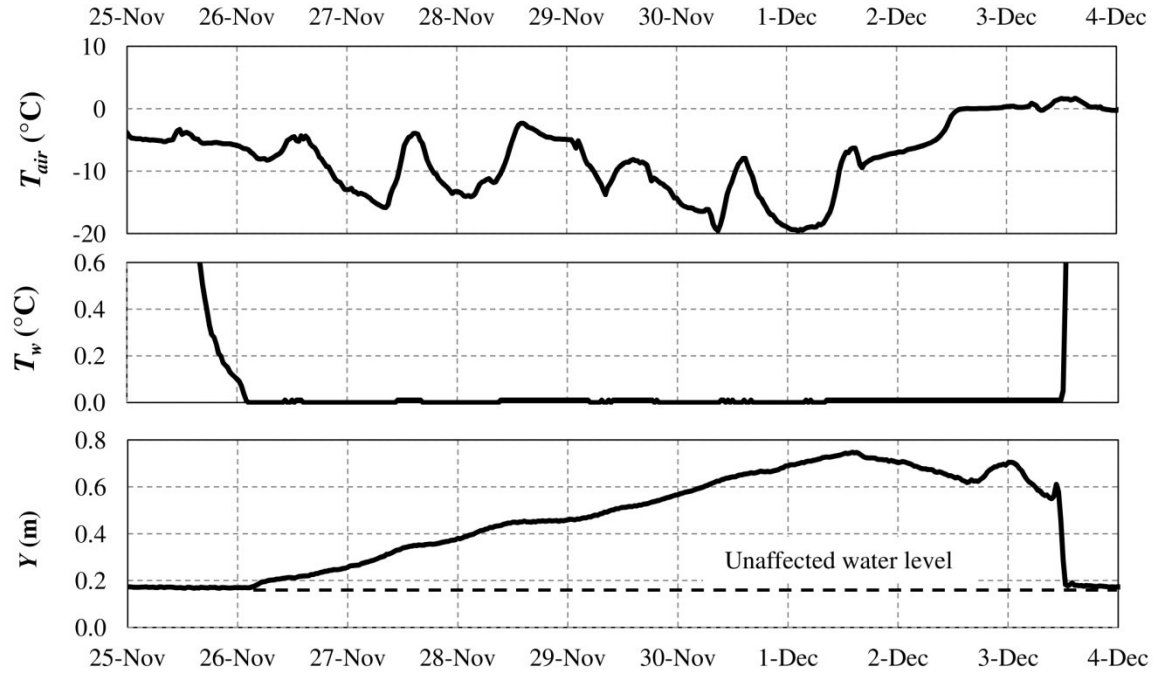

Figure 4.4. Environmental data (Nov. 25th to Dec. 4th, 2012) showing a freezeup cycle in the Creek at Site 3.

When T_{air} dropped to -6.5°C, T_w dropped to 0°C and *Y* began to increase as a result of ice development (confirmed with fixed cameras),. Between Nov. 26th and Dec. 3rd, *Y* varied in synchronicity with T_{air} (ice development [*Y* increase] during cold nights and ice melt [stable or decreasing *Y*] during mild days) before dramatically dropping back to the open water level (unaffected by ice). This sudden drop occurred exactly when T_w rose above 0°C. Cameras confirmed that ice dams had been breached along that reach.

Ice-induced *Y* variations were measured at studied Sites 1 to 6, less than 2 m upstream of ice dams development locations. Ice dams' height (*h*) was calculated by subtracting the open water (ice-free) *Y* value from the measured ice-affected *Y* value. The open water *Y* value prevailing during freezeup cycles was linearly interpolated between the open water *Y* values measured before and after each freezeup cycle (see Fig. 4), a reasonable approximation since no major discharge variation was measured at the upstream discharge measurement site during freezeup cycles and since the discharge trend is usually monotonic during winter flow recession trends events. With the calculated values of *h*, ice dam *buildup* and *breaching* rates were calculated on a 30-minute basis. Two types of buildup events were distinguished: ice dam *activations* (Δh^{+}) events defined by $T_w \leq 0.00$°C and by increasing *h* values, and ice dam *reactivations* (Δh^{++}) events defined by $T_w \leq$ 0.00°C and by increasing *h* values smaller than the maximum *h* previously reached (existing breached ice dam patching up). *Reactivation* events could eventually become *activation events* as ice development continued above the previous ice dam crest. In turn, *breaching* (Δh^{-}) events were defined by $T_w \geq 0.00$°C and by decreasing values of *h* eventually dropping to 0 m once the water stored upstream of ice dams had been released.

One can note that the *breaching* event in Fig. 4 (Dec. 3rd) is preceded by a sudden and brief Y rise while T_{air} is close to 0°C. This variation can either be caused by the jamming of drifting ice pieces or by the rapid release of water stored by upstream ice dams. This type of pre-breaching variation is not part of the statistical analysis presented here. Sudden and rapid ice dam *breaching* events lasting a maximum of 2 hours were measured on 29 occasions during winter 2012-2013. Though not observed in the present study, ice dam collapse can generate flood waves (e.g. Tesaker, 1994; 1996). On the other hand, some breaching events were more gradual and lasted several hours.

4.4.2 Ice dam buildup and breaching rates

Ice dam buildup and breaching rates (Δh^{+}, Δh^{++}, Δh^{-}) were calculated for each time step (30 min) and expressed in cm/hour. Figure 5 presents the data for the studied Creek sites from Nov. 26th, 2012 to Apr. 8th, 2013.

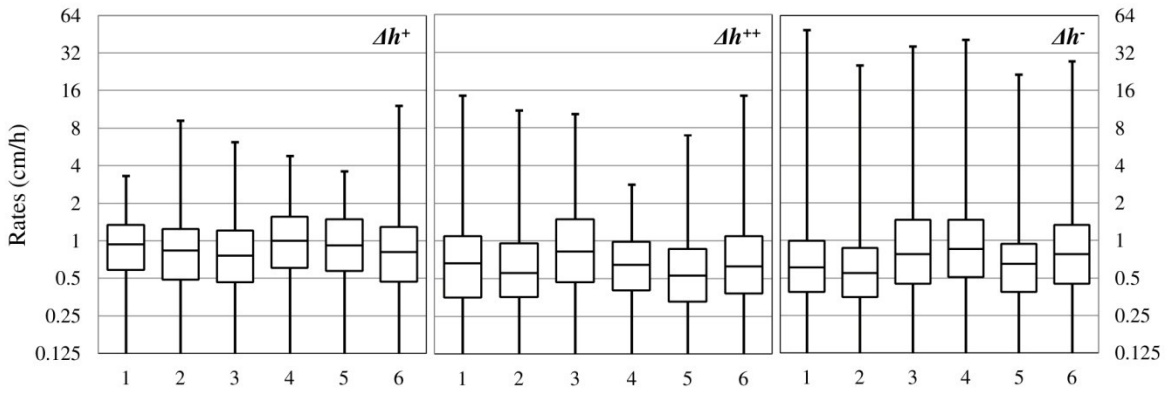

Figure 4.5. Ice dam activation (Δh^+ ; total of 653 hours for the 6 sites), reactivation (Δh^{++}; 1,363 hours) buildup rates and breaching (Δh^-; 1,714 hours) rates (max, min, 75%, 50% and 25% quartiles) for each site from Nov. 26th, 2012 to Apr. 8th, 2013 (note the log scale).

Results show that *activation* rates present higher quartiles values (25%, 50% and 75%) than *reactivation* rates at all sites but Site 3. In contrast, *maximum* buildup rates were greater during *reactivation* events at all sites but Site 4. This was expected because less ice development is required to "repair" or "patch-up" an existing, breached ice dam than to create a new ice dam The range of site-averaged rates and maximum rates during activation, reactivation and breaching events are summarized in Table 1. Large variability in breaching rates come from the fact that breaching processes are very chaotic: they are associated with preferential melting patterns and the development of water tunnels within the dam core while hydrological instabilities occur unexpectedly.

Table 4.1. Site-averaged and sites' maximum rates during activation, reactivation and breaching events.

	Average rates at six sites (cm/h)	Maximum rates at six sites (cm/h)
Δh^+	1.0 to 1.4	3.3 to 12.1
Δh^{++}	0.7 to 1.2	2.8 to 14.5
Δh^-	-0.9 to -1.6	-21.6 to -49.0

In Fig. 6, development rates from the 6 Creek sites in winter 2012-2013 are combined with development rates measured along the Creek (2 sites) and two additional channels (3 sites) during the winter of 2011-2012 (Turcotte et al., 2013) and with development rates from 13 sites in the Montmorency watershed during the winter of 2013-2014. This data set includes activation (3,381 data points), reactivation (3,329 data points) and breaching (4,847 data points) rates for ice dam of few centimeters to more than a meter-high (h) monitored along channels draining sub watersheds of 5 km^2 to 1000 km^2 and presenting different channel morphologies (step-pools, rapids, riffle-pools).

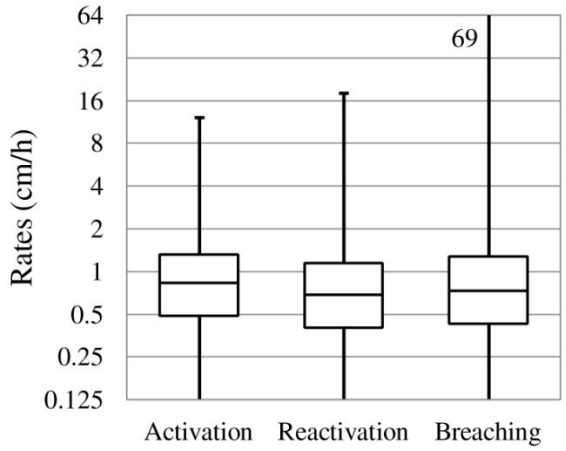

Figure 4.6. Ice dam activation (Δh^{+}), reactivation (Δh^{++}) and breaching (Δh^{-}) rates for 3 consecutive winters over 24 sites in channels of order 2, 3 and 4.

The data show that ice dam development rates (and the overall freezeup process) in different channel sizes and morphology patterns is similar to that observed in the Creek (Fig. 5). Reactivation rates present higher maximums than activation rates and breaching rates present quartiles that are comparable to those of activation and reactivation rates, but their maximum is dramatically higher. This confirms that the breaching process is on average relatively gradual while potentially leading to a sudden water storage release. Sudden breaching events or ice dam collapse events can potentially trigger a chain reaction and a jave (Jasek and Beltaos, 2008, Turcotte et al., 2014).

In order to investigate year to year variations, data at Site 3 is presented for 3 consecutive winters in Figure 7. Δh^{+} rates from all three winters are comparable while Δh^{++} rates are significantly higher in 2013-2014 for both quartiles and maximum values. Δh^{-} rates present some inter-annual variability in quartile values but exhibit similar ranges.

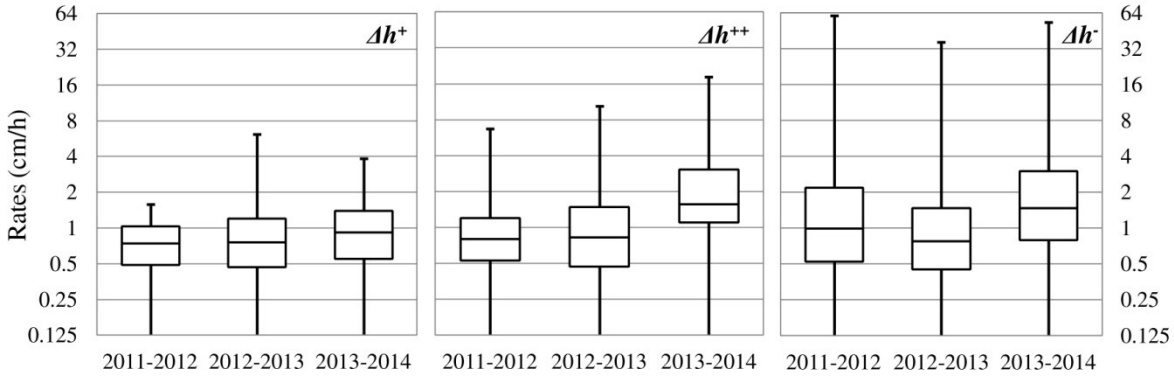

Figure 4.7. Ice dam activation (Δh^{+}), reactivation (Δh^{++}) and breaching (Δh^{-}) rates for 3 consecutive winters at Creek's Site 3.

4.5 Ice dam modeling: heat budget method

Dynamic ice processes are complex, spatially variable, and difficult to simulate, especially in small channels where heat fluxes can vary significantly along a short reach. Indeed, steep channels are often located in hilly forested areas. The canopy and watershed topography partially prevent short wave radiation from reaching the channel and also affect long wave radiation fluxes as the local tree steams supply thermal radiation (Stähli et al. 2009) back to the channel. Evaporation and convection heat fluxes vary on a small spatial scale as the wind is greatly influenced by the forest canopy. For example, a wind speed reduction of 75-80% is generally assumed between open areas and forested areas (e.g. Metcalfe and Buttle, 1998; Tribbeck and Gurney, 2006). Small channels are also significantly affected by groundwater heat fluxes compared to larger channels. Input locations, unit discharge per channel length, and temperature (the groundwater temperature is assumed to be 1°C higher than the year-averaged air temperature (Caissie, Pers. Com.) play a significant role in ice development patterns.

In order explain the great spatial and temporal variability of Δh^{+}, Δh^{++} and Δh^{-} rates as well as ice dam elevation over time, and given the great heterogeneity of the Canadian boreal forest (density and canopy composition) added to the complexity of in groundwater patterns in the Canadian Shield, the physical model presented here was fed with site-specific input parameters. The authors improved the watershed-scale heat budget model presented by Turcotte et al. (2013) and adapted the equation scheme in order to create a local-scale water heat budget model with an ice development and melting component. The objective of this model is to successfully predict *Y* variations for a single step-pool sequence. The sequence located at Site 4 was chosen for the model application because of the presence of the meteorological station. The following sections present the heat fluxes (in Watts per m^2) considered in the model and describe how they were obtained, i.e., either from *in-situ* measurements or from calculations.

4.5.1 Short wave radiation (E_{sw})

In-situ measurements of short wave radiation were essential to the model accuracy. Unfortunately, upwelling short wave radiation measurements (from the water to the atmosphere) were contaminated by snow cover reflection and could therefore not be used in the model. The net short wave radiation reaching the water (E_{sw}) was obtained by measuring downwelling radiation and by multiplying this value by ($1-\alpha_w$), where α_w is the water albedo, which was set to 0.12 (e.g., Beltaos, 2008, 2013).

4.5.2 Long wave radiation (E_{lw})

Because of the forest effect, direct *in-situ* measurements of long wave radiation were also required. The radiometer measured upwelling long wave radiation emitted from water, ice and snow cover surfaces all together. Therefore, net long wave radiations reaching the water (E_{lw}) was obtained by subtracting the

upwelling radiation emitted by water only (E_{lww}) from the measured downwelling long wave radiation. E_{lww} was obtained using the Stefan-Boltzmann law:

$$E_{lww} = \xi \sigma T_w^{\,4} \tag{1}$$

Where ξ is the emissivity (typically 0.97 for water), σ is the Stefan-Boltzmann constant (5.67×10^{-8} W/m² °K⁴) and T_w is the water temperature in Kelvin [273.2 + T(°C)].

4.5.3 Evaporation (E_{evap}) and convection (E_{conv})

Evaporation and convection heat fluxes were calculated using the following *in-situ* measured parameters: wind speed, T_{air}, T_w, atmospheric pressure and relative humidity. Figure 8 shows that forest wind speed measured at Site 4 was dramatically different from the wind speed measured at a nearby (33 km) airport (Environment Canada "Quebec/Jean Lesage INTL A" station). Linear regression (grey dashed line) suggests that the studied hilly forested terrain reduced wind speed by 91% on average.

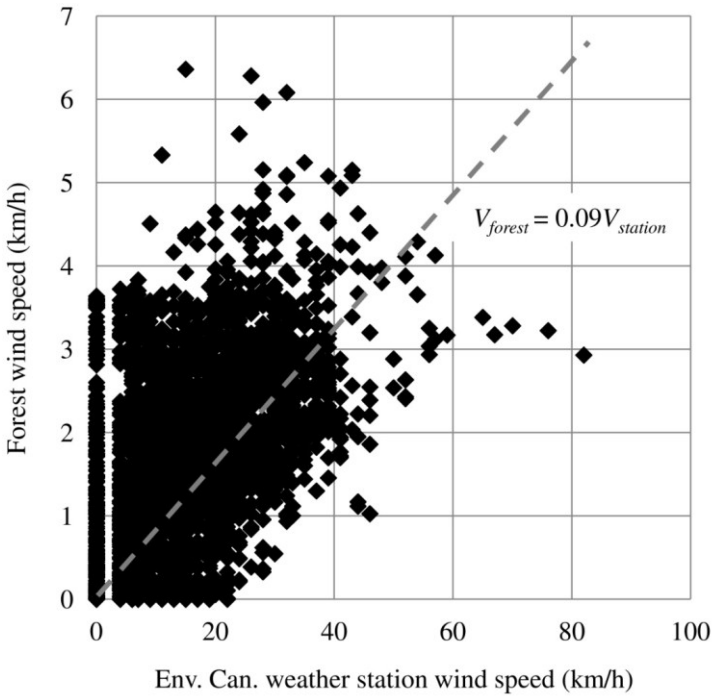

Figure 4.8. Hourly wind speed comparison between Environment Canada weather station and forested study Site 4 (comparison of 2874 measurements).

The evaporation heat flux (E_{evap}) was given by the Kuzmin formula:

$$E_{evap} = (0.013 + 0.00016 V_2)(e_w - e_{air}) \rho_w L_V \,/\, 8.64 x 10^6 \tag{2}$$

where V_2 is the wind speed (km/day), e_w and e_{air} are respectively the vapor pressure of water and air (mb), ρ_w is the water density (kg/m³) and L_v is the latent heat of vaporization of water (MJ/kg).

The convection heat flux (E_{conv}) is obtained by multiplying E_{evap} by the Bowen ratio (B_R):

$$B_R = 0.6\left(\frac{P_a}{1000}\right)\frac{(T_w - T_{air})}{(e_w - e_a)} \tag{3}$$

where P_a is the atmospheric pressure (mb). All input parameters in Equations (2) and (3) where measured at Site 4 except T_w, which was measured at Site 6.

4.5.4 Conductive energy from the bed (E_{bed})

As the ground temperature sufficiently below the channel bed remains above 0°C during the entire winter period, heat is constantly transferred from the ground to the water by conductive transport driven by temperature gradient between the ground and water. As the Creek watershed lays on a granitic geologic formation (Canadian Shield), thermal conductivity (k_s) of 2.5 W/m°C for granite was considered (Côté and Konrad, 2005). Based on year-averaged measured air temperatures at that site, a ground temperature of 5°C was estimated at 10 m below the channel bed. The ground temperature drops to 0°C at the bed level at the beginning of winter (mandatory for anchor ice formation), which represents an average heat flux of 1.25 W/m² reaching the water. This heat flux value was used though it is smaller than what other studies have proposed (e.g. Marsh, 1990).

4.5.5 Energy from the groundwater (E_{gw})

Groundwater characteristics (temperature and flow rate) were not measured *in-situ* but were carefully estimated in order to calculate the resulting heat flux (E_{gw}) using this equation:

$$E_{gw} = \frac{T_{gw}\Psi C_w \rho_w}{P} G \tag{4}$$

Here, T_{gw} is the groundwater temperature (°C), Ψ is the groundwater flow per unit length (m²/s), C_w is the specific heat of water (4,220 J/kg°C at 0°C), P is the wetted perimeter (m) and G is a modulator coefficient accounting for groundwater inflow reduction caused by an ice-induced increase in Y. G was set to vary linearly with the depth, having a value of 0.1 when the water depth was at its measured maximum and a value of 1.0 when the water depth was at its measured minimum value. T_{gw} was set to 4°C, a lower value than the estimated ground temperature of 5°C, to account for groundwater cooling as it approached the channel through cold channel banks. Ψ was determined at the upstream site. The base flow was obtained with a rating

curve developed by Turcotte et al. (2014) for that site and using a hydrograph separation technique. This base flow was divided by the estimated total channel length upstream of Site 4 (4,800 m) to obtain Ψ. The value of E_{gw} obtained from Equation (4) can be considered as a fair estimation of the groundwater heat flux at that site though the actual local flux may be different, depending on local fractures in the bedrock along the banks and underneath the channel.

4.5.6 Energy from friction (E_{fr})

The heat contribution from flow friction on the channel bed and banks is expressed by:

$$E_{fr} = \frac{\rho_w g Q S_f}{P} \tag{5}$$

where g is the gravitational constant (9.81 m/s²), Q is the channel flow rate at site 4 (m³/s) and S_f is the friction slope (m/m). Winter-time Q at Site 4 could not be directly measured because of ice effects. Therefore, it was calculated using measured flow rate at the upstream site (Q_{up}) with this equation:

$$Q = \left(R_w Q_{up} - \frac{\Delta S}{\Delta t} \right)(1 - R_{SC}) \tag{6}$$

R_w is the watershed flow ratio between Site 4 and the upstream site (estimated to 1.85 based on flow rate measurements before winter), S is water storage and release (m³) respectively caused by ice dam development and breaching between both sites (time dependent values based on ice effect estimations with a maximum storage rate of 153 m³/h [0.04 m³/s] and a maximum release rate of 90 m³/h [0.02 m³/s]), and R_{SC} is the incoming flow ratio diverted to the secondary channel at Site 4 (estimated to 0.25).

The Creek channel wetted perimeter (P) was calculated using a geometry specific to Site 4. Since P varies as the ice forms and as Y increases, a freezeup scheme of the pool at Site 4 was used to estimate the relationship between P and Y over time (Fig. 9). As the prevailing water level just before freezeup (Y_{ini}) increased, icing started to develop from the banks and extended toward the center of the channel in a triangular shape (inverted slope of 1:1 as observed in the field). Time laps photographs revealed that anchor ice accumulations were sparse and their presence as thin layers covering some protruding rocks was not considered for the determination of the wetted perimeter nor the channel cross-sectional area (A).

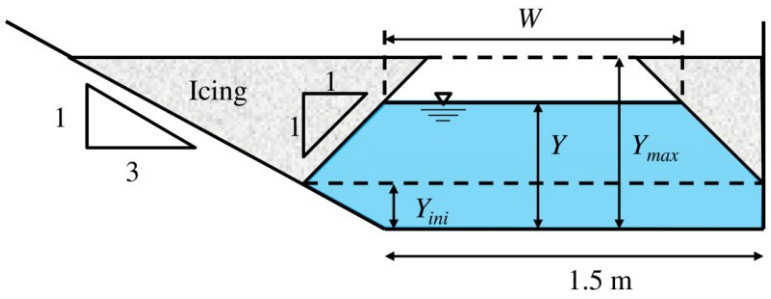

Figure 4.9. Approximate cross-section and ice development geometry at Site 4.

The local pool friction slope (S_f) in Equation (5) was calculated using Manning. The Meyer-Peter and Muller (1948) formula was used to estimate the ice-free n value (0.031 based on an observed d_{90} [largest 10% submerged rocks] of about 30 cm). Under partial anchor ice coverage conditions, n was set to 0.04, in agreement with Kerr et al. (2002). Calculated S_f varied from $1x10^{-7}$ m/m during the most intense ice dam buildup event to 0.007 m/m at peak flow during a mid-winter breakup event.

4.5.7 Suspended ice cover insulation

Suspended ice covers (SIC) are unique ice features found in steep channels (Tesaker, 1994; 1996; Stickler and Alfrendsen, 2009; Turcotte et al. 2014). Turcotte et al. (2013) proposed a simple approach to account for the insulating properties of SIC. In order to quantify this aspect of SIC, air temperatures above (T_{air}) and under the SIC (T_{SIC}) were measured from Feb. 7th to Mar. 7th, 2013 at Site 4. Results (Fig. 10) show that T_{SIC} is most often warmer than T_{air} (when T_{air} is below -5°C or so) and occasionally cooler (during mild spells and/or when the ice is melting). The linear regression (white dashed line in Fig. 10) suggests that the SIC reduces air temperature by 75% on average. This buffer effect is the combined result of (1) SIC insulation from heat exchanges with the cold atmosphere with (2) continuous heat release from the water. The SIC extended over 90-95% of the channel surface near Site 4 during the measurement period. Cold air found below the ice and heat released from the relatively warm water probably respectively came and escaped through open areas (5-10%).

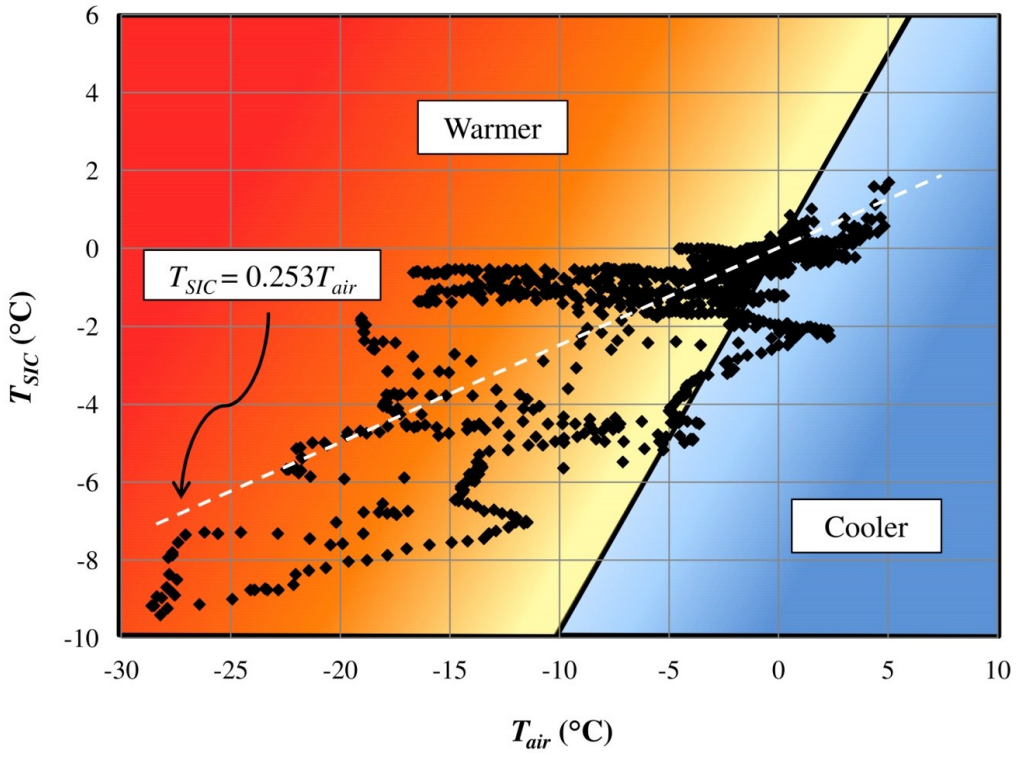

Figure 4.10. Air temperatures measured below the suspended ice cover compared to those above from Feb. 7th to Mar. 7th, 2013 (1,320 measurements).

In order to adapt this information to the heat budget model, the ratio of SIC divided by the total channel area (or channel ice coverage; I_c) was manually determined using 30-minute basis time-lapse photographs and regular field visits. Short wave radiation, long wave radiation, evaporation and convection heat fluxes were reduced proportionally to I_c. Heat fluxes from the bed, groundwater, and friction remained unchanged as they occur at the water-bed interface.

4.5.8 Total energy and ice formation

The net heat flux (E_{net}) expressed in W/m² was obtained using the following equation:

$$E_{net} = (E_{sw} + E_{lw} + E_{evap} + E_{conv})(1 - I_c) + E_{bed} + E_{gw} + E_{fr} \quad (7)$$

The total energy (Ω) of a single step-pool sequence (i.e., Site 4) expressed in Watts was obtained with:

$$\Omega = (E_{sw} + E_{lw} + E_{evap} + E_{conv})(1 - I_c)(Wl) + (E_{bed} + E_{gw} + E_{fr})(Pl) \quad (8)$$

where l is the channel segment length (8 m for the step-pool sequence at Site 4) and W is the channel width. Ω is either positive (the water gains heat) or negative (the water loses heat). During ice-free conditions, a heat

gain or loss respectively results in T_w increase or decrease. Once T_w drops to 0°C or less (supercooling), a negative heat budget generates ice formation. The volume of ice produced for each time step (ΔV_{ice}) is given by the following relation:

$$\Delta V_{ice} = \frac{-\Omega t}{\rho_i L_f} \tag{9}$$

ΔV_{ice} is expressed in m³, t is the time step (1,800 sec.), ρ_i is the density of ice (916 kg/m³) and L_f is the latent heat of fusion of water (3.34×10^5 J/kg). Equation 9 is also applicable for a positive heat budget which leads to negative ΔV_{ice} values (i.e. ice melting).

4.6 Model parameterization

4.6.1 Ice dam characteristics

The local production of ice can go into ice dam formation, anchor ice formation, ice cover formation and/or frazil ice formation. The frazil ice can attach to any of the other formations or it can stay suspended in the flow. It is assumed that the amount of frazil ice leaving the reach is equal to the amount of frazil entering the reach. The user must specify to the model the percentage of ice that will be used building up the dam. This ratio is referred to as the *damming energy ratio* (D). Given an assumed ice dam geometry, the rise in the ice dam level will therefore be calculated and hence the rise in water level (Y) known.

In order to avoid undesirable Y disturbances, the ice dam at site 4 was not sampled for porosity (ϕ). Based on data from Dubé et al. (2014), a ϕ value of 40% was adopted. Using D and ϕ, the change in ice dam volume at each time step is given by:

$$\Delta V_{dam} = D\left(\frac{1}{1-\phi}\right)\Delta V_{ice} \tag{10}$$

Ice dam shapes can vary significantly from one site to another and the relationship between the volume of ice and the backwater effect is consequently very site-specific. In order to successfully predict Y variations at Site 4, the geometry of the ice dam was determined and schematized (Fig. 11). The trapezoidal dam shape was set to present a fixed crest length (L) and fixed lateral slopes. The ice dam volume (V_{dam}) was obtained as a function of width (W_D) and height (Y_D). The resulting equation is:

$$V_{dam} = Y_D^{\,3}\left(\frac{-2S_D L_D^{\,2}}{H_D^{\,2}}\right) + Y_D^{\,2}\left((L+L_D)\frac{-2L_D S_D}{H_D} + \left(\frac{L_D}{H_D}\right)W_i\right) + Y_D\left((L+L_D)W_i\right) \tag{11}$$

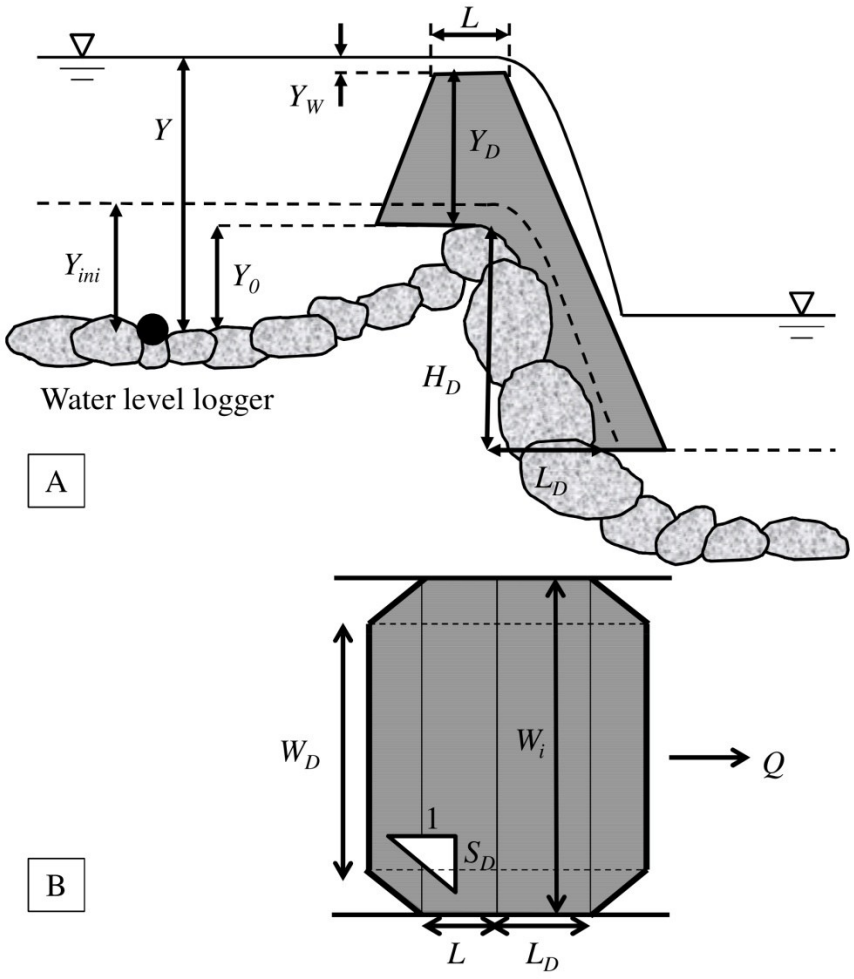

Figure 4.11. Modeled ice dam geometry at Site 4. (A) Profile view and (B) overhead view in stream wise direction.

This third order equation, solved for Y_D, is also expressed as a function of the drop height (H_D), the drop length (L_D), the initial dam width (W_i) and the narrowing slope (S_D). S_D was included to address the observed dam's crest narrowing while extending further upstream and downstream. This implies that the surface on which the ice forms becomes smaller as the dam builds up and hence, for a given ΔV_{dam}, Y_D increases more rapidly. Another hypothesis underlying the ice dam geometry in Fig. 11A is that the lateral slopes are equal to L_D/H_D. This means that lateral slopes remain unchanged as the dam builds up (as observed on time-lapse photographs). As long as Ω remains negative, the ice dam builds up and Y increases.

When Ω becomes positive in Eq. (9), ice melting occurs and a different component of the model intervenes. Field observations and time-lapse photographs revealed that during breaching events, the dam crest and lateral slopes remained intact (negligible melting). As observed by Turcotte et al. (2011) a typical breaching event is characterized by a perforation of the ice dam core through a complex matrix of tunnels and galleries. For modeling purposes, this process was schematized with the melting of a rectangular section of fixed width

(W_T) extending over the entire dam's base length (L_{TOT}) and with an height (h_T) increasing upward from the channel bed (as long as Ω remained positive). The height h_T of the tunnel over time is expressed as:

$$\Delta h_T = \frac{\Gamma \Delta V_{dam}}{L_{TOT} W_T} \tag{12}$$

where Γ represent the heat transfer efficiency as water melts the tunnel. To simplify the model, Γ was set to a constant value that was independent of other parameters. In reality Γ it is likely to depend on other parameters such as the water velocity through the tunnel (V_T).

The flow rate conveyed by the tunnel (Q_T) is the product of V_T and the tunnel cross-section. Based on a simple Bernoulli equation, considering a difference in water elevation from upstream to downstream of the dam equal to H_D, and neglecting the upstream flow velocity, V_T becomes:

$$V_T = \sqrt{\frac{2gH_D}{1 + \frac{fL_{TOT}}{D_h}}} \tag{13}$$

In Equation 13, f is the friction coefficient set to 0.005 and D_h is the hydraulic diameter for a rectangular tunnel.

4.6.2 Water depth simulation parameters

As shown in Figure 11A, total Y in the pool is the combination of the initial level of the ice dam relatively to the water level logger (Y_0), the ice dam height (Y_D) and the water depth over the dam (Y_W). The present model considers a linear storage release equation to calculate Y over time if Q_W is the flow rate over the dam crest, Q_T is the flow rate under the dam, Q is the channel discharge entering the pool, and V is the water volume in the pool (cross-section presented in Fig. 9 and length l equal to 8 m). This storage equation is:

$$Q_T + Q_W = Q - \frac{dV}{dt} \tag{14}$$

Based on a weir equation, Q_W is expressed as:

$$Q_W = {Y_W}^{3/2} W_D \left(\frac{2C_d \sqrt{2g}}{3} \right) \tag{15}$$

where C_d is the discharge coefficient (set to 0.7). Eq. (14) only depends on Y which values are solved for each time step and sent back to the heat budget model.

4.7 Model calibration and results

Two freezeup events, during which the radiometer at Site 4 was not affected by ice or snow are available and were simulated with the model. The first event (Dec. 1st to Dec. 2nd, 2012) only included the last *buildup* hours and the first *breaching* hours of a freezeup cycle. The second event (Feb. 1st to Feb. 4th, 2013) occurred after a mid-winter breakup and included a complete *buildup* cycle followed by most of the *breaching* cycle. This second event was used to calibrate (and evaluate the sensitivity of) the many parameters of the model.

Figure 12 presents the measured air temperature (T_{air}), measured and simulated heat fluxes (E_{sw}, E_{lw}, E_{evap}, E_{conv}, E_{gw}, E_{fr}), the channel ice coverage (I_c), as well as the resulting net heat flux (E_{net}) at Site 4 from Feb. 1st to Feb. 4th, 2013. E_{bed} is not presented as its value is considered to be constant (1.25 W/m²). Atmospheric heat fluxes (E_{sw}, E_{lw}, E_{evap}, E_{conv}), as presented in Fig. 12, are not affected by I_c while E_{net} is the result of the interaction between atmospheric fluxes and the ice cover.

Measured short wave radiation (E_{sw}) data show important variations over time because of the distribution of different tree species and the presence of hills at Site 4. Besides these variations the canopy greatly reduced the overall solar radiation reaching the channel (theoretical values of E_{sw} in open fields should have been about 450 W/m² while the highest value in Fig. 12 is 160 W/m²). Measured long wave radiation (E_{lw}) was relatively constant at about -50 W/m². This was expected because of the stable water temperature (at 0°C or slightly supercooled) during the entire event combined with the reflective effect of the forest surrounding the channel. E_{lw} was relatively insensitive to T_{air} variations compared with E_{evap} E_{conv}. The irregular aspect of the latter two parameters' trend was mainly induced by wind speed variations.The calculated friction heat flux (E_{fr}) dropped from 0.50 to 0.01 W/m². Those seemingly insignificant values came from the low flow rate combined with the decreasing water velocity (and friction slope) as the downstream ice dam was building up. In contrast, at peak flow during the mid-winter breakup event of Jan 31st, the simulated E_{fr} had reached a value of 60 W/m².

As presented on Fig. 12, initially, the surface ice coverage (I_c) remained fairly low since water levels were increasing (drowning the ice as it formed). When the water level dropped, the developing cover emerged as on Feb. 2nd near noon (reaching 50%) and on Feb. 3rd near 3:00 a.m. (reaching 85%).

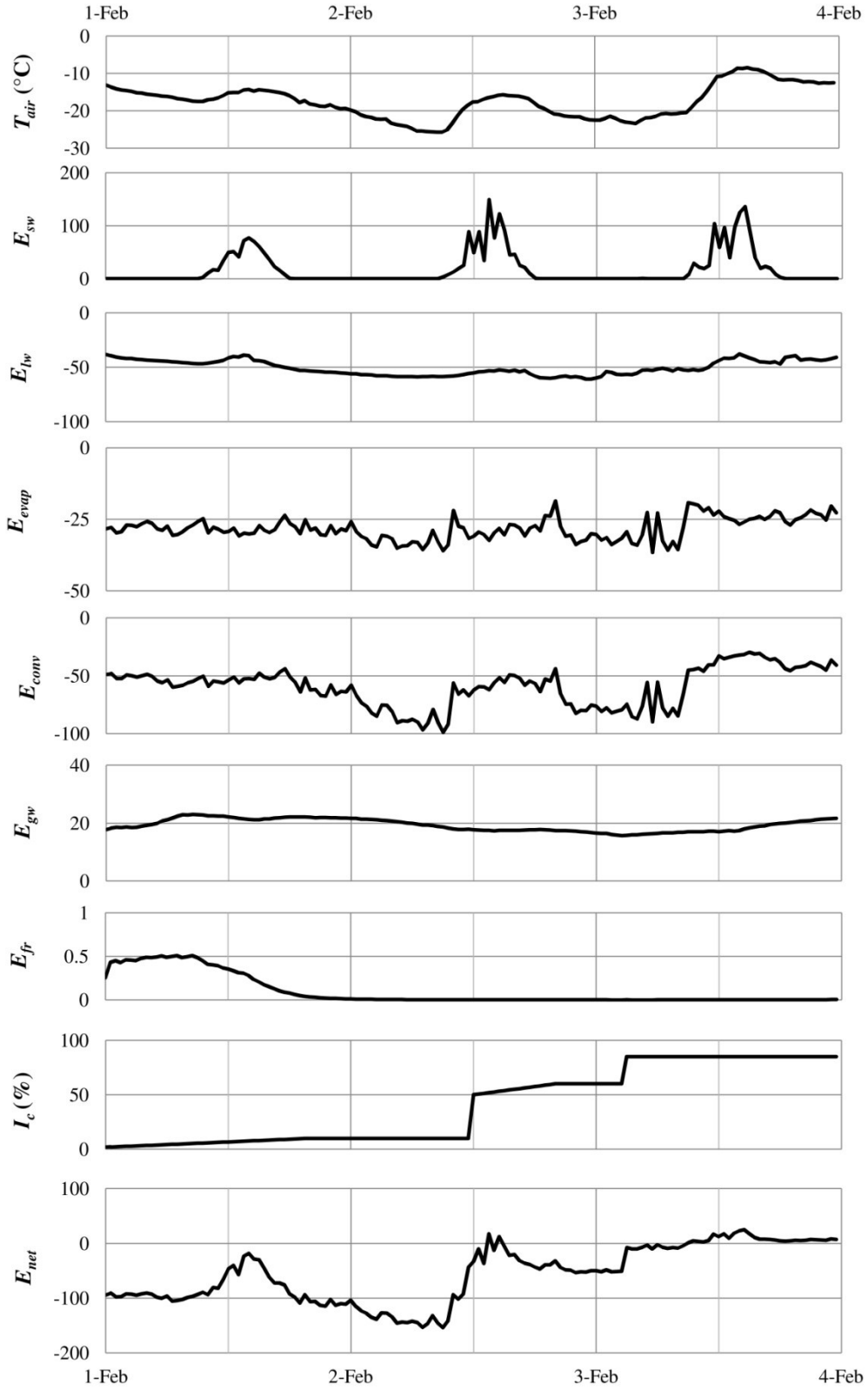

Figure 4.12. Measured air temperature (T_{air}), heat fluxes (in W/m²) from short wave radiation (E_{sw}) and long wave radiation (E_{lw}), simulated heat fluxes from evaporation (E_{evap}), convection (E_{conv}), groundwater (E_{gw}) and friction (E_{fr}), observed channel ice coverage (I_c) and simulated net heat flux (E_{net}) from Feb. 1st to Feb. 4th, 2013 at Site 4.

The total energy per unit length (Ω/l) trend is shown in Fig. 13. The water continuously lost heat to the atmosphere until Feb. 2nd, at 1:00 p.m. The transient, slightly positive heat budget that followed was sufficient to cause some ice melting and a momentarily drop in the measured Y (Fig. 13). Subsequently, with a return to negative heat budget, ice dam buildup resumed and Y further increased. Then, in the first hours of Feb. 3rd, E_{net} and Ω/l became irreversibly positive, the ice dam at Site 4 was breached and Y dropped back towards ice-free condition (Fig. 13).

The resulting simulated Y variations in Fig. 13 were obtained by introducing the following values, estimated with field observations and time-lapse photographs, into the ice dam geometry component of the model: initial dam width (W_i) of 3 m, ice dam crest length (L) of 10 cm, drop height (H_D) of 0.75 m, drop length (L_D) of 0.5 m, narrowing slope (S_D) of 1 m/m, and pool length (l) of 8 m. Parameter values that were estimated based on theoretical assumptions included the weir discharge coefficient (C_d) set to 0.7, the heat transfer efficiency through the tunnel (Γ) set to 60%, the friction coefficient (f) in the tunnel set to 0.005, and the tunnel breaching width (W_T) set to 1 m. The best fit (simulated Y vs. measured Y) was obtained by setting the damming energy ratio (D), the last remaining degree of freedom, to 75%.

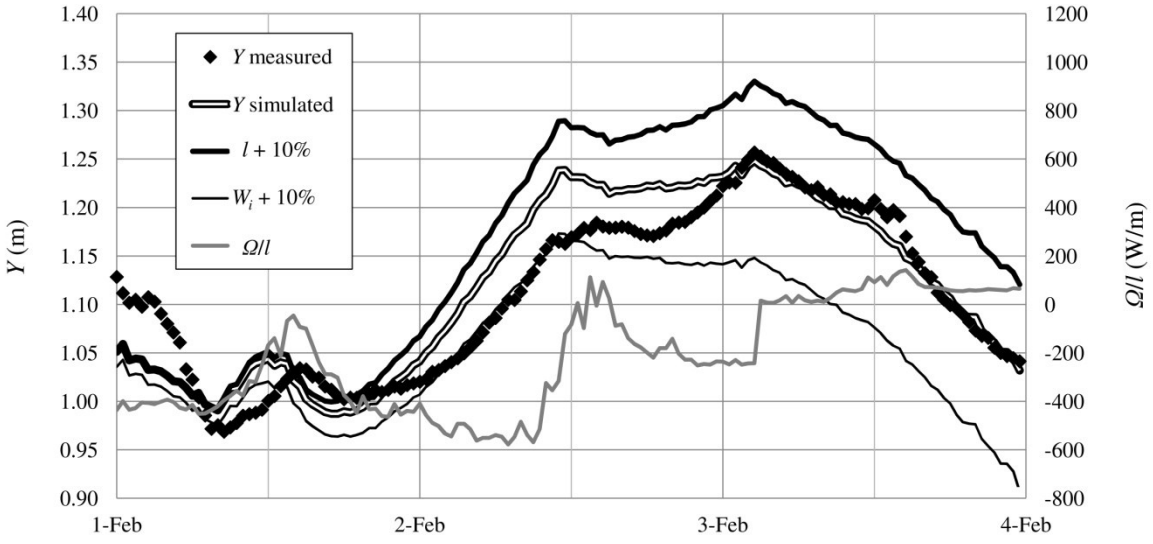

Figure 4.13. Measured water depth (Y), simulated Y, l and W_i sensitivity trends and total energy per unit length (Ω/l) at Site 4 (Feb. 1st to Feb. 4th, 2013).

General water level variations of the freezeup event were relatively successfully calibrated, especially during the last breaching period. However, the model could not simulate adequately some Y variations such as the lump taking place on the afternoon of Feb. 1st, 2013. At that time, the simulated Ω/l also varied but remained negative. It is possible that this Y variation could have actually been a flow rate (Q) variation caused by a transient hydraulic storage release from an upstream reach where the local heat budget was momentarily positive. This type of local discharge variation could not be taken into account in the present model and

illustrates the great complexity of hydro-cryologic processes at the watershed scale (Turcotte et al., 2014). A second model mismatch (Feb. 2nd, 2013) occurred during the main ice dam buildup period whereas the *Y* rise was overestimated by a maximum of 8 cm. Beyond the complexity of the process, this mismatch can be explained by a lack of accuracy of (1) the ice dam volume equation as a function of its height (Eq. 11), (2) the weir equation evaluating the water depth over the dam crest as a function of *Q*, or (3) the actual evaluation of *Q* (under estimation of upstream storage).

The model includes 30 degrees of freedom, some of which have a significant effect on simulated *Y* values. For instance, in Fig. 13, a 10% increment of the pool length (l) or the dam width (W_i) generate a significant impact on the overall *Y* amplitude over time. A broad sensitivity analysis was performed by increasing the following parameters by 10%: pool length (l), narrowing slope (S_D), drop height (H_D), drop length (L_D), weir discharge coefficient (C_d), crest length (L), initial dam width (W_i) and ground water temperature (T_{gw}). Figure 14 presents the relative increase or decrease of the maximum resulting values of *Y* (on Feb. 3rd) for each parameter.

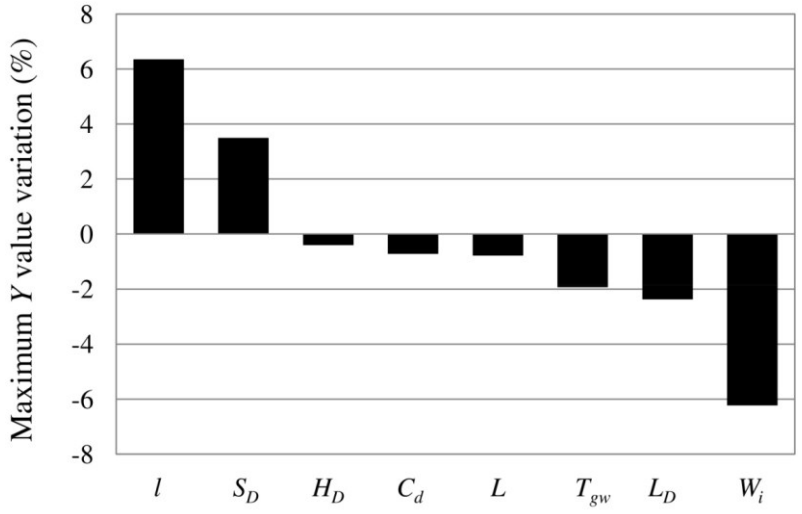

Figure 4.14. Sensitivity analysis on simulated maximum *Y* value.

Results show that, under the same given heat fluxes, *Y* is mostly sensitive to l and W_i variations. This implies that under specific meteorological conditions, buildup rates and the maximum ice dam height will depend heavily on the local channel geometry and morphology. Steep channels can be characterized by very heterogeneous profiles, patterns, and large rock arrangements (steps or other hydraulic control sections). As a result, it is expected that ice dams will development at different rates and will present different shapes along the same gravel bed channel reach. It also appears virtually impossible to predict the development of a specific ice dam if local channel parameters are not methodically characterized.

4.7.1 Heat fluxes and air temperature vs. growth rates

The link between measured *buildup* rates (Δh^+), simulated energy budget E_{net} values, and air temperature (T_{air}) values for each time step was analysed for the Feb. 1st to Feb. 4th (Fig. 15). In order to present a valid comparison with E_{net}, T_{air} was multiplied by 1-I_c (open area ratio). This yielded the *effective* T_{air} value. While the overall scatter between E_{net} and Δh^+ is important (R^2=0.12 for an imposed intercept at 0 cm/h), it is interesting to note that E_{net} values under -100 W/m^2 are consistently associated with Δh^+ greater than 1.5 cm/h. The overall scatter (R^2=0.5) between the *effective* T_{air} and Δh^+ is comparable to what had been obtained for a measured T_{air} by Turcotte et al. (2013) for multiple freezeup events along different steep streams. Nonetheless, for *effective* T_{air} under -15°C, ice dam growth rates were also constantly higher than 1.5 cm/h. From a practical standpoint, the *effective* T_{air} is easier to calculate than E_{net}.

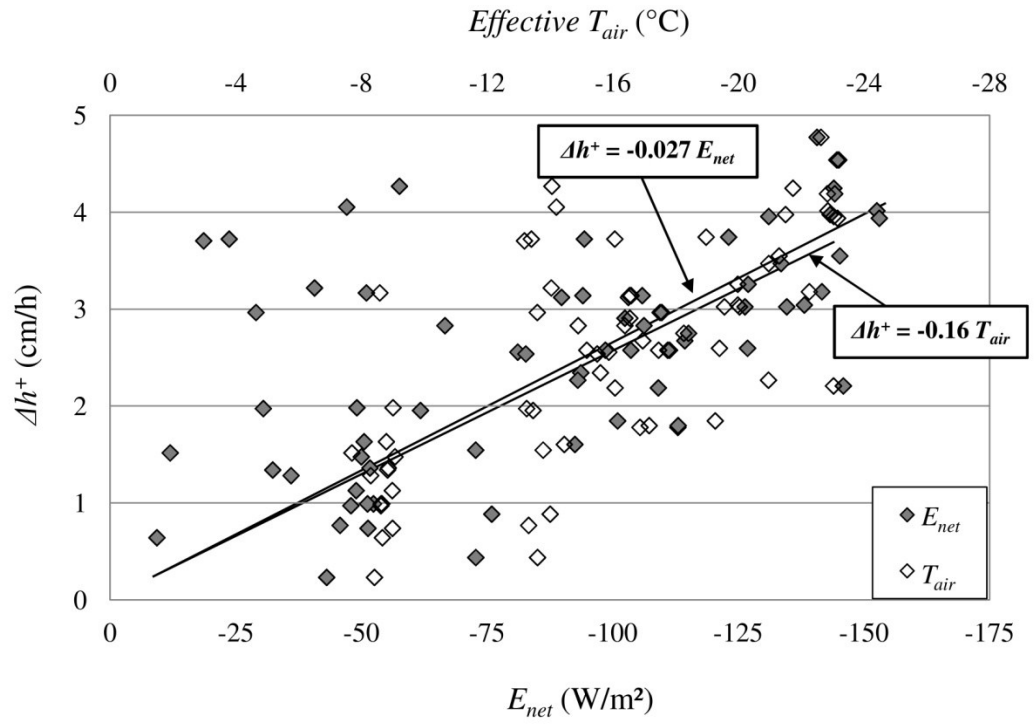

Figure 4.15. Measured ice dam *buildup* rates (Δh^+) versus simulated net heat flux (E_{net}) and measured *effective* air temperature (T_{air}) for the Feb. 1st to Feb. 4th, 2013 freezeup event at Site 4.

Questions arise regarding (1) the intercept value of those relationships (not necessarily going through 0 cm/h), (2) the effect of *Q* (ice-induced hydrological) instabilities on *Y* measurements, (3) the potential effect of drifting ice pieces (broken ice features from upstream dams being trapped by ice dams) on *Y* measurements and (4) the overall chaotic nature of dynamic ice production in steep channels. Further field investigations and laboratory experiments in cold rooms should explore the relationship between Δh^+ and E_{net} (or T_{air}, a dominant energy budget parameter).

4.8 Discussion

The purpose of this paper was to provide useful data on dynamic ice processes to practicing engineers and scientists. The dominant freezeup processes in steep, gravel bed channels is the development (and breaching) of ice dams. The main metric that describes ice dam buildup and breaching is the rise and fall of their upstream water level (Y). Of interest are the maximum values of Y, especially compared with the floodplain level or overall channel depth, and the rates at which Y increases (Δh^{+}, Δh^{++}) or decreases (Δh^{-}), mostly for flooding rates evaluations and for hydrological budget calculations.

The field data show that the all of these quantities are within predictable ranges. This means that scientists, streamside residents, and practicing engineers have a quantitative basis for making decisions: in the studied Creek as well as along many other gravel bed channels across the Montmorency River watershed during three consecutive winters, ice dams typically reached a maximum height of 50 to 100 cm (note that Tesaker [1994] had reported an ice dam which crest was 4 meters above the channel bed), sometimes after many buildup and breaching cycles, at median buildup and breaching rates of about 1 cm/h. Maximum buildup rate values reached over 10 cm/h and ice dams could breach, or collapse, at rates above 50 cm/h.

Furthermore, this paper has quantified the individual contributions of the many winter energy flux components of a step-pool channel located in a forested area. Net shortwave radiation was the most variable and could momentarily reach 100 W/m^2 at noon, net long wave radiation and convective heat exchanges were about -50 W/m^2, both groundwater and evaporative energy fluxes were about -20 W/m^2 and the net energy flux could drop to -140 W/m^2 when the air temperature was below -25 °C or so. It was also shown that a complete heat budget evaluation can be used to estimate the volume of ice generated per channel length. If the geometry of an ice dam can be determined, the ice volume generation rate can be used to calculate the rate at which this ice dam will buildup, its maximum elevations, and, to some extent, its breaching rate.

The model also demonstrated that the predicted parameters (Y and h) are very sensitive to (1) the pool length, (2) the relative amount of heat that is lost to the dam as compared to shore ice and anchor ice and (3) the initial dam width, which is mostly dictated by the local hydraulic control (or step) geometry. Given the sensitivity of the model and the uncertainty of various input parameters, it is probably suitable to perform many simulations with different sets of input parameters and to express the maximum height (and buildup or breaching rates) of an ice dam as a possible range rather than as a single value. It would also be of interested to develop a synthetic (universal) ice dam geometry equation (e.g., Eq. 11) that fits most ice dams with less degrees of freedom or to develop a set of ice dam geometry equations that would be associate with different types of hydraulic controls or morphologies (narrow steps, wide steps, large stone clusters in a flatbed

channel, etc.). Note that it is possible to predict where an ice dam will form based on previous winter observations or on experience.

There are further interactions and feedback mechanisms in dynamic ice processes that make the deterministic prediction of ice dam almost impossible. For example, some ice dams are so dominant or fast growing that they can drown several ice dams and pools located upstream. This process lengthens the pool associated with a given dam and modifies a very sensitive input parameter of the model. Another example of this freezeup process complexity is the likely effect of a snowfall on ice dam growth rates and on channel insulation properties. Saturated snowflakes can stick to the channel bed (e.g., Turcotte et al., 2012) or to existing ice features and a snow layer can be flooded by the increasing water level to generate white ice within an ice dam core (Dubé et al., 2013). Snowfalls have been associated with ice dam buildup (activation and reactivation) and breaching events (Turcotte et al., 2013).

Despite the complexity of freezeup processes in steep channels and the sensitivity of the model to many input parameters, the data and equations presented here can be adapted to, or coupled with, an existing ice-hydrodynamic model that would simulate steep channel ice processes, which has not specifically been done so far. The authors believe that a simplified version of the model could be calibrated to relatively large drainage systems, yielding primary information on water levels and discharge depressions during the freezeup period.

4.9 Conclusion

This paper has presented a framework for practicing engineer and scientists working in cold region gravel bed channels. Results showed that ice dam buildup and breaching rates should be expected to greatly vary around a median value of about 1 cm/h. This great variability was explained with a local-scale ice dam development model that successfully predicted the behavior of a single ice dam. This model showed that numerous degrees of freedom are inherent to the process and that local morphology characteristics play an important role in ice dam development. This implies that any engineering or scientific project in steep channels must account for local ice processes and that the simulation of multiple sets of input parameters would yield a range of possible ice dam development scenarios.

The model presented here can be improved by better field data including (1) using a heated net radiometer (2) measuring groundwater flow rates and temperatures (3) precisely measuring local flow rates during freezeup (possibly using a dye dilution technique), (4) exploring ice dam breaching mechanisms, and (5) developing synthetic or morphology specific ice dam geometry equations.

List of symbols

Symbol	Parameter	Unit
A	Cross section area	m²
C_d	Discharge coefficient	-
C_w	Specific heat of water	J/kg°C
C_{WR}	Weir coefficient	-
D	Damming energy ratio	-
e_{air}	Vapor pressure of air	mb
e_w	Vapor pressure of water	mb
E_{bed}	Conductive heat flux from the channel bed	W/m²
E_{conv}	Convective heat flux	W/m²
E_{evap}	Evaporative heat flux	W/m²
E_{fr}	Friction heat flux	W/m²
E_{gw}	Groundwater heat flux	W/m²
E_{lw}	Long wave radiation heat flux	W/m²
E_{net}	Net heat flux	W/m²
E_{sw}	Short wave radiation heat flux	W/m²
f	Friction coefficient	-
g	Gravitational constant	m/s²
G	Groundwater inflow modulator coefficient	-
h	Ice dam height	m
H_D	Ice dam drop height	m
h_T	Breaching tunnel height	m
I_c	Channel ice coverage	%
k_s	Thermal conductivity	W/m°C
l	Pool length	m
L	Ice dam crest length	m
L_D	Ice dam drop length	m
L_f	Latent heat of fusion of water	J/kg
L_{TOT}	Total ice dam base length	m
L_v	Latent heat of vaporization of water	MJ/kg
n	Manning roughness coefficient	-
P	Wetted perimeter	m
P_a	Atmospheric pressure	mb
Q	Flow rate	m³/s
Q_T	Breaching tunnel flow rate	m³/s
Q_{up}	Flow rate at the upstream site	m³/s
Q_W	Flow rate over the ice dam crest (weir)	m³/s
R_h	Relative humidity	%
R_{SC}	Secondary channel flow rate ratio	-
R_w	Watershed flow ratio	-
S	Water storage	m³
S_D	Ice dam narrowing slope	m/m
S_f	Friction slope	m/m
T_{air}	Air temperature	°C
T_{gw}	Groundwater temperature	°C
T_{SIC}	Air temperature under the suspended ice cover	°C
T_w	Water temperature	°C
V	Volume of water in the pool section	m³

(continued)

Symbol	Parameter	Unit
V_{dam}	Ice dam volume	m³
V_{ice}	Volume of ice produced	m³
V_T	Breaching tunnel flow velocity	m/s
V_2	Wind speed measured at 2 m above the ground	km/day
W	Channel width	m
W_D	Ice dam width	m
W_i	Initial ice dam width	m
W_T	Breaching tunnel width	m
Y	Water level	m
Y_D	Ice dam height	m
Y_{ini}	Freezeup water depth	m
Y_W	Water depth over the ice dam crest	m
Y_0	Ice dam height relativity to the water logger	m
Γ	Heat transfer efficiency	%
Δh^+	Ice dam activation growth rate	cm/h
Δh^{++}	Ice dam reactivation growth rate	cm/h
Δh^-	Ice dam breaching rate	cm/h
Ψ	Groundwater flow per unit length	m²/s
Ω	Total energy	W
Ω/l	Total energy per unit length	W/m
α_w	Water albedo	-
ξ	Emissivity of water	-
ρ_i	Ice density	kg/m³
ρ_w	Water density	kg/m³
σ	Stefan-Boltzmann constant	W/m² °K⁴
ϕ	Ice porosity	%

Acknowledgments

This research was partially funded by the Canada Foundation for Innovation (CFI) and by the Natural Sciences and Engineering Research Council of Canada (NSERC). The authors would also like to recognize the contribution of a number of river ice scientists and engineers who provided useful comments for the paper, particularly the two reviewers. Finally, field work was greatly facilitated at all levels by Dany Crepault and François Anctil from Laval University.

References

Ashton, G.D., 1986. River Lake Ice Engineering. Water Resources Publications, LLC.

Beltaos, S., 2008. River Ice Breakup. Water Resources Publications, LLC.

Beltaos, S., 2013. River Ice Formation. Committee on River Ice Processes and the Environment, CGU-HS.

Côté, J., Konrad, J.M., 2005. Thermal conductivity of base-course materials. Can.Geotech. Journal 42: 61-78.

Dubé, M., Turcotte, B., Morse, B., Stander, E. 2013. Formation and inner structure of ice dams in steep channels. Proceedings of the 17th CGU-HS CRIPE Workshop on River Ice, Edmonton, Alberta, Canada.

Dubé, M., Turcotte, B., Morse, B., 2014. Inner structure of anchor ice and ice dams in steep channels. Cold Regions Science and Technology 106-107, 194-206.

Jasek, M., Beltaos, S., 2008. Ice-jamrelease: javes, ice runs and breaking fronts. In: Beltaos, S. (Ed.), River Ice Breakup. Water Resources Publications, Highland Ranch, CO.

Kerr DJ, Shen HT, Daly SF. 2002. Evolution and hydraulics of anchor ice on gravel bed. Cold Reg. Sci. Technol. 35: 101–114.

Malenchak, J., Morris, M., Shen, H.T., Doering, J., 2006. Modeling anchor ice growth at Sundance Rapids. Proceedings of the 18th IAHR International Symposium on Ice.

Malenchak, , M., Doering, J., Shen, H.T., 2011. Modeling of Anchor Ice and Aufeis Formation at Sundance Rapids. CGU HS Committee on River Ice Processes and the Environment, 16th Workshop on River Ice, Winnipeg, Manitoba.

Marsh, P., 1990. Modelling water temperature beneath river ice covers. Canadian Journal of Civil Engineering 17, 36–44.

Metcalfe, R.A., Buttle, J.M., 1998. A statistical model of spatially distributed snowmelt rates in a boreal forest basin. Hydrological Processes, *Hydrol. Process.* 12, 1701-1722.

Meyer-Peter, E., Muller, R., 1948. Equations to bed load transport. Proc., 4th Meeting International Association to Hydraulic Research, Paper, No. 2, pp. 39-64.

Montgomery, D.R., Buffington, J.M., 1997. Channel-reach morphology in mountain drainage basins. GSA Bulletin 109 (5), 596-611.

Stähli, M., Jonas, T., Gustafsson, D., 2009. The role of snow interception in winter-time radiation processes of a coniferous sub-alpine forest. Hydrological Processes, *Hydrol. Process*. 23, 2498-2512.

Stickler, M., Alfredsen, K., 2005. Factors controlling anchor ice formation in two Norwegian rivers. 13th Workshop on the Hydraulics of Ice Covered Rivers.

Stickler M, Alfredsen KT. 2009. Anchor ice formation in streams: a field study. Hydrol. Process. 23: 2307–2315. DOI: 10.1002/hyp.7349.

Stickler M, Alfredsen KT, Linnansaari T, Fjeldstad H-P. 2010. The influence of dynamic ice formation on hydraulic heterogeneity in steep streams. River Res. Applic. 26: 1187–1197. DOI: 10.1002/rra.1331.

Tesaker E. 1994. Ice formation in steep rivers. In: Proceedings of the 12th International IAHR Ice Symposium.

Tesaker E. 1996. Interaction between ice and water flow in rapids. In: Proceedings of the 13th International IAHR Ice Symposium.

Timalsina, N.P., Charmasson, J., Alfredsen, K.T., 2013. Simulation of the ice regime in a Norwegian regulated river. Cold Regions Science and Technology 94, 61-73.

Tribbeck, M.J., Gurney, R.J., Morris, E.M., 2006. The Radiative Effect of a Fir Canopy on a Snowpack. Journal of Hydrometeorology, Volume 7, 880-895.

Turcotte B, Morse B, Anctil F. 2011. Steep channels freezeup processes. Proceedings of the 16th CGU-HS CRIPE Workshop on the Hydraulics of Ice Covered Rivers, Winnipeg, MB, Canada.

Turcotte, B., Morse, B., Anctil, F., 2012a. Cryologic continuum of a steep watershed. Hydrol. Process. DOI: 10.1002/hyp.9629

Turcotte, B., Morse, B., Anctil, F., 2012. Impacts of precipitation on the cryologic regime of stream channels, Hydrol. Process. 26, 2653–2662.

Turcotte, B., Morse, B., Dubé, M., Anctil, F., 2013. Quantifying steep channel freezeup processes, Cold Regions Science and Technology 94, 21-36.

Turcotte, B., Morse, B., Anctil, F., 2014. The hydro-cryologic continuum of a steep watershed at freezeup. Journal of hydrology 508, 397-409.

Yamazaki, M., Hirai, Y., Hasegawa, K., Hirayama, K., 1998. Anchor ice formation and discharge change on a cold region river. Ice in Surface Waters, Shen (ed.), Balkema, Rotterdam.

5. Conclusion

Ce projet de recherche a présenté des données et des résultats originaux et innovateurs qui permettent de mieux comprendre les processus dynamiques de formation et de fonte de la glace dans les cours d'eau à forte pente. Le travail réalisé a permis d'atteindre avec succès l'ensemble des cinq objectifs énoncés. En effet, une première caractérisation de la structure interne des barrages de glace a été décrite au Chapitre 2. En utilisant une combinaison des analyses par sections minces et par *CAT scan*, il a été possible de documenter les différentes structures de glace composant les barrages de glace, d'en calculer avec précision la porosité et de décrire les processus de croissance en fonction des arrangements cristallographiques observés. Le Chapitre 3 se voulait une extension du deuxième chapitre en analysant cette fois non seulement des échantillons de barrages de glace mais également des échantillons de glace de fond. De plus, en appliquant des techniques d'analyse plus poussées aux résultats du *CAT scan*, il a été possible de caractériser les différents types de cristaux observés et de quantifier statistiquement les différences et les similitudes entre les structures cristallographiques retrouvées dans la glace de fond et celles retrouvées dans les barrages de glace. Les résultats fournissent également une compréhension supplémentaire des processus d'initiation et de développement de la glace de fond et des barrages de glace. Le Chapitre 4 s'est quant à lui étendu au niveau macroscopique en étudiant le développement des barrages de glace à l'échelle du chenal. En mesurant l'évolution des niveaux d'eau durant un hiver complet (2012-2013), il a été possible de quantifier les taux de croissance et de fonte de six différents barrages de glace situés sur un même cours d'eau. Ainsi, la variabilité spatiale et temporelle du développement des barrages de glace à l'intérieur d'un chenal a pu être observée et documentée. Cette variabilité a pu être expliquée grâce à la modélisation innovatrice d'un barrage de glace tenant compte des particularités de la formation de glace dans les chenaux à forte pente situés en forêt. Le modèle a également permis de déterminer les paramètres environnementaux qui influencent le plus le développement des barrages de glace. De façon plus spécifique, les résultats présentés à l'intérieur des trois articles scientifiques qui composent ce mémoire permettent de tirer les conclusions suivantes :

- Les barrages de glace peuvent être composés à la fois de frasil-fixé et de glace colonnaire alors que la glace de fond est strictement composée de frasil-fixé.
- La porosité des accumulations de frasil-fixé varie entre 23% et 52% alors que la porosité des accumulations de glace colonnaire varie entre 0% et 1,5%.
- L'émergence de la surface du substrat est une condition nécessaire pour la formation de la glace colonnaire.
- La glace colonnaire peut se développer sur un substrat solide comme une roche mais également sur les accumulations de frasil-fixé émergentes.

- Les cristaux de frasil-fixé et de glace colonnaire sont significativement différents en longueur de segments et en longueur totale alors que leur porosité n'est pas significativement différente.
- La glace de fond est initiée par l'attachement et l'interception de particules de frasil.
- La croissance en place (*in situ*) des cristaux de frasil-fixé est le processus dominant de développement de la glace de fond et des barrages de glace.
- Les taux de croissance et de fonte des barrages de glace présentent une grande variabilité spatiale et temporelle et ce, à l'intérieur d'un même chenal.
- Le développement d'un barrage de glace est très sensible aux conditions météorologiques, hydrauliques et hydrologiques locales propres à la section d'écoulement marche-mouille dans laquelle il se forme.
- Les conditions hydrauliques et hydrologiques locales sont influencées par le développement des barrages de glace situés à l'amont. Il s'ensuit donc une boucle de réactions dont le comportement complexe est pratiquement impossible à prévoir.
- Pour l'ingénieur praticien, ces résultats impliquent que la conception d'ouvrages hydrauliques dans les cours d'eau à forte pente doit absolument tenir compte des particularités propres à chaque unité géomorphologique (seuil-mouille, marche-mouille, etc.).

À la lumière des résultats obtenus et des analyses réalisées, certaines recommandations peuvent être énoncées en vue de poursuivre la recherche dans le domaine. Bien que les résultats démontrent que l'initiation de la glace de fond est assurée par l'attachement et l'interception de particules de frasil, il n'a pas été possible d'observer ces phénomènes en temps réel. Une telle observation fournirait une meilleure compréhension des processus d'attachement et de croissance des cristaux de frasil dans les premières minutes/heures du développement de la glace de fond. Il serait également intéressant de réaliser une nouvelle campagne d'échantillonnage de glace de fond et de barrages de glace en mesurant de façon systématique les conditions hydrauliques (e.g. vitesse de l'écoulement, niveau d'eau) au moment de la collecte pour ensuite procéder à l'analyse par *CAT scan*. Le tout permettrait de mieux documenter et de confirmer les résultats obtenus dans le présent projet quant au lien entre la cristallographie des échantillons et les conditions hydrauliques aux sites de collecte. En vue d'améliorer la modélisation proposée, il serait important de mesurer une plus grande quantité, voire tous les intrants thermiques utilisés dans le modèle. Parmi ceux-ci, la température et le débit de l'eau souterraine représentent deux paramètres ayant une grande influence sur le bilan énergétique et sont probablement les plus difficiles à mesurer précisément. Pour simuler efficacement la période de fonte (*breaching*) du barrage de glace, une investigation des processus de perforation à la base du barrage doit être menée. Bien que la littérature offre une description de ce phénomène, les processus physiques sont encore mal compris.